NASA Technical Memorandum 100916
ICOMP-88-11

Universal Limiter for Transient Interpolation Modeling of the Advective Transport Equations: The ULTIMATE Conservative Difference Scheme

B.P. Leonard
Institute for Computational Mechanics in Propulsion
Lewis Research Center
Cleveland, Ohio

September 1988

NASA

NASA
LEWIS RESEARCH CENTER
ICOMP
CASE WESTERN
RESERVE UNIVERSITY

UNIVERSAL LIMITER FOR TRANSIENT INTERPOLATION MODELING OF THE

ADVECTIVE TRANSPORT EQUATIONS: THE **ULTIMATE**

CONSERVATIVE DIFFERENCE SCHEME

B.P. Leonard*
Institute for Computational Mechanics in Propulsion
Lewis Research Center
Cleveland, Ohio 44135

SUMMARY

A fresh approach is taken to the embarrassingly difficult problem of
adequately modeling simple pure advection. An explicit conservative control-
volume formulation makes use of a universal limiter for transient interpolation
modeling of the advective transport equations. This ULTIMATE conservative dif-
ference scheme is applied to unsteady, one-dimensional scalar pure advection
at constant velocity, using three critical test profiles: an isolated sine-
squared wave, a discontinuous step, and a semi-ellipse. The goal, of course,
is to devise a single robust scheme which achieves sharp monotonic resolution
of the step without corrupting the other profiles. The semi-ellipse is partic-
ularly challenging because of its combination of sudden and gradual changes in
gradient. The ULTIMATE strategy can be applied to explicit conservative
schemes of any order of accuracy. Second-order schemes are unsatisfactory,
showing steepening and clipping typical of currently popular so-called "high
resolution" shock-capturing or TVD schemes. The ULTIMATE third-order upwind
scheme is highly satisfactory for most flows of practical importance. Higher
order methods give predictably better step resolution, although even-order
schemes generate a (monotonic) waviness in the difficult semi-ellipse simula-
tion. But little is to be gained above ULTIMATE fifth-order upwinding which
gives results close to the ultimate one might hope for.

INTRODUCTION

In a landmark series of papers in the 1970's, Bram van Leer worked
"Towards the Ultimate Conservative Difference Scheme" for computational fluid
dynamics (refs. 1 to 5). This work spawned a body of literature in the present

decade involving advective modeling methods which are sometimes classified as "shock-capturing" schemes or, more recently, as "TVD" schemes, referring to the oscillation-suppression strategy of total-variation diminution (ref. 6). The ultimate conservative difference scheme for CFD has proven surprisingly elusive. There have been notable "successes" such as impressive demonstrations of nonoscillatory high resolution of steps and shock waves, for example; but progress has been unexpectedly slow. It seems that correction of one defect always introduces another, equally severe. Unphysical oscillations inherent in classical second-order methods were eliminated by switching to first-order upwinding; but this merely replaced unacceptable oscillations with (what was ultimately realized to be) unacceptable global artificial diffusion. By devising methods with locally varying artificial diffusion (small in smooth regions, larger in sharply varying regions), it is possible to achieve somewhat better resolution than global first-order upwinding without introducing spurious numerical oscillations.

Some forms of shock-capturing (or TVD) schemes achieve their impressive results for step resolution by the use of locally varying positive artificial diffusion or viscosity (first-order upwinding) to suppress oscillations, combined with local negative viscosity (such as first-order downwinding) to artificially compress or steepen the front. Unfortunately, this inherent negative diffusion is responsible for artificial steepening of (what should be) gentle gradients, as well, as will be demonstrated. Because of the concomitant flattening of local extrema (due to the local positive artificial diffusion), this defect has become known as "clipping," although the problem is initiated by the artificial steepening introduced to give high resolution to simulated fronts. In some cases (for example, a step-function followed by a ramp), inherent oscillations, rather than being suppressed, are converted into a series of small monotonic steps, a phenomenon known as "stair-casing."

As will be clearly demonstrated here, currently popular forms of TVD schemes achieve monotonic (although not always sharp) resolution of steps at the expense of gross (albeit nonoscillatory) distortion of simple smooth profiles. Thus, A.R. Mitchell's characterization of advective modeling as computational dynamics' ultimate embarrassment (ref. 7) is still appropriate, given the current state of the art. The ultimate goal of the current research program is to inject some self-confidence (as opposed to self-satisfaction) into

2

computational fluid dynamics by developing a truly robust (i.e., universally applicable) framework on which further refinements can be constructed.

The present paper is the first in a proposed series presenting a fresh approach to simulating the advective term, which, being an odd-order (first-) derivative, is the most significant aspect of CFD (ref. 8). An extremely simple form of "monotonizing" universal limiter is described which can be applied to explicit conservative difference schemes, with no constraints on the order of accuracy and resolution. The universal limiter banishes unphysical over-shoots and nonmonotonic oscillations without corrupting the expected accuracy of the underlying method. In particular, when used with (artificial-viscosity-free) third or higher order base schemes, it does not induce artificial com-pression (steepening) or clipping, typical of so-called "high resolution" (actually, second-order) shock-capturing methods.

Conservative explicit advection schemes of arbitrarily high order can be composed from "transient interpolation modeling" (TIM); i.e., for pure advec-tion of a scalar ϕ at constant vector velocity v, the exact transient solu-tion over time Δt is

$$\phi(x,\Delta t) = \phi(x-v\Delta t,0) \qquad (1)$$

where the accuracy (in both space and time) of the approximate numerical method is determined solely by (multidimensional) spatial interpolation at the earlier time-level. The ULTIMATE conservative difference scheme then consists of using the universal limiter (UL) for transient interpolation modeling (TIM) of the advective transport equations (ATE).

Since accurate modeling of the advective term is one of the more challeng-ing aspects of CFD (in addition to nonlinearities, multidimensionality, etc.), attention will be focused, in this first article, on the superficially simple but embarrassingly difficult problem of unsteady one-dimensional pure advection of scalar profiles at constant velocity. Three critical test profiles are con-sidered: an isolated sine-squared wave, representing smooth functions with a continuously turning gradient; a step discontinuity in value; and a semi-ellipse, combining discontinuous and continuous changes in gradient. At first, several (unlimited) explicit schemes are surveyed, together with some popular shock-capturing methods which are explained in terms of the Normalized

Variable Diagram (NVD). The NVD is also used as the basis for development of the universal limiter, which is then explained in terms of unnormalized variables and applied to explicit polynomial TIM methods of second through eighth order. For most (relatively smooth) flows, the cost-effective third-order upwind ULTIMATE scheme gives excellent practical results. Local higher order resolution can be automatically built in with almost negligible additional cost.

SCALAR ADVECTION

Unsteady, one-dimensional, pure advection of a scalar ϕ at constant velocity u is described by

$$\frac{\partial \phi}{\partial t} = -u \frac{\partial \phi}{\partial x} \tag{2}$$

This equation can be integrated in time over a time-step Δt and in space over a control volume (CV) at station i from $-\Delta x/2$ to $+\Delta x/2$, assuming a uniform grid. This gives the exact conservative difference scheme

$$\bar{\phi}_i^{n+1} = \bar{\phi}_i^n - c\left(\phi_r^* - \phi_\ell^*\right) \tag{3}$$

where the bars represent spatial averages, and the asterisks time averages, the superscripts designate time-levels, c is the Courant number $u\Delta t/\Delta x$, and right and left time-averaged face values are indicated. The CV spatial averages can be written in terms of central node values plus a deviation term

$$\bar{\phi}_i = \phi_i + DEV \tag{4}$$

Now assume that node values are related by an exact equation of the form

$$\phi_i^{n+1} - \phi_i^n = -c\left(\phi_r - \phi_\ell\right) \tag{5}$$

where the face values now include the effects of the deviation terms. The deviation terms themselves will then satisfy

$$DEV^{n+1} - DEV^n = -c(DEV_r - DEV_\ell) \tag{6}$$

given suitable definitions of the terms on the right. Thus, from equations (3), (4), and (6),

$$\phi_i^{n+1} - \phi_i^n = -c\left[\left(\phi_r^* - DEV_r\right) - \left(\phi_\ell^* - DEV_\ell\right)\right] \qquad (7)$$

which can be put in the form of equation (5) provided the effective average face value at any face f is defined as

$$\phi_f = \phi_f^* - DEV_f \qquad (8)$$

In this interpretation, equation (5) rewritten as

$$\phi_i^{n+1} = \phi_i^n - c\left(\phi_r - \phi_\ell\right) \qquad (9)$$

can still be considered exact for constant c, given appropriate definitions of the effective face values. In practical simulations, the face values are approximated and the form of the equation is extended to variable advecting velocity (including sign-reversals), i.e.,

$$\phi_i^{n+1} = \phi_i^n - \left(c_r\phi_r - c_\ell\phi_\ell\right) \qquad (10)$$

Transient Interpolation Modeling

One method of generating advective algorithms in the form of equation (9) is based on equation (1), which in one dimension can be written, for constant u,

$$\phi_i^{n+1} = \phi(x,\Delta t) = \phi(x-u\Delta t,0) = \phi^n(x-u\Delta t) \qquad (11)$$

where $\phi^n(x)$ can be considered to be a function of the normalized local coordinate, $\xi = (x - x_i)/\Delta x$, and given by

$$\phi^n(x) = \phi_i^n + f(\xi) \qquad (12)$$

The homogeneous spatial interpolation function f can in turn be written as

$$f(\xi) = \xi g(\xi) \qquad (13)$$

where g might be a polynomial with coefficients depending on differences (of various orders) of local node variables. For a conservative scheme, these coefficients can always be written as follows

$$g(\xi) = (A_{i+1/2} - A_{i-1/2}) + (B_{i+1/2} - B_{i-1/2})\xi + \cdots \qquad (14)$$

5

or

$$g(\xi) = h_{i+1/2}(\xi) - h_{i-1/2}(\xi) \tag{15}$$

where $h_{i-1/2}$ can be obtained from $h_{i+1/2}$ by the indicated reduction in index by 1 on all involved node variables. Then, by defining

$$\phi_r(-\xi) = h_{i+1/2}(\xi) \tag{16}$$

and

$$\phi_\ell(-\xi) = h_{i-1/2}(\xi) \tag{17}$$

Equations (11) to (17) can be combined into a form identical to equation (9)

$$\phi_i^{n+1} = \phi_i^n - c\left[\phi_r(c) - \phi_\ell(c)\right] \tag{18}$$

Note that the effective face values are in general functions of Courant number and that conservation is guaranteed by equations (16) and (17). (Extension to variable velocity parallels eq. (10), with face values being functions of their respective local Courant numbers.)

For example, for first-order upwinding, transient interpolation modeling is based on a linear function

$$f(\xi) = \xi\left(\phi_i^n - \phi_{i-1}^n\right) \quad \text{for} \quad c > 0 \tag{19}$$

$$= \xi\left(\phi_{i+1}^n - \phi_i^n\right) \quad \text{for} \quad c < 0 \tag{20}$$

Thus, for positive or negative c, ϕ_r can be written in terms of quantities centered at the right CV face

$$\phi_r(c) = \frac{1}{2}\left[\left(\phi_{i+1}^n + \phi_i^n\right) - \text{SGN}(c)\left(\phi_{i+1}^n - \phi_i^n\right)\right] = \phi_r^{(1)}, \text{ say} \tag{21}$$

and, of course, ϕ_ℓ is obtained by reducing all indexes by 1. Note that the first term in brackets is the sum of node values straddling the CV face, whereas the second term involves the difference of these values.

Similarly, the well-known Lax-Wendroff scheme (second-order central TIM) corresponds to centered quadratic spatial interpolation

6

$$f(\xi) = \xi \left[\frac{\left(\phi_{i+1}^n - \phi_{i-1}^n\right)}{2} + \frac{\left(\phi_{i+1}^n - 2\phi_i^n + \phi_{i-1}^n\right)}{2} \xi \right] \tag{22}$$

and the corresponding right face value is

$$\phi_r(c) = \frac{1}{2} \left[\left(\phi_{i+1}^n + \phi_i^n\right) - c\left(\phi_{i+1}^n - \phi_i^n\right) \right] = \phi_r^{(2)} \tag{23}$$

valid for both positive and negative c values. Comparing equations (21) and (23), it is seen that these two schemes differ by the Courant-number-dependence of the coefficient of the first-difference term. Both give exact point-to-point transfer when $c \equiv 1$: $\phi_r = \phi_i^n$, $\phi_\ell = \phi_{i-1}^n$, $\phi_i^{n+1} = \phi_{i-1}^n$; and similarly when $c \equiv -1$.

The QUICKEST scheme (third-order upwinding TIM), is based on upwind biassed cubic interpolation (ref. 9)

$$\phi_r^{(3)} = \phi_r^{(2)} - \frac{(1 - c^2)}{2 \cdot 3!} \left(2\mathscr{D}_r^2 - \text{SGN}(c) \, \delta_r^3 \right) \tag{24}$$

where $2\mathscr{D}_r^2$ is the (right-face-centered) sum of second-differences centered at i and $i+1$

$$2\mathscr{D}_r^2 = \left(\phi_{i+2}^n - 2\phi_{i+1}^n + \phi_i^n \right) + \left(\phi_{i+1}^n - 2\phi_i^n + \phi_{i-1}^n \right)$$

$$= \phi_{i+2}^n - \phi_{i+1}^n - \phi_i^n + \phi_{i-1}^n \tag{25}$$

and δ_r^3 is the difference of the above second-differences, i.e., the third-difference (centered at the right face)

$$\delta_r^3 = \phi_{i+2}^n - 3\phi_{i+1}^n + 3\phi_i^n - \phi_{i-1}^n \tag{26}$$

Note that $\left(2\mathscr{D}_r^2 - \text{SGN}(c)\delta_r^3 \right)/2$ is the upwind biassed second-difference, proportional to the upwind curvature. Conversely, for fourth-order central TIM (centered quartic interpolation), less weight is placed on δ_r^3

$$\phi_r^{(4)} = \phi_r^{(2)} - \frac{(1 - c^2)}{2 \cdot 3!} \left(2\mathscr{D}_r^2 - \frac{c}{2} \delta_r^3 \right) \tag{27}$$

7

Second-order upwinding, based on upwind shifted quadratic interpolation, has a similar form to QUICKEST, but with a different coefficient of the upwinded curvature term:

$$\phi_r^{(2U)} = \phi_r^{(2)} - \frac{(1 - |c|)}{4} \left(2\mathscr{D}_r^2 - \text{SGN}(c)\ \delta_r^3 \right) \tag{28}$$

and Fromm's method (ref. 10) is simply the average of equations (23) and (28), thereby cutting the curvature coefficient in half.

Fifth-order upwinding and sixth-order central follow a similar pattern

$$\phi_r^{(5)} = \phi_r^{(4)} + \frac{(1 - c^2)(4 - c^2)}{2 \cdot 5!} \left(2\mathscr{D}_r^4 - \text{SGN}(c)\ \delta_r^5 \right) \tag{29}$$

and

$$\phi_r^{(6)} = \phi_r^{(4)} + \frac{(1 - c^2)(4 - c^2)}{2 \cdot 5!} \left(2\mathscr{D}_r^4 - \frac{c}{3} \delta_r^5 \right) \tag{30}$$

respectively, where $2\mathscr{D}_r^4$ is the sum of fourth-differences

$$2\mathscr{D}_r^4 = \phi_{i+3}^n - 3\phi_{i+2}^n + 2\phi_{i+1}^n + 2\phi_i^n - 3\phi_{i-1}^n + \phi_{i-2}^n \tag{31}$$

and δ_r^5 is the face-centered fifth-difference

$$\delta_r^5 = \phi_{i+3}^n - 5\phi_{i+2}^n + 10\phi_{i+1}^n - 10\phi_i^n + 5\phi_{i-1}^n - \phi_{i-2}^n \tag{32}$$

Finally, seventh-order upwinding and eighth-order central are summarized by

$$\phi_r^{(7)} = \phi_r^{(6)} - \frac{(1 - c^2)(4 - c^2)(9 - c^2)}{2 \cdot 7!} \left(2\mathscr{D}_r^6 - \text{SGN}(c)\ \delta_r^7 \right) \tag{33}$$

and

$$\phi_r^{(8)} = \phi_r^{(6)} - \frac{(1 - c^2)(4 - c^2)(9 - c^2)}{2 \cdot 7!} \left(2\mathscr{D}_r^6 - \frac{c}{4} \delta_r^7 \right) \tag{34}$$

respectively, where

$$2\mathscr{D}_r^6 = \phi_{i+4}^n - 5\phi_{i+3}^n + 9\phi_{i+2}^n - 5\phi_{i+1}^n - 5\phi_i^n + 9\phi_{i-1}^n - 5\phi_{i-2}^n + \phi_{i-3}^n \tag{35}$$

and

$$\delta_r^7 = \phi_{i+4}^n - 7\phi_{i+3}^n + 21\phi_{i+2}^n - 35\phi_{i+1}^n + 35\phi_i^n - 21\phi_{i-1}^n + 7\phi_{i-2}^n - \phi_{i-3}^n \tag{36}$$

8

Note that for Nth-order central methods, the coefficient of δ_r^{N-1} is proportional to $c/(N/2)$, as compared with $SGN(c)$ for the related $(N-1)$th-order upwind scheme.

Central or upwinded polynomial TIM methods of the above forms can, of course, be continued up to arbitrarily high order via straight-forward recursion formulas, based on Binomial coefficients or Pascal's triangle. For the methods considered in this study, figure 1 shows the one-dimensional control-volume stencils involved as the order is increased. The stencils are shown for variable, possibly reversing, velocities, corresponding to equation (10), even though the test problems used in this study involve only constant velocity, positive to the right. For this reason, first-order upwinding, for example, involves the same three-point stencil as second-order central, corresponding to equations (21) and (23), respectively. QUICKEST, second-order upwinding, Fromm's method, and fourth-order central each involve a five-point stencil, when velocity reversals are allowed for. Four grid points are involved for each face, as seen from equations (25) and (26). This is the same stencil used by all (second-order) shock-capturing TVD schemes. Clearly, as the order of accuracy is increased, a wider stencil is necessitated; an Nth-order central scheme and its related $(N-1)$th-order upwind scheme require an $(N+1)$-point stencil in one dimension.

Test Problems

The following three test problems are selected on the basis of simplicity and ease of reproducibility, and are intended to represent basic characteristics of behavior that might be encountered in practice. A given numerical scheme is considered successful if it is able to simulate all three test problems to within some desired level of performance; if a scheme fails one or more of the tests, it is deemed unsatisfactory no matter how accurately it simulates any one of the other tests. Performance is judged on the basis of two basic criteria: (1) total absolute error (ABSERROR)

$$\mathscr{E} = \sum_{i=1}^{N} \left| \varepsilon_i \right| \tag{37}$$

where ε is the local error at each node

$$\varepsilon = \phi_{computed} - \phi_{exact} \qquad (38)$$

and (2) the WAVINESS or total variation of error

$$\mathcal{W} = \sum_{i=1}^{N} \left| \varepsilon_{i+1} - \varepsilon_i \right| \qquad (39)$$

In addition, it is usually desirable to monitor monotonicity; i.e., does an initially monotonic profile remain so? In fact, strict monotonicity maintenance is a basic (in fact the only) constraint determining the nature of the universal limiter to be developed here.

The first test profile follows that used by Sweby (ref. 11), an isolated sine-squared wave of width $20\Delta x$

$$\phi(t=0) = \sin^2\left(\frac{\pi x}{20\Delta x}\right) \quad \text{for} \quad 0 \leq x \leq 20\Delta x$$

$$= 0 \quad \text{otherwise} \qquad (40)$$

This function represents a relatively smooth profile with a continuously turning gradient and a single local maximum. In order to simulate practical situations, it is important to run the test problems over the same prescribed distance in all cases, irrespective of time-step (Courant number) or initial profile shape. In the tests described here, for example, the exact solutions advance by 45 mesh-widths. Two Courant numbers are used: $c = 0.05$ (900 time steps), representing "small" Δt; and a "moderate" value of $c = 0.5$ (90 time steps). The 25-time-step simulation used by Sweby was not long enough to see significant differences between the methods studied, or to allow their gross deficiencies to develop (which are typically worse at small Courant numbers, for a fixed distance).

The second test profile is a unit step change in ϕ over one mesh width. Initially, $\phi = 0$ everywhere to the right of a specified jump point; all other points, including the upstream boundary, are set at 1.0. The unit step profile

is more fundamental than the isolated "square-wave," or box, used in some previous studies (e.g., Sweby used an isolated rectangular box of width 20Δx in addition to the isolated sine-squared function of the same width). The box profile, at best, merely gives twice as much information as the unit step; but for highly oscillatory methods, oscillations excited by the step-up interfere with those due to the step-down, and the resulting complex wave-pattern is not as enlightening as that of the simple step simulation. The unit step is also a basic test of monotonicity, a fundamental aspect of advective modeling. A "good" step simulation is one which monotonically resolves the step in a "small" number of mesh widths - the smaller the (monotonic) "numerical width," the better the method (for this test!).

The third test profile follows one used by Steven Zalesak (ref. 12) that he attributes to B.E. McDonald. It consists of a semi-ellipse of width $2i_w\Delta x$, initially centered at i_c,

$$\phi_i(t=0) = \sqrt{1 - (i - i_c)^2/i_w^2} \quad \text{if} \quad |i - i_c| < i_w$$

$$= 0 \quad \text{otherwise} \tag{41}$$

This is a rigorous test in that an initial (leading) step change in gradient is followed by a region of continuously changing gradient and finally by a trailing step. Methods which are oscillation-free in the simple step simulation may generate significant waviness just behind the leading step or just ahead of the trailing step. The test used here differs slightly from that used by Zalesak in being 20Δx wide to conform to Sweby's sine-squared profile, rather than 30Δx; this does not have any significant qualitative effect on results.

Figure 2 shows the three initial profiles and the grid used for all tests. For reference, the leading-edge of each profile is positioned at the same location; the initial value is 0 for $i \geq 23$ in each case, and nonzero for smaller values. Grid-points 1 and 2 are used for boundary-condition treatment. Numerical boundary conditions are very simple: $\phi_\ell \equiv 1$ for the step profile and $\phi_\ell \equiv 0$ for the other two tests. Higher order methods (above fourth) require the designation of pseudonode values conforming to the above pattern. In all cases, computation begins with grid-point 1. To normalize the x-domain to order unity, Δx is taken as 1/100; but this is irrelevant to the computation,

since the only parameter is the Courant number c. As mentioned, all tests are run so that the exact solution would translate a fixed distance, taken to be 45Δx. Thus, the total number of update steps, N_t, is related to the Courant number by

$$c = \frac{45}{N_t} \tag{42}$$

Results for Polynomial TIM Methods

Figures 3 to 12 show the results of simulating pure advection of the three test profiles for first-order upwinding, the Lax-Wendroff scheme, second-order upwinding, Fromm's method, QUICKEST, fourth-order central, fifth-order upwinding, sixth-order central, seventh-order upwinding, and eighth-order central, respectively. Each case is run at both a representative small Courant number (c = 0.05, N_t = 900) and a moderate Courant number (c = 0.5, N_t = 90). First-order upwinding is the only polynomial method which gives monotonic step resolution; but the width of the resolution is poor and the other profiles show the well-known effects of this method's inherently large global artificial numerical diffusion, which is worse at smaller Courant numbers, as seen in figure 3. The Lax-Wendroff method (fig. 4) generates trailing oscillations (phase-lag dispersion) typical of central-difference methods; in these cases, phase lag is worse at smaller Courant numbers (compare figs. 4, 8, 10, and 12). Second-order upwinding gives rise to leading oscillations, as seen in figure 5. It was this observation that led to the idea of averaging the Lax-Wendroff method with second-order upwinding in an effort to cancel phase-lead and phase-lag, at least in some "average" sense (ref. 10). Fromm's zero-average-phase-error method indeed shows marked improvement (fig. 6), with much less sensitivity to Courant number, as seen. Fromm's method actually cancels the leading dispersion term in the truncation error only at c = 0.5; in this case it is identical to third-order upwinding (QUICKEST), as seen in the second half of figure 7. QUICKEST gives markedly better performance at other Courant numbers, but the two methods are qualitatively very similar. Note that the smooth (sine-squared) function is particularly well modeled. Fourth-order central is again highly oscillatory, with large ABSERROR and WAVINESS for each profile, as seen in figure 8. The fact that fourth-order central methods are substantially

12

inferior to third-order upwinding is apparently not well known, and one continues to hear of researchers who switch to central fourth-order schemes after experiencing "difficulties" with second-order.

With fifth-order upwinding (fig. 9), one begins to see a trend which continues to higher order: simulation of the smooth profile is excellent; as order increases, the step rise is steeper but the odd-order overshoots are larger and the even-order methods continue to be highly oscillatory, albeit with shorter wavelength; with the even-order central methods, significant waviness develops in the semi-ellipse simulation just behind the initial jump in gradient. These trends are seen by scanning across figures 7 to 12. Finally, note that central (necessarily even-order) methods are much more sensitive to Courant number. This is because the highest order term in the face-value expression is proportional to c rather than $SGN(c)$; compare equations (23), (27), (30), and (34) with (21), (24), (29), and (33), respectively. All the methods considered here give exact point-to-point transfer at $c \equiv 1$, as seen from the formulas for ϕ_r; i.e., $\phi_r = \phi_i^n$, $\phi_\ell = \phi_{i-1}^n$, and $\phi_i^{n+1} = \phi_{i-1}^n$. For the higher order methods, point-to-point transfer also occurs (over more than one mesh width) for larger integer values of c; however, in the absence of modeled physical diffusion, these methods are not all stable over a continuous range, except for $0 \leq c \leq 1$.

NORMALIZED VARIABLE DIAGRAM

Normalized Variables

Figure 13 shows a one-dimensional control-volume with attention focussed on one face (in this case, the left). In determining the effective face value, ϕ_f, the most influential nodes are the two straddling the face and the next upstream node, the latter depending of course on the flow direction at the face in question, i.e., the sign of u_f. These three node values can be labeled ϕ_D (downstream), ϕ_U (upstream), and ϕ_C (central), as shown. Note the difference in definition of these nodes, depending on $SGN(u_f)$. In terms of original variables, there are clearly a very large number of cases to consider: combinations of positive or negative u_f, positive or negative ϕ, and positive or

negative values of gradient and curvature. Variations in sign, flow direction, and scale can be normalized out by defining the normalized variable (at any point) as

$$\tilde{\phi} = \frac{\phi - \phi_U^n}{\phi_D^n - \phi_U^n} \qquad (43)$$

Now, in a case when ϕ_f is a function of ϕ_D^n, ϕ_C^n, ϕ_U^n, and Courant number, the normalized face value is only a function of its adjacent normalized upstream node value and c

$$\tilde{\phi}_f = f\left(\tilde{\phi}_C^n, c\right) \qquad (44)$$

since the other normalized node values are constant:

$$\tilde{\phi}_U^n = 0 \quad \text{and} \quad \tilde{\phi}_D^n = 1 \qquad (45)$$

Equation (44) includes first-order methods, second-order central and upwind schemes, and third-order upwinding, in addition to second-order (and third-order) shock-capturing algorithms. Higher order methods involve more distant nodes but the normalized $\tilde{\phi}_f$ will still depend most strongly on $\tilde{\phi}_C^n$.

Second-Order Time Averaging

In general, for transient-interpolation-modeling methods based on equation (11), the time accuracy of the resulting control-volume algorithm (eq. (18)), is the same order as the degree of the spatial interpolation used in equation (12). Many advection schemes in common use (including TVD schemes) are based on second-order time averaging, which can be made explicit by straight-forward integration. Specifically, for spatially second-order-accurate methods, the deviation term in equation (4) is formally neglected; thus, from equation (8), the effective face values are just the estimated time averages. If these time averages are based on locally advected face-value linear behavior spatially, the method is second-order accurate in time, as well. For example if $\hat{\phi}_f$ is the instantaneous face value, the time-averaged face value over Δt is

$$\phi_f \approx \phi_f^* = \frac{1}{\Delta t} \int_0^{\Delta t} \hat{\phi}_f(\tau) \, d\tau = \phi_f^n - \frac{u\Delta t}{2} \left(\frac{\partial \phi}{\partial x}\right)_f^n \qquad (46)$$

where ϕ_f^n is the estimated face value at time-level n. In most cases, the spatial gradient is estimated as

$$\left(\frac{\partial \phi}{\partial x}\right)_f^n = \frac{\left(\phi_f^n - \phi_C^n\right)}{\Delta x / 2} \qquad (47)$$

so that

$$\phi_f = \phi_f^n - c\left(\phi_f^n - \phi_C^n\right) \qquad (48)$$

or, in terms of normalized variables,

$$\tilde{\phi}_f = (1 - c)\tilde{\phi}_f^n + c\tilde{\phi}_C^n \qquad (49)$$

where, now, the linear Courant number weighting is explicit and $\tilde{\phi}_f^n$ depends only on $\tilde{\phi}_C^n$

$$\tilde{\phi}_f^n = fn\left(\tilde{\phi}_C^n\right) \qquad (50)$$

Figure 14 shows the normalized variable diagram (NVD), plotting characteristics of the form of equation (50), for

(1) First-order upwinding (1U):

$$\tilde{\phi}_f^n = \tilde{\phi}_C^n \qquad (51)$$

(2) The Lax-Wendroff method (2C):

$$\tilde{\phi}_f^n = \frac{1}{2}\left(1 + \tilde{\phi}_C^n\right) \qquad (52)$$

(3) Second-order upwinding (2U):

$$\tilde{\phi}_f^n = \frac{3}{2}\,\tilde{\phi}_C^n \qquad (53)$$

and

(4) Fromm's method (2F):

$$\tilde{\phi}_f^n = \frac{1}{4} + \tilde{\phi}_C^n \tag{54}$$

Note that the latter three spatially second-order methods all pass through the point (0.5, 0.75); in fact, any method whose $\tilde{\phi}_f^n\left(\tilde{\phi}_C^n\right)$ characteristic passes through this point with a finite slope is (at least) second-order accurate in space, since $\tilde{\phi}_f^n$ can then be written

$$\tilde{\phi}_f^n = \frac{1}{2}\left(1 + \tilde{\phi}_C^n\right) - CF\left(1 - 2\tilde{\phi}_C^n\right) \tag{55}$$

where the curvature factor CF is a constant or, in the case of nonlinear schemes, a function of $\tilde{\phi}_C^n$. This is more apparent in terms of unnormalized variables

$$\phi_f^n = \frac{1}{2}\left(\phi_D^n + \phi_C^n\right) - CF\left(\phi_D^n - 2\phi_C^n + \phi_U^n\right) \tag{56}$$

or

$$\phi_f^n = \frac{1}{2}\left(\phi_D^n + \phi_C^n\right) - CF\left(\frac{\partial^2\phi}{\partial x^2}\right)_f^n \Delta x^2 + \ldots \tag{57}$$

thus, deviating from the second-order-accurate linear interpolation by second or higher order terms, provided CF is finite. Note that first-order upwinding, equation (51), and

(5) First-order downwinding (1D):

$$\tilde{\phi}_f^n = 1 \tag{58}$$

cannot be written in the form of equation (55) for finite CF.

The characteristics shown in figure 14 are in the form of equation (50), i.e., the estimated face value at time-level n as a function of $\tilde{\phi}_C^n$. It is also important to portray the time-averaged face value in the same way, $\tilde{\phi}_f$ (no superscript), according to the linear weighting, equation (49). Figures 15 to 17 show the NVDs corresponding to $\tilde{\phi}_f\left(\tilde{\phi}_C^n, c\right)$ for the Lax-Wendroff, second-order upwinding and Fromm methods, respectively. The characteristics are shown for five different values of Courant number: $c \rightarrow 0$, $c = 1/4$, $1/2$, $3/4$, and 1. The zero-value is distinguished by a dashed line, since this can only be

approached in an explicit calculation. Note that all these methods revert to $\tilde{\phi}_f = \tilde{\phi}_C^n$ when $c = 1$, as seen from equation (49), giving exact point-to-point transfer as discussed previously.

Nonlinear "Shock-Capturing" Schemes

For lack of better categorizing terminology, a number of currently popular algorithms have become known as "shock-capturing" schemes. When applied to the pure advection problems studied here, these second-order methods (in space and time) can be portrayed either in the $\tilde{\phi}_f^n$ NVD or in the $\tilde{\phi}_f$ NVD, corresponding to equations (50) or (49), respectively. However, in contrast to the linear characteristics of figure 14 (or of figs. 15 to 17), these methods are distinguished by nonlinear characteristics, although they remain linear in c according to equation (49). All schemes revert to first-order upwinding outside the monotonic range, i.e., for $\tilde{\phi}_C^n < 0$ or $\tilde{\phi}_C^n > 1$. They all pass through the origin (0,0) and the point (1,1) in either NVD. For the $\tilde{\phi}_f^n$ NVD, they all pass through (0.5, 0.75), as required for second-order methods.

Figure 18 shows the so-called minimum-modulus (Minmod) method (ref. 13) which is seen to follow second-order upwinding for $0 \leq \tilde{\phi}_C^n \leq 0.5$ and Lax-Wendroff for $0.5 \leq \tilde{\phi}_C^n < 1$. Part (a) of the figure shows $\tilde{\phi}_f^n$ as a function of $\tilde{\phi}_C^n$, whereas part (b) shows $\tilde{\phi}_f$ as the c-weighted average between $\tilde{\phi}_f^n$ and $\tilde{\phi}_C^n$, equation (49), again for discrete values of c. A related method used by Chakravarthy and Osher (ref. 14) consists of second-order upwinding combined with first-order downwinding at time-level n. This is shown in figure 19. The MUSCL scheme of van Leer (ref. 5) is shown in figure 20; it consists of Fromm's method in the "smooth" (small curvature) region near $\tilde{\phi}_C^n \to 0.5$, with piecewise linear deviations to pass through (0,0) and (1,1). In terms of $\tilde{\phi}_f^n$, the prescription for this method is

(1) A sufficient (although not necessary) "monotonic" limiter:

$$\tilde{\phi}_f^n = 2\tilde{\phi}_C^n \qquad \text{for} \qquad 0 \leq \tilde{\phi}_C^n \leq \frac{1}{4} \tag{59}$$

(2) Fromm's method in "smooth" regions:

$$\tilde{\phi}_f^n = \frac{1}{4} + \tilde{\phi}_C^n \qquad \text{for} \qquad \frac{1}{4} \leq \tilde{\phi}_C^n \leq \frac{3}{4} \tag{60}$$

17

and

(3) First-order downwinding:

$$\tilde{\phi}_f^n = 1 \qquad \text{for} \qquad \frac{3}{4} \leq \tilde{\phi}_C^n \leq 1 \qquad\qquad (61)$$

with first-order upwinding elsewhere, as usual. Another scheme due to van Leer (ref. 2) can be described by replacing the piecewise linear characteristic of MUSCL with a curved line (a parabola) for $\tilde{\phi}_f^n$ in the monotonic range; this has the same slope as MUSCL for $\tilde{\phi}_f^n = 0_+$ and 1_-, as seen in figure 21. For convenience, this scheme will be referred to as van Leer's "curved-line advection method" (CLAM); in the Sweby diagram (see appendix) the characteristic forms portion of a hyperbola, thus the scheme is sometimes referred to as van Leer's "harmonic" advection method. A scheme developed by Roe (ref. 6), nicknamed "Superbee," is shown in figure 22. Again piecewise linear, the $\tilde{\phi}_f^n$ characteristic (as $\tilde{\phi}_C^n$ increases from 0) consists of a portion of slope 2, a portion of slope 1/2 (following Lax-Wendroff), a portion of slope 3/2 (second-order upwinding), and a portion of zero slope (first-order downwinding). This is considered to be one of the most "compressive" of the second-order schemes with respect to its narrow step resolution, as will be seen. This idea can be taken to extremes, however; another formally second-order scheme, which might aptly be called "Super-C" (for "compressive") is shown in figure 23(a); and an extremely "compressive" limited first-order downwinding scheme, "Hyper-C," is shown in figure 23(b). Note that both of these figures involve the time-averaged normalized face value, $\tilde{\phi}_f$. The Super-C scheme requires $\tilde{\phi}_f$ to be the smaller of the upper universal limiter boundary (developed in the next section) and Lax-Wendroff, i.e., the smaller of

$$\tilde{\phi}_f = \frac{\tilde{\phi}_C^n}{c} \qquad \text{and} \qquad \tilde{\phi}_f = \frac{1}{2}(1 - c) + \frac{1}{2}(1 + c)\tilde{\phi}_C^n \qquad\qquad (62)$$

for $0 \leq \tilde{\phi}_C^n \leq 1/2$; with limited second-order upwinding, i.e., the smaller of

$$\tilde{\phi}_f = 1 \qquad \text{and} \qquad \tilde{\phi}_f = \frac{1}{2}(3 - c)\tilde{\phi}_C^n \qquad\qquad (63)$$

for $1/2 < \tilde{\phi}_C^n \leq 1$, with first-order upwinding elsewhere. Hyper-C (limited first-order downwinding) simply requires $\tilde{\phi}_f$ to be the smaller of

18

$$\frac{\tilde{\phi}_C^n}{c} \quad \text{and} \quad 1 \tag{64}$$

in the monotonic regime, with $\tilde{\phi}_f = \tilde{\phi}_C^n$ elsewhere, as usual. Finally, note that the Courant-number-dependence of Super-C and Hyper-C is no longer linear.

Results for the Nonlinear Schemes

Figures 24 through 30 show the results of simulating the three test problems with each of the nonlinear schemes just described; again, the two representative Courant numbers (0.05 and 0.5) are used. As seen in figure 24, although Minmod resolves the step monotonically, the structure is not at all sharp and the other profiles are rather diffusive, especially at smaller Courant numbers. In the Chakravarthy-Osher simulations, shown in figure 25, the leading-edge steepening effects of the first-order downwinding are seen, with concomitant clipping due to first-order upwinding; again, profiles are more diffusive at small c values. The two van Leer schemes, MUSCL and CLAM (figs. 26 and 27), give similar results to each other, as perhaps expected from the qualitative similarity of their NVDs (figs. 20 and 21). The MUSCL scheme in particular is one of the more successful of the well-known second-order non-linear schemes, considering overall performance for all three test problems. Once again, both MUSCL and CLAM deteriorate at small Courant-number values, due primarily to the unnecessarily restrictive TVD limiter, equation (59).

Superbee (fig. 28) gives significantly sharper results for the step simu-lation at all c values. The smooth-function (sine-squared) simulation is slightly better than that of MUSCL; however, there is a degree of artificial steepening inherent in this method, as seen in the semi-ellipse computation. In the presence of rapid changes in gradient (large curvature) - near the leading and trailing edges of the profile - the scheme has a tendency to con-vert all gentle slopes into sharp steps followed by plateaus. This defect is purposely taken to extremes with Super-C (fig. 29) and Hyper-C (fig. 30). Clearly, in terms of step performance, Super-C supersedes Superbee and Hyper-C supersedes Super-C. Super-C also does an excellent job of simulating the sine-squared profile; however, the semi-ellipse results are rather bizarre, showing stair-casing for small c values and gross artificial steepening at

c = 0.5. Although Hyper-C gives virtually exact step simulation at all c
values, the other profiles are totally corrupted. These schemes were included
to show the futility of designing a method on the basis of a single criterion
(in this case, sharp monotonic resolution of steps); consequently the almost
incredible step simulation of these artificial-compression methods should not
be used as a standard for judging the overall performance of truly robust
schemes.

In order to show the effect of Courant number over a wider range, fig-
ure 31 gives a log-log plot of ABSERROR for the sine-squared profile (lower
curves) and the semi-ellipse (upper curves) versus ABSERROR for the step simu-
lation for Minmod, MUSCL, Superbee, and Super-C, with Courant number as a
parameter ranging from 0.01 to 0.978, with points shown at values of 0.1, 0.5,
and 0.9 on each curve. At very small c values, Minmod produces large errors
for all test profiles. The other schemes' semi-ellipse errors are comparable,
with step errors decreasing in the order: MUSCL, Superbee, Super-C. The sine-
squared error follows the same order. Superbee and, in particular, Super-C,
show much less sensitivity to Courant number than the other schemes. Although
all methods' trajectories in this plane approach the origin (exact point-to-
point transfer) as $c \rightarrow 1$, the tendency is rather slow, and even at c = 0.9,
the sine-squared error in particular is unacceptably large, compared with what
can be achieved with higher order methods.

THE UNIVERSAL LIMITER

The normalized-variable plane, with $\tilde{\phi}_C^n$ as abscissa and $\tilde{\phi}_f$ (no super-
scrip) as ordinate, can be used to construct a very simple diagram representing
constraints on the effective time-averaged normalized face value so as to guar-
antee maintenance of monotonic profiles, thereby suppressing extraneous over-
shoots or nonmonotonic oscillations, but allowing arbitrarily high resolution
depending on the formal order of accuracy (in both space and time) of the base
method. As seen in the previous section, nonlinear second-order schemes (lin-
ear in c) can be represented by a single curve in the $\left(\tilde{\phi}_C^n , \tilde{\phi}_f \right)$ plane for any
fixed value of the Courant number. This is true for the nonlinear third-order
scheme as well (to be described), but the Courant-number dependence is then
also nonlinear, as will be seen. All the nonlinear second-order schemes

(except Super-C) satisfy Sweby's sufficient TVD criteria (ref. 10) (translated into present notation)

$$\tilde{\phi}_f = \tilde{\phi}_f^n = \tilde{\phi}_C^n \quad \text{for} \quad \tilde{\phi}_C^n \leq 0 \quad \text{and} \quad \tilde{\phi}_C^n \geq 1 \tag{65}$$

and

$$\tilde{\phi}_C^n \leq \tilde{\phi}_f^n \leq \min\left[2\tilde{\phi}_C^n, 1\right] \quad \text{for} \quad 0 \leq \tilde{\phi}_C^n \leq 1 \tag{66}$$

In particular, all nonlinear characteristics pass through (0,0) and (1,1). These criteria are in terms of $\tilde{\phi}_f^n$; they are thus limited to temporally second-order schemes linear in c, according to equation (49).

To allow higher order accuracy, it is extremely important to work directly with the effective time-averaged normalized face value $\tilde{\phi}_f$, rather than $\tilde{\phi}_f^n$. By imposing simple monotonicity-maintenance criteria, much less restrictive constraints - the universal limiter - are placed on the allowable face values. The computational strategy is then, in principle, as follows: (1) formulate ϕ_f by some desired high-order method; (2) compute the actual normalized $\tilde{\phi}_C^n$ value and the intended normalized $\tilde{\phi}_f$ value, (3) if $\tilde{\phi}_f$ falls within the allowable universal limiter range, simply proceed; (4) if $\tilde{\phi}_f$ lies outside this range, reset (limit) its value to that of the nearest constraint boundary at the given $\tilde{\phi}_C^n$ value; (5) reconstruct the new ϕ_f from $\tilde{\phi}_f$; (6) repeat the procedure for all other faces; (7) update according to equation (10). In actual practice, it is less expensive computationally to carry out this strategy directly in terms of unnormalized variables, as will be described in detail.

Monotonicity-Maintenance Criteria

Figure 32 shows normalized node values with $\tilde{\phi}_C^n$ in the monotonic range, $0 \leq \tilde{\phi}_C^n \leq 1$. As suggested by the cross-hatching, monotonic behavior requires necessary conditions on $\tilde{\phi}_f$:

$$\tilde{\phi}_C^n \leq \tilde{\phi}_f \leq 1 \tag{67}$$

and on the corresponding face value of the adjacent upstream CV face, $\tilde{\phi}_u$:

$$0 \leq \tilde{\phi}_u \leq \tilde{\phi}_C^n \tag{68}$$

Consider equation (9), written for $\tilde{\phi}_C^n$ in normalized variables

$$\tilde{\phi}_C^{n+1} = \tilde{\phi}_C^n - c\left(\tilde{\phi}_f - \tilde{\phi}_u\right) \tag{69}$$

In order to maintain monotonicity, the new $\tilde{\phi}_C$ value must be constrained by

$$\tilde{\phi}_U^{n+1} \leq \tilde{\phi}_C^{n+1} \leq \tilde{\phi}_D^{n+1} \tag{70}$$

For pure advection at constant velocity, the right-hand inequality is less restrictive than $\tilde{\phi}_f \geq \tilde{\phi}_C^n$, but the left-hand inequality results in

$$\tilde{\phi}_f \leq \tilde{\phi}_u + \frac{1}{c}\left(\tilde{\phi}_C^n - \tilde{\phi}_U^{n+1}\right) \tag{71}$$

And since $\tilde{\phi}_u$ is nonnegative and $\tilde{\phi}_U^{n+1}$ nonpositive, the worst-case condition is given by $\tilde{\phi}_u = 0$ and $\tilde{\phi}_U^{n+1} = 0$, i.e.,

$$\tilde{\phi}_f \leq \frac{\tilde{\phi}_C^n}{c} \quad \text{for} \quad 0 < \tilde{\phi}_C^n \leq 1 \tag{72}$$

This, combined with inequality (67)

$$\tilde{\phi}_C^n \leq \tilde{\phi}_f \leq 1 \quad \text{for} \quad 0 \leq \tilde{\phi}_C^n \leq 1 \tag{73}$$

constitutes the universal limiter in the monotonic range of $\tilde{\phi}_C^n$. For $\tilde{\phi}_C^n < 0$ or > 1, numerical experimentation has shown that the simple condition

$$\tilde{\phi}_f = \tilde{\phi}_C^n \quad \text{for} \quad \tilde{\phi}_C^n < 0 \quad \text{or} \quad \tilde{\phi}_C^n > 1 \tag{74}$$

gives the most satisfactory overall performance; this, of course, is equivalent to first-order upwinding as used by other nonlinear (second-order) TVD schemes. It does not erode the accuracy of the overall scheme, which is determined solely by behavior in the smooth region, near $\tilde{\phi}_C^n \rightarrow 0.5$.

The universal limiter, equation (74) together with inequalities (72) and (73), is shown in diagrammatic form in figure 33; the Courant-number-dependent boundary, $\tilde{\phi}_f = \tilde{\phi}_C^n/c$, is shown dashed to stress the fact that its slope changes with different values of c. Note that for $c \rightarrow 0$, this boundary approaches the vertical axis; while for $c = 1$, it degenerates into $\tilde{\phi}_f \equiv \tilde{\phi}_C^n$

22

(everywhere), corresponding to exact point-to-point transfer as usual. For reference to previous work, the corresponding criteria in terms of Sweby's variables, r and φ, are given in the appendix.

For clarity, the precise steps in applying the universal limiter to transient interpolation modeling of the advective transport equations are given, as follows, using normalized variables.

<u>ULTIMATE strategy (normalized variables)</u>:

(1) Designate upstream (U), downstream (D), and central (C) nodes on the basis of $SGN(u_f)$ for each face in turn.

(2) Compute $DEL = \phi_D^n - \phi_U^n$; if $|DEL| < 10^{-5}$ (say), set $\phi_f = \phi_C^n$ and proceed to the next face.

(3) Otherwise, compute $\tilde{\phi}_C^n = \left(\phi_C^n - \phi_U^n\right)\!\Big/ DEL$; if this is less than 0 or greater than 1, again set $\phi_f = \phi_C^n$ and proceed.

(4) If not, compute $\tilde{\phi}_f = \left(\phi_f - \phi_U^n\right)\!\Big/ DEL$, where ϕ_f is based on a desired high-order TIM method.

(5) If $\tilde{\phi}_f < \tilde{\phi}_C^n$, reset (the lower limit) $\tilde{\phi}_f = \tilde{\phi}_C^n$; if $\tilde{\phi}_f > \tilde{\phi}_C^n/c$, reset (the upper limit) $\tilde{\phi}_f = \tilde{\phi}_C^n/c$; if $\tilde{\phi}_f > 1$, reset (the absolute upper limit) $\tilde{\phi}_f = 1$.

(6) Reconstruct $\phi_f = \tilde{\phi}_f \cdot DEL + \phi_U^n$ (this is the face value used in the update algorithm).

(7) After finding all face values in this way, explicitly update according to equation (10).

In order to avoid divisions and multiplications involved in constructing normalized variables and reconstructing the unnormalized variables, it is better to work directly with the unnormalized variables.

ULTIMATE strategy (unnormalized variables):

(1) Designate upstream (U), downstream (D), and central (C) nodes on the basis of $SGN(u_f)$ for each face in turn, and compute $DEL = \phi_D^n - \phi_U^n$ and $ADEL = |DEL|$ for each face.

(2) Compute $ACURV = \left| \phi_D^n - 2\phi_C^n + \phi_U^n \right|$ for each face; if $ACURV \geq ADEL$ (nonmonotonic), set $\phi_f = \phi_C^n$ and proceed to the next face.

(3) Compute the reference face value $\phi_{REF} = \phi_U^n + \left(\phi_C^n - \phi_U^n \right) \Big/ c$ for each face.

(4) Set up some desired high order face value ϕ_f .

(5) If $DEL > 0$, limit ϕ_f by ϕ_C^n below and the smaller of ϕ_{REF} and ϕ_D^n above.

(6) If $DEL < 0$, limit ϕ_f by ϕ_C^n above and the larger of ϕ_{REF} and ϕ_D^n below.

(7) Update according to equation (10).

In order to get some feeling for the ULTIMATE strategy, figures 34 to 37 show normalized variable diagrams, $\tilde{\phi}_f = f\left(\tilde{\phi}_C^n , c \right)$ for the universal limiter applied to Lax-Wendroff, second-order upwinding, Fromm's method, and the third-order QUICKEST scheme, respectively. Note similarities (and differences) between figures 35 and 19(b), and between figures 36 and 20(b). Also note qualitative similarities between the limited versions of Fromm's method and QUICKEST (figs. 36 and 37) respectively; they are identical at $c = 0.5$ (as well as at $c = 1$, of course).

Results for the ULTIMATE Schemes

Figures 38 to 46 show the results for the three standard test problems obtained by applying the universal limiter to the Lax-Wendroff scheme, second-order upwinding, Fromm's method, QUICKEST, fourth-order central, fifth-order upwinding, sixth-order central, seventh-order upwinding, and eighth-order

central, respectively, each for the two Courant numbers c = 0.05 and 0.5.
Note the inadequacies of the limited Lax-Wendroff scheme (fig. 38) and limited
second-order upwinding (fig. 39) similar in some respects to the nonlinear
shock-capturing schemes. Especially note the poor performance at the smaller
c value; the reversed asymmetry of the profiles corresponds to the respective
asymmetry of these two methods' NVDs (figs. 34 and 35).

The limited Fromm method (fig. 40) is clearly an improvement over the
simple second-order schemes, and has qualitatively similar performance to
limited QUICKEST, as expected from the similarity of their NVDs (figs. 36
and 37). The limited QUICKEST scheme (fig. 41) gives results which are
probably entirely adequate for most practical situations. The sine-function
error, in particular, is now within tolerable bounds. Although the limited
fourth-order method (fig. 42) gives lower ABSERROR for each profile, there is
a clearly discernible increase in WAVINESS in the semi-ellipse simulation,
especially at small Courant number values; this is a typical shortcoming of
even-order methods. Overall, the limited-QUICKEST scheme seems to be the best
of the schemes using the five-point stencil of figure 1; it is certainly far
superior to any of the second-order shock-capturing schemes (which involve the
same stencil). The artificial waviness of the limited fourth-order method
(which also uses this stencil) detracts from an otherwise excellent
performance.

If better step resolution is required, the limited fifth-order upwinding
scheme (fig. 43) gives highly satisfactory results, although of course this
requires a seven-point stencil in general (allowing for velocity reversals).
The limited sixth-order central method (which uses the same seven-point sten-
cil), figure 44, gives slightly better step resolution, but worse performance
for the semi-ellipse (in terms of both ABSERROR and WAVINESS) and a slightly
higher ABSERROR in the sine-squared simulation at smaller Courant numbers (due
to slight asymmetric clipping, typical of even-order methods).

The higher order schemes follow a predictable pattern, with better step
resolution, and essentially exact smooth-function simulation, but with annoy-
ing waviness in the challenging semi-ellipse problem - now even noticeable in
the upwind schemes, but still much worse with the even-order central methods,

especially at small c values. Clearly, the ULTIMATE strategy could be continued to arbitrarily high order, either with polynomial TIM schemes of the type considered here or with alternate forms of interpolation such as splines, for example. The only stipulation is that the base method must be explicit in determining the intended ϕ_f - step (4) of the ULTIMATE strategy.

Once again, to see the effect of Courant number over the complete stable range, figure 47 shows ABSERROR of the sine-squared and semi-ellipse profiles plotted on a log-log scale against ABSERROR of the step for the ULTIMATE Fromm, QUICKEST, fifth- and seventh-order upwind schemes, with Courant number as a parameter ranging from 0.01 to 0.978, with points shown at c = 0.1, 0.5, and 0.9 on each curve. For clarity, the ULTIMATE even-order schemes have been omitted. The limited version of Fromm's method is perhaps of academic interest (being slightly better than MUSCL in the region near c = 0.5); but since the limited QUICKEST third-order upwind scheme requires the same stencil and essentially the same number and type of computations, it is clearly a more attractive method. Figure 47 should be compared with figure 31 giving the corresponding results for second-order shock-capturing methods. The obvious global characteristic for the higher-order ULTIMATE schemes is their much lower error for the smooth-function simulation, due to their lack of artificial steepening and concomitant clipping. As expected, step-simulation error decreases monotonically with the order of the underlying base method. The semi-ellipse and step errors of the higher order ULTIMATE schemes are strongly correlated, whereas for the second-order artificial compression methods of figure 31, the semi-ellipse error is roughly the same for each scheme, again reflecting the artificial steepening and clipping of these methods.

Simplified ULTIMATE QUICKEST Strategy

Referring to figure 37, it is seen that in the range

$$0.2 \leq \tilde{\phi}_C^n \leq 0.8 \tag{75}$$

the ULTIMATE QUICKEST scheme is in fact identical to the unconstrained QUICKEST scheme. Thus, considerable simplification can be made in the algorithm without any approximation or effect on results. Inequality (75) can be rewritten as

$$|\tilde{\phi}_C^n - 0.5| \leq 0.3 \tag{76}$$

or, multiplying by 2,

$$|1 - 2\tilde{\phi}_C^n| \leq 0.6 \tag{77}$$

Rewriting in terms of unnormalized variables results in

$$|CURV| \leq 0.6 \ |DEL| \tag{78}$$

where CURV is the upwind-biased second-difference

$$CURV = \phi_D^n - 2\phi_C^n + \phi_U^n \tag{79}$$

and DEL is the normalization difference

$$DEL = \phi_D^n - \phi_U^n \tag{80}$$

Thus, if inequality (78) is satisfied, the unconstrained QUICKEST scheme can be used directly, with no need for testing of universal-limiter constraints. In any practical flow, this criterion will be satisfied in the overwhelming bulk of the flow domain, being violated (if at all) only at a small fraction of grid points near where sharp changes in gradient occur.

Of course, if

$$\tilde{\phi}_C^n \leq 0 \quad \text{or} \quad \tilde{\phi}_C^n \geq 1 \tag{81}$$

all ULTIMATE schemes (of any order) will use (in terms of unnormalized variables)

$$\phi_f = \phi_C^n \tag{82}$$

Inequalities (81) are equivalent to

$$|\tilde{\phi}_C^n - 0.5| \geq 0.5 \tag{83}$$

or, equivalently

$$|CURV| \geq |DEL| \tag{84}$$

Thus, the simplified ULTIMATE QUICKEST strategy is as follows:

(1) Designate "D," "C," and "U" nodes based on $SGN(u_f)$ in the usual way, for each face.

(2) Compute $|DEL|$ and $|CURV|$.

(3) If inequality (78) is satisfied, use the unconstrained and unnormalized QUICKEST face value,

$$\phi_f = \frac{1}{2}\left(\phi_D^n + \phi_C^n\right) - \frac{|c|}{2}\left(\phi_D^n - \phi_C^n\right) - \frac{1}{6}\left(1 - c^2\right)CURV \qquad (85)$$

(4) Otherwise, if inequality (84) is satisfied, use equation (82).

(5) Otherwise, compute the limited QUICKEST face value according to the (unnormalized) ULTIMATE strategy.

(6) Proceed to the next CV face.

(7) Update in the usual way.

Note that step (5) occurs only in the small ranges

$$0 < \tilde{\phi}_C^n < 0.2 \quad \text{or} \quad 0.8 < \tilde{\phi}_C^n < 1 \qquad (86)$$

Cost-Effective High-Resolution Hybrid Scheme

The ULTIMATE QUICKEST scheme is a simple, robust algorithm using the same stencil as second-order shock-capturing schemes but with much better global accuracy. If higher resolution of near-discontinuities is deemed necessary, it is clearly possible to use higher order (upwind) schemes globally. However, since the need for higher resolution occurs only in small localized regions, a cost-effective strategy is to use the efficient simplified ULTIMATE QUICKEST scheme as a base method, automatically switching to a higher resolution ULTIMATE scheme only where needed.

Numerical experimentation has shown that the need for a higher resolution scheme can be determined by monitoring the absolute value of the unnormalized average "curvature," $\mathscr{D}_r^2$, defined in equation (25). If this is less than a specified constant, the limited QUICKEST scheme is used; if the critical value is exceeded locally, the algorithm branches to a higher order scheme (typically fifth- or seventh-order upwinding), returning to ULTIMATE QUICKEST wherever $\mathscr{D}_r^2$ drops below the threshold. By judicious choice of the threshold constant, the algorithm will use the ULTIMATE (probably unlimited) QUICKEST algorithm almost everywhere (i.e., in smooth regions) and switch to the higher order scheme at just the right grid points to give the desired high resolution. Figures 48 and 49 show results for the usual test-problems for a hybrid-3/5 and hybrid-3/7 strategy, respectively, using a value of 0.015 for the threshold constant. Node values involved in the higher order component on either left or right CV faces (or both) are shown by black dots; open circles designate that the simpler limited third-order scheme is to be used on both faces of the respective control volume.

SOME ASPECTS OF GENERALIZATION

Clearly in this initial paper outlining the priciples of the universal limiter, attention has been narrowly focussed on the idealized academic (yet still very challenging) problem of one-dimensional pure advection at constant velocity on a uniform grid. This was done purposely, of course, to identify the basic problems associated with the advection term, the modeling of which is by far the most difficult numerical aspect and major pacing item in the development of computational fluid dynamics. [It makes absolutely no sense, logically or practically, to simulate a flow using highly sophisticated multi-equation turbulence models, for example, with an advection method which essentially replaces modeled physical viscosity with inherent (or explicit) artificial viscosity throughout the bulk of the flow domain - but this is still the "state-of-the-art" in a disturbingly large (and growing) number of commercial and research codes, especially in heat transfer and related industries.] But, obviously, in order for the universal limiter to be of practical value in a general-purpose code, several generalizations will need to be made. Space in a single (already lengthy) article does not permit detailed expositions of such generalizations or verification using classical test-problems. This will be taken up in future papers - both by the author and presumably by other

researchers who may wish to extend and apply the theory in various ways. However, some generalizations are fairly straight-forward and will be sketched in this section, without showing specific results. Other generalizations of a more obvious nature (diffusion, nonuniform grids) or a more controversial one (systems of nonlinear equations) will be briefly addressed in the closing section.

Variable Advecting Velocity

The ULTIMATE strategy is easily extended to unsteady one-dimensional advection, where the advecting velocity is a function of space and time. For simplicity, assume that the right-face Courant number is positive

$$c_r > 0 \tag{87}$$

and that in a local region, ϕ is increasing monotonically

$$\phi_{i-1}^n < \phi_i^n < \phi_{i+1}^n < \phi_{i+2}^n \tag{88}$$

The update algorithm is based on equation (10), repeated here for convenience

$$\phi_i^{n+1} = \phi_i^n + c_\ell \phi_\ell - c_r \phi_r \tag{89}$$

where the face Courant numbers are considered to be known quantities at time-level n. As usual, ϕ_r is first estimated using some desired high order method. This is limited by the adjacent node values

$$\phi_i^n \leq \phi_r \leq \phi_{i+1}^n \tag{90}$$

Now require, conservatively, for monotonicity maintenance

$$\phi_i^{n+1} \geq \phi_{i-1}^n \tag{91}$$

This can be rewritten, using equation (89), as

$$c_r \phi_r \leq c_\ell \phi_\ell + \phi_i^n - \phi_{i-1}^n \tag{92}$$

and using a worst-case estimate of ϕ_ℓ, this becomes

$$c_r \phi_r \leq c_\ell \phi_{i-1}^n + \phi_i^n - \phi_{i-1}^n \tag{93}$$

for $c_\ell > 0$. (If $c_\ell < 0$, it may not be appropriate to require persistence of monotonicity.) Of course, for constant velocity, inequality (93) is equivalent to inequality (72). One further condition is necessary in the variable-velocity case, guaranteeing

$$\phi_i^{n+1} \leq \phi_{i+1}^n \tag{94}$$

which results in a condition on ϕ_ℓ, for control-volume (i), given by

$$c_\ell \phi_\ell \leq c_r \phi_r + \phi_{i+1}^n - \phi_i^n \tag{95}$$

or, in terms of ϕ_r, viewed as the left face of CV(i+1), using a worst-case estimate for the "far-right" face value,

$$c_r \phi_r \leq c_{rr} \phi_{i+1}^n + \phi_{i+2}^n - \phi_{i+1}^n \tag{96}$$

assuming $c_{rr} > 0$. In the constant-velocity case, this is superseded by the right-hand inequality of (90). The equivalent restrictions for monotonic decreasing regions should be clear. Local extrema are treated in the usual way.

Nonlinear Advection

Consider one-dimensional nonlinear advection

$$\frac{\partial \phi}{\partial t} + \frac{\partial f(\phi)}{\partial x} = 0 \tag{97}$$

where $f(\phi)$ is monotonic increasing. This can be rewritten in control-volume form as

$$\phi_i^{n+1} = \phi_i^n + \lambda\left(f_\ell - f_r\right) \tag{98}$$

where $\lambda = \Delta t/\Delta x$, $f_\ell = f\left(\phi_\ell\right)$, and $f_r = f\left(\phi_r\right)$. Again, for definiteness, assume that

$$\phi_{i-1}^n < \phi_i^n < \phi_{i+1}^n < \phi_{i+2}^n \tag{99}$$

First, estimate ϕ_r by some desired high order method. As usual, this will be limited by interpolative monotonicity

$$\phi_i^n \leq \phi_r \leq \phi_{i+1}^n \tag{100}$$

which is equivalent to

$$\lambda f\left(\phi_i^n\right) \leq \lambda f\left(\phi_r\right) \leq \lambda f\left(\phi_{i+1}^n\right) \tag{101}$$

Then, to assure inequality (91),

$$\lambda f_r \leq \lambda f\left(\phi_{i-1}^n\right) + \phi_i^n - \phi_{i-1}^n \tag{102}$$

which is the generalization of equation (93). The condition analogous to inequality (96) is superseded by the right-hand member of equation (101). Clearly if

$$f(\phi) = u\phi \tag{103}$$

for constant u, the limiting conditions revert back to inequality (72).

Multidimensional Algorithm

Because of the control-volume formulation of the one-dimensional algorithm, it is a straight-forward procedure to extend the ULTIMATE strategy to two and three dimensions. For two dimensions, the explicit update step analogous to equation (10) is

$$\phi_i^{n+1} = \phi_i^n - \left(c_r\phi_r - c_\ell\phi_\ell\right) - \left(c_b\phi_b - c_t\phi_t\right) \tag{104}$$

where "bottom" and "top" CV faces have been introduced, in addition to "left" and "right." Because of strict conservation,

$$\phi_r(i,j) = \phi_\ell(i+1,j) \tag{105}$$

and

$$\phi_t(i,j) = \phi_b(i,j+1) \tag{106}$$

(and similarly with the Courant numbers). Cell-averaged source-terms can be added to the right-hand side of equation (104), if appropriate.

Focusing attention on one CV face (say the left), the first step is to compute some explicit high (third or higher) order multidimensional estimate for ϕ_ℓ. This is then limited in a manner similar to figure 33, where $\tilde{\phi}_C^n$ is

based on three node values in a direction normal to the face: the two strad-
dling the face together with the next upstream-biased node in the normal direc-
tion, determined by $SGN(u_n)$, where u_n is the normal component of velocity at
the face in question. Thus, in general terms, the limiting step is "locally
one-dimensional" in the normal direction for each face, even though the high-
order base method is multidimensional.

For example, figure 50 shows the nodes involved for the left face (for u_ℓ
and v_ℓ as shown) using the author's uniformly third-order polynomial interpo-
lation algorithm (UTOPIA) as the base method, with the limiter-nodes shown as
black dots and the remaining nodes as open circles. Allowing for all velocity
directions on all four faces results in a 13-point stencil (the same as that
used for the second-order discrete biharmonic operator). Higher order schemes
can be designed in a similar way. Making use of additional nodes in the normal
direction for each face appears to be more effective than involving other nodes
in the transverse direction. Extension to three dimensions follows an entirely
similar procedure. Details and results of rigorous test problems will be
presented in a subsequent paper.

DISCUSSION AND FORECAST

The universal limiter, portrayed in figure 33, represents an extremely
simple way to produce explicit "monotonic" advection schemes of arbitrarily
high order. Potential numerical oscillations are suppressed without corrupt-
ing the expected resolution of the underlying scheme. It has been seen that
second-order methods (including well-known shock-capturing or TVD schemes) are
significantly inferior to the third-order ULTIMATE QUICKEST scheme, which uses
the same five-point stencil. Better resolution of sharp changes in gradient
can be achieved by using a higher order base method, and concomitantly wider
computational stencil. However, higher (even) order central methods are sus-
ceptible to a degree of waviness under some circumstances, as seen with the
semi-ellipse simulation. In terms of overall performance, there seems little
to be gained beyond the ULTIMATE fifth-order upwind scheme, or the highly cost-
effective hybrid scheme which uses ULTIMATE QUICKEST in smooth regions and
automatically switches to a higher order ULTIMATE upwind scheme in isolated
regions of high curvature. More precise simulation of narrow local extrema can

be built into the algorithm by using a weighting strategy which relies more heavily on an unlimited higher order scheme in such regions, provided a suitable monitor can be devised to discriminate between physical and numerically produced extrema. This now appears to be possible, using simple pattern-recognition techniques.

Some insight into the step-resolution of various schemes can be gained by correlating portions of a step simulation with regions of the $\left(\tilde{\phi}_C^n, \tilde{\phi}_f\right)$ plane. Figure 51(a) shows schematically a simulated step profile, inverted for more direct reference to the NVD. In the leading-edge (LE) region, $\tilde{\phi}_C^n$ is slightly less than 1; in the trailing-edge (TE) region, it is slightly greater than 0. This is reflected in figure 51(b). As seen in figure 51(c), sharper resolution corresponds to larger $\tilde{\phi}_f$ values relative to the corresponding $\tilde{\phi}_C^n$ values, in both regions. This correlation can be quite clearly seen, for example, with the Chakravarthy-Osher scheme (figs. 19 and 25) or ULTIMATE second-order upwinding (figs. 35 and 39) where the NVD characteristic is relatively low in the TE region corresponding to a "blunt" trailing edge step simulation, and relatively high in the LE region, giving a sharp leading edge. The reverse is true for the ULTIMATE Lax-Wendroff scheme, resulting in a blunt leading edge and a sharp trailing edge. The Minmod scheme selects the lower characteristic in each region, leading to rather diffuse performance; whereas Superbee (or more effectively, Super-C) relies on the higher characteristic in each region of the NVD, and this results in the combination of sharp leading and trailing edges with concomitant narrow resolution of the step.

The artificially high values of $\tilde{\phi}_f$ for the latter schemes is equivalent to artificial compression, or (to the extent that the NVD characteristic lies above a well-behaved scheme such as ULTIMATE QUICKEST) to negative artificial diffusion. For example, the limited Lax-Wendroff scheme exhibits artificial negative diffusion for $\tilde{\phi}_C^n < 0.5$; whereas for limited second-order upwinding and the Chakravarthy-Osher scheme, this appears in the leading edge region, where the NVD characteristic is based on first-order downwinding. This interpretation correlates with the observed trailing oscillations of the unlimited Lax-Wendroff scheme (fig. 4) and the leading oscillations of unlimited second-order upwinding (fig. 5).

34

The great advantage of the ULTIMATE strategy is that it can be used with explicit schemes of arbitrarily high order, giving concomitant resolution of sudden changes in gradient without artificial steepening and clipping. The limited polynomial schemes reviewed here already give excellent results (above second order), but clearly the ULTIMATE philosophy can be used with other more sophisticated and more appropriate forms of spatial interpolation. One such method currently under investigation involves exponential ("tension") splines applied locally; this technique offers possibilities of very high resolution on a compact stencil.

Extension to multidimensional flow is straightforward and, as mentioned, this will form the subject of future papers. Although not addressed in this paper (since attention has been focused on the critical problem of pure advection) it should be clear that the introduction of modeled physical diffusion to an order consistent with the advection scheme presents absolutely no problems. The inclusion of physical diffusion in fact puts less demands on the advective algorithm; in most cases of practical interest, the ULTIMATE QUICKEST scheme gives results which are graphically indistinguishable from the exact solution (when known). In a similar way, extension to spatially varying grids presents no problems. The higher order accuracy of the base method can be formally maintained (refs. 9 and 16); or, provided the expansion ratio does not exceed about 125 percent, the simpler uniform-grid formulas for third- and higher order methods can be used directly without reducing the practical order of accuracy - although the formal order is, of course, reduced (ref. 17).

One of the most important questions, of course, concerns how well the ULTIMATE strategy generalizes to handle systems of nonlinear equations such as the Euler (or Navier-Stokes) equations of gasdynamics, and the "shallow-water" and related equations of oceanography and meteorology. This is by no means a trivial generalization and will no doubt form the subject of future papers; however, it is fair to predict that ULTIMATE simulations will be at least as successful as the better shock-capturing schemes, since the underlying philosophy is very similar. In particular, because of natural physical compression, shock-wave or hydraulic jump (or atmospheric front) resolution can be expected to be narrower than the scalar step resolution studied here. And because of

the ability to use arbitrarily high order resolution, unsteady gasdynamic simulations can be expected to give extremely reliable results, even at very high Mach numbers and nonideal conditions. Because of the conservative control-volume formulation, multidimensional gasdynamic, and geophysical algorithms are expected to be similarly robust. The general philosophy here is to model the control-volume advective modes precisely and let the physics (as reflected in the governing equations) take care of the "acoustic" or wave modes. This idea seems not to work well with currently popular second-order flux-limited schemes because of these schemes' addictive reliance on locally varying (positive or negative) artificial viscosity, requiring precise knowledge of characteristic speeds and directions. But the principle has great potential when used with higher order ULTIMATE multidimensional algorithms, which, by design, require only advective velocities at the CV cell faces, as prescribed by the governing equations.

Finally, the ULTIMATE strategy can be applied to steady-flow multidimensional simulations (even though the acronym might be somewhat out of place). Quite simply, the steady-state limiter consists of ULTIMATE with the Courant number set to zero. This, of course, results in the extremely simple condition in the monotonic regime

$$\tilde{\phi}_C \leq \tilde{\phi}_f \leq 1 \quad \text{for} \quad 0 < \tilde{\phi}_C \leq 1 \tag{107}$$

with $\tilde{\phi}_f = \tilde{\phi}_C$, or similar characteristic passing through (0,0) and (1,1), in the nonmonotonic range. In other words, for locally monotonic behavior in the direction normal to a given CV face, after a high-order multidimensional estimate of ϕ_f is made, the face value actually used is constrained simply to lie between the adjacent upstream and downstream node values: ϕ_U and ϕ_D, respectively. The author's multidimensional SHARP algorithm (ref. 15), simple high accuracy resolution program, is a third-order nonlinear scheme conforming to these requirements; it is based on an exponential upwinding or linear extrapolation refinement of the multidimensional QUICK scheme (ref. 16). But, of course, the principle can be extended to arbitrarily high order using the universal limiter for tight resolution and accuracy, thus giving ULTRA-SHARP simulation of steady multidimensional flows containing near-discontinuities. In a practical algorithm, it is important to construct a single-valued upper boundary

for the allowable NVD region near $\tilde{\phi}_C \rightarrow 0_+$. This is most conveniently achieved by requiring

$$\tilde{\phi}_f \leq \text{const } \tilde{\phi}_C \quad \text{for} \quad 0 \leq \tilde{\phi}_C \tag{108}$$

in addition to inequality (107), with suitably large values of the slope constant (~10 or 100). The piecewise linear NVD characteristic of the steady two-dimensional SMART algorithm of Gaskell and Lau (ref. 18) is also of this form. Steady-state methods based on second- and third-order schemes (including TVD limiters) can be solved with straight-forward ADI scalar penta-diagonal matrix algorithms using Gaskell-and-Lau's modified (nonlinear) curvature-factor technique, similar to the curvature factor, $\text{CF}\left(\tilde{\phi}_C^n\right)$, appearing in equation (55). Alternatively, arbitrarily high order limited schemes can be solved by popular ADI tridiagonal methods using the author's downwind weighting factor technique (ref. 19), thus rendering the ULTRA-SHARP very-high-order multidimensional nonoscillatory steady-flow schemes immediately compatible with many of the general-purpose commercial and research steady-state elliptic solvers currently in use, which are typically based on low-accuracy blended combinations of first- and second-order advection methods.

ACKNOWLEDGMENTS AND PERSPECTIVE

"TVD region," conforming to current practice in operational schemes, although the less restrictive conditions would have been known to him, since they had appeared in a GAMM proceedings paper by Roe and Baines (ref. 24) in 1982 and in other proceedings papers by Roe (refs. 6 and 25) in 1983. The author's attention was directed toward the latter papers by S.T. Zalesak in November 1987 and by P.L. Roe in May 1988. Interestingly enough, Roe's 1986 review article (ref. 26) makes no mention of the less restrictive limiter boundaries, but rather describes instead only some of the more restrictive limiters (such as Minmod, "CLAM," and Superbee), even though the earlier proceedings papers are referenced.

Zalesak's IMACS paper (ref. 12) describes work by his colleague, John Lyon, at the Naval Research Laboratory, who appears to be the only other researcher to have used arbitrarily high (up to eighth) order advection schemes constrained by an equivalent of the universal limiter. Finally, P.H. Gaskell and A.K.C. Lau, at the University of Leeds, have (again independently, following from their steady-flow work (ref. 18)) developed an equivalent limiting strategy for unsteady flow applied to a quasi-third-order advection scheme. They report highly accurate simulations of standard shock-tube test problems without resorting to flux vector splitting, Riemann solvers, or any of the other complexities associated with currently popular forms of first/second-order shock-capturing schemes. This confirms the author's belief that characteristic decomposition is not a necessity, but rather a symptom of poorly designed advection schemes, based on variable artificial viscosity, which require detailed explicit knowledge of all characteristic velocities and amplitudes. If the advection (macroflux) terms appearing in the conservation equations for mass momentum and energy are carefully modeled with suitably limited higher order methods and microflux terms (pressure tensor, etc.) treated appropriately, the governing equations themselves will automatically generate the correct additional wave modes. The far-reaching implications of this, especially for multidimensional flows, should be clear.

APPENDIX

In a well-known paper (ref. 10), Sweby introduced sufficient conditions for schemes to have total-variation-diminishing properties, and portrayed these conditions in what has become known as the "Sweby diagram," a plot of the flux-limiter factor, φ, against the local gradient ratio, r. For constant Courant number, the flux-limiter factor is defined as

$$\varphi = \frac{\left(\phi_f - \phi_C^n\right)}{\left(\phi_f^{LW} - \phi_C^n\right)} \tag{A.1}$$

where ϕ_f is the limited face value, ϕ_C^n is the adjacent upstream node value, and ϕ_f^{LW} is the face value according to second-order central differencing (Lax-Wendroff)

$$\phi_f^{LW} = \frac{1}{2}\left(\phi_D^n + \phi_C^n\right) - \frac{|c|}{2}\left(\phi_D^n - \phi_C^n\right) \tag{A.2}$$

where ϕ_D^n is the adjacent downstream value, as usual. All of the schemes considered by Sweby are linear in Courant number in the form of equation (49), rewritten for $c \gtrless 0$, as

$$\phi_f = (1 - |c|)\phi_f^n + |c|\phi_C^n \tag{A.3}$$

The Lax-Wendroff face value can also be written in this form

$$\phi_f^{LW} = (1 - |c|)\phi_f^{CEN} + |c|\phi_C^n \tag{A.4}$$

where ϕ_f^{CEN} is the linear interpolation $1/2\left(\phi_D^n + \phi_C^n\right)$. Substituting (A.3) and (A.4) into (A.1) results in an equivalent expression for the flux-limiter factor

$$\varphi = \frac{\left(\phi_f^n - \phi_C^n\right)}{\left(\phi_f^{CEN} - \phi_C^n\right)} \tag{A.5}$$

which can be rearranged as

$$\phi_f^n = \phi_C^n + \varphi \cdot \left(\phi_f^{CEN} - \phi_C^n\right) \tag{A.6}$$

interpreted as first-order upwinding modified by adding a term proportional to the difference between linear interpolation and first-order upwinding.

In terms of the normalized variables as defined in the present paper, it is not difficult to show that

$$\varphi = \frac{\left(\tilde{\phi}_f^n - \tilde{\phi}_C^n\right)}{\frac{1}{2}\left(1 - \tilde{\phi}_C^n\right)} = \frac{\left(\tilde{\phi}_f - \tilde{\phi}_C^n\right)}{\frac{1}{2}(1 - |c|)\left(1 - \tilde{\phi}_C^n\right)} \tag{A.7}$$

Similarly, the gradient ratio used by Sweby is

$$r = \frac{\left(\phi_C^n - \phi_U^n\right)}{\left(\phi_D^n - \phi_C^n\right)} = \frac{\tilde{\phi}_C^n}{\left(1 - \tilde{\phi}_C^n\right)} \tag{A.8}$$

The so-called TVD region proposed by Sweby consists of first-order upwinding ($\varphi = 0$) for negative r, followed by

$$0 \le \varphi \le 2r \quad \text{for} \quad 0 \le r \le 1 \tag{A.9}$$

and then limited by first-order downwinding at time-level n, $\tilde{\phi}_f^n = 1$ in equation (A.7), giving

$$0 \le \varphi \le 2 \quad \text{for} \quad r \ge 1 \tag{A.10}$$

Note that equation (A.9) can be interpreted as

$$\tilde{\phi}_f^n = 2\tilde{\phi}_C^n \quad \text{for} \quad 0 < \tilde{\phi}_C^n < \frac{1}{2} \tag{A.11}$$

Figure A.1 compares Sweby's TVD region (shaded) interpreted in the $\left(\tilde{\phi}_C^n, \tilde{\phi}_f^n\right)$ plane and in the (r, φ) plane. For reference, Roe's Superbee scheme is shown, passing through the "second-order" point, (0.5, 0.75) in figure A.1(a), and (1,1) in figure A.1(b). By contrast, figure A.2 gives the "extended Sweby diagram" corresponding to the ULTIMATE strategy of figure 33; recall that that figure involved $\tilde{\phi}_f$ rather than $\tilde{\phi}_f^n$, as used in fig. A.1(a). Note that the sloping boundary OB in the extended Sweby diagram has a slope of $2/|c|$ as compared with the slope of 2 for OC in the original Sweby diagram. Also note that the upper boundary of the extended diagram increases in height as $|c| \rightarrow 1$; in fact

$$\varphi_B = \frac{2}{1 - |c|} \tag{A.12}$$

whereas, in the original diagram figure A.1(b), the upper boundary is independent of c:

$$\varphi_C \equiv 2$$

As the Courant number varies, the point B in figure A.2 "slides" along the line $\varphi_B = 2(1 + r_B)$, where $r_B = |c|/(1 - |c|)$. For reference, the Super-C scheme is shown in figure A.2. Hyper-C simply follows the upper boundary: AOBA. As is immediately obvious, Sweby's TVD region is grossly over-restrictive, resulting in predicted (normalized) face values which are too small, especially for $\tilde{\phi}_C^n$ values slightly larger than 0 or slightly smaller than 1. This is one reason for the poor performance of currently popular second-order TVD schemes.

REFERENCES

1. van Leer, B.: Towards the Ultimate Conservative Difference Scheme, I - The Quest of Montonicity. Proceedings of the Third International Conference on Numerical Methods in Fluid Mechanics, Vol. 1 (Lecture Notes in Physics, Vol. 18) H. Cabannes and R. Temam, eds., Springer-Verlag, 1973, pp. 163-168.

2. van Leer, B.: Towards the Ultimate Conservative Difference Scheme. II. Monotoncity and Conservation Combined in a Second-Order Scheme. J. Comput. Phys., vol. 14, no. 4, Mar. 1974, pp. 361-370.

3. van Leer, B.: Toward the Ultimate Conservative Difference Scheme. III. Upstream-Centered Finite-Difference Schemes for Ideal Compressible Flow. J. Comput. Phys., vol. 23, no. 3, Mar. 1977, pp. 263-275.

4. van Leer, B.: Towards the Ultimate Conservative Difference Scheme. IV. A New Approach to Numerical Convection. J. Comput. Phys., vol. 23, no. 3, Mar. 1977, pp. 276-299.

5. van Leer, B.: Towards the Ultimate Conservative Difference Scheme. V. A Second-Order Sequel to Godunov's Method. J. Comput. Phys., vol. 32, no. 1, July 1979, pp. 101-136.

6. Roe, P.L.: Some Contributions to the Modelling of Discontinuous Flows. Large Scale Computations in Fluid Mechanics, Pt. 2, (Lectures in Applied Mathematics, Vol. 22) E. Engquist, S. Osher, and R.C.J. Sommerville, eds., American Mathematical Society, 1985, pp. 163-193.

7. Mitchell, A.R.: Recent Developments in the Finite Element Method. Computational Techniques and Applications: CTAC-83, J. Noye and C.A.J. Fletcher, eds., Elsevier North-Holland, 1984, pp. 2-14.

8. Leonard, B.P.: Third-Order Upwinding as a Rational Basis for Computational Fluid Dynamics. Computational Techniques and Applications: CTAC-83, J. Noye and C.A.J. Fletcher, eds., Elsevier North-Holland, 1984, pp. 106-120.

9. Leonard, B.P.: A Stable and Accurate Convective Modelling Procedure Based on Quadratic Upstream Interpolation. Computer Methods in Applied Mechanics and Engineering, vol. 19, no. 1, June 1979, pp. 59-98.

10. Fromm, J.E.: A Method for Reducing Dispersion in Convective Difference Schemes. J. Comput. Phys., vol. 3, no. 2, Oct. 1968, pp. 176-189.

11. Sweby, P.K.: High Resolution Schemes Using Flux Limiters for Hyperbolic Conservation Laws. SIAM J. Numer. Anal., vol. 21, no. 5, Oct. 1984, pp. 995-1011.

12. Zalesak, S.T.: A Preliminary Comparison of Modern Shock-Capturing Schemes: Linear Advection. Advances in Computer Methods for Partial Differential Equations VI, R. Vichnevetsky and R.S. Stepelman, eds., IMACS, Rutgers University, 1987.

13. Harten, A.: High Resolution Schemes for Hyperbolic Conservation Laws. J. Comput. Phys., vol. 49, no. 3, Mar. 1983, pp. 357-393.

14. Chakravarthy, S.R.; and Osher, S.: High Resolution Applications of the Osher Upwind Scheme for the Euler Equations. AIAA Paper 83-1943, July 1983.

15. Leonard, B.P.: SHARP Simulation of Discontinuities in Highly Convective Steady Flow. NASA TM-100240, 1987.

16. Leonard, B.P.: Elliptic Systems: Finite Difference Method IV. Handbook of Numerical Heat Transfer, W.J. Minkowicz, E.M. Sparrow, G.E. Scheider, and R.H. Pletcher, eds., Wiley, 1988, Chapter 9, pp. 347-378.

17. Castro, I.P.; and Jones, J.M.: Studies in Numerical Computations of Recirculating Flows. Int. J. Numer. Methods Fluids, vol. 7, no. 8, Aug. 1987, pp. 793-823.

18. Gaskell, P.H.; and Lau, A.K.C.: Curvature Compensated Convective Transport: SMART, a New Boundedness Preserving Transport Algorithm. Int. J. Numer. Methods Fluids, vol. 8, no. 6, June 1988, pp. 617-641.

19. Leonard, B.P.: Sharp Numerical Simulation of Thin Layers in Highly Convective Flows. In BAIL V -- Proceedings of the Fifth International Conference on Computational and Asymptotic Methods for Boundary and Interior Layers, Shanghai, June 1988, J.J.H. Miller and B.Y. Guo, eds., Boole Press, Dublin (in press).

20. Leonard, B.P.: Adjusted Quadratic Upstream Algorithms for Transient Incompressible Convection. Computational Fluid Dynamics Conference, AIAA, 1979, pp. 226-233.

21. Leonard, B.P.: A Survey of Finite Differences with Upwinding for Numerical Modelling of the Incompressible Convective Diffusion Equation. Computational Techniques in Transient and Turbulent Flow, C. Taylor and K. Morgan, eds., Pineridge Press, Swansea, UK, 1981, pp. 1-23.

22. Leonard, B.P.; Vachtsevanos, G.J.; and Abood, K.A.: Unsteady-State, Two Dimensional Intrusion Model for an Estuary. Applied Numerical Modelling, C.A. Brebbia, ed., Wiley, 1978, pp. 113-123.

23. Yee, H.C.: Upwind and Symmetric Shock-Capturing Schemes. NASA TM-89464, 1987.

24. Roe, P.L.; and Baines, M.J.: Algorithms for Advection and Shock Problems. Proceedings of the 4th GAMM Conference on Numerical Methods in Fluid Mechanics, H. Viviand, ed., Vieweg, West Germany, 1982, pp. 281-290.

25. Roe, P.L.; and Baines, M.J.: Asymptotic Behaviour of Some Non-Linear Schemes for Linear Advection. Proceedings of the 5th GAMM Conference on Numerical Methods in Fluid Mechanics, M. Pandolfi, and R. Piva, eds., Vieweg, West Germany, 1983, pp. 283-290.

26. Roe, P.L.: Characteristic-Based Schemes for the Euler Equations. Annual Reviews of Fluid Mechanics, Vol. 18, M. Van Dyke, J.V. Wehausen, and J.L. Lumley, eds., Annual Reviews Inc., 1986, pp. 337-365.
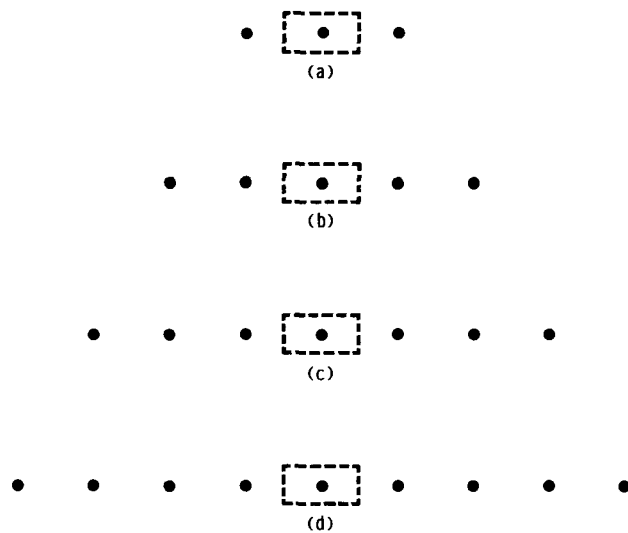
FIGURE 1. - CONTROL-VOLUME STENCILS FOR (a) FIRST-ORDER UPWINDING AND SECOND-ORDER CENTRAL; (b) SECOND- AND THIRD-ORDER UPWINDING, FROMM'S METHOD AND FOURTH-ORDER CENTRAL; (c) FIFTH-ORDER UPWINDING AND SIXTH-ORDER CENTRAL; (d) SEVENTH- AND EIGHTH-ORDER SCHEMES.
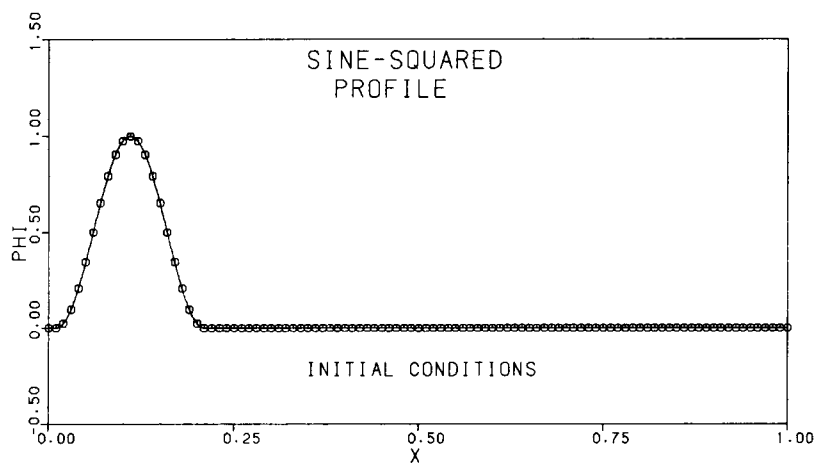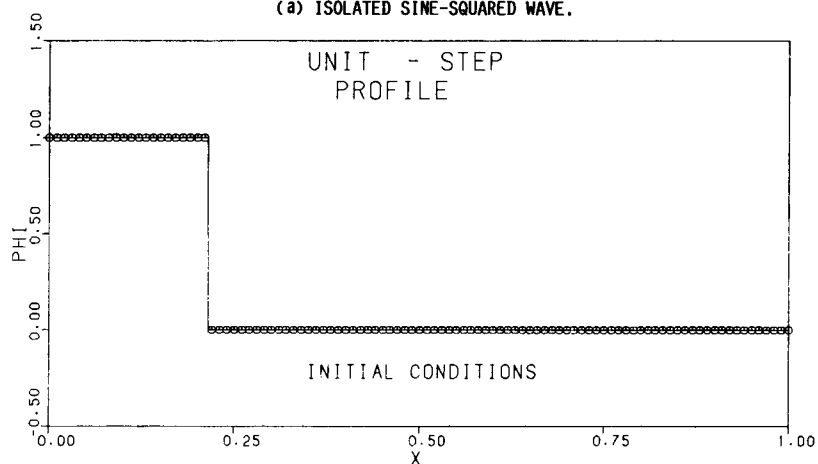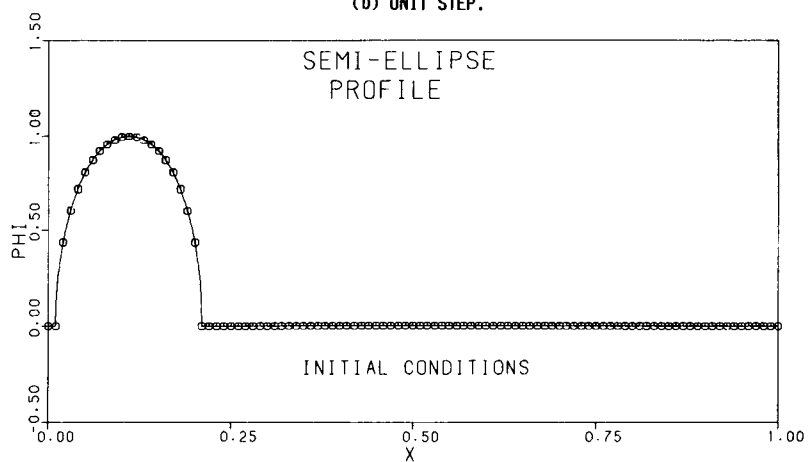
FIGURE 2. - INITIAL CONDITIONS FOR THE THREE TEST PROFILES.
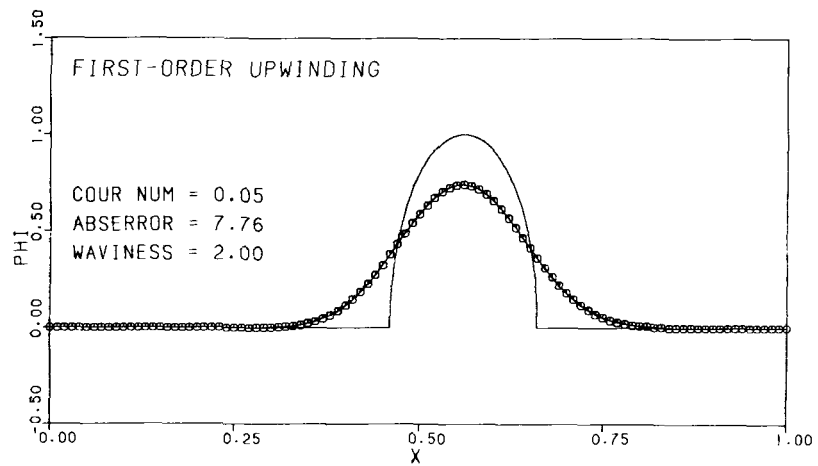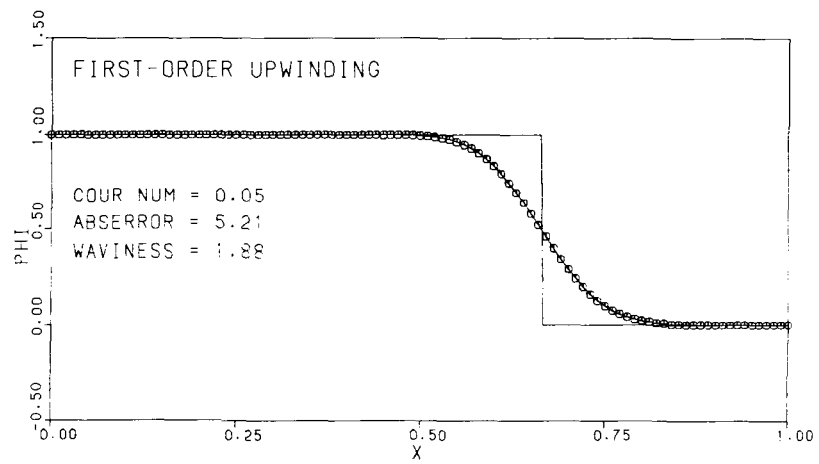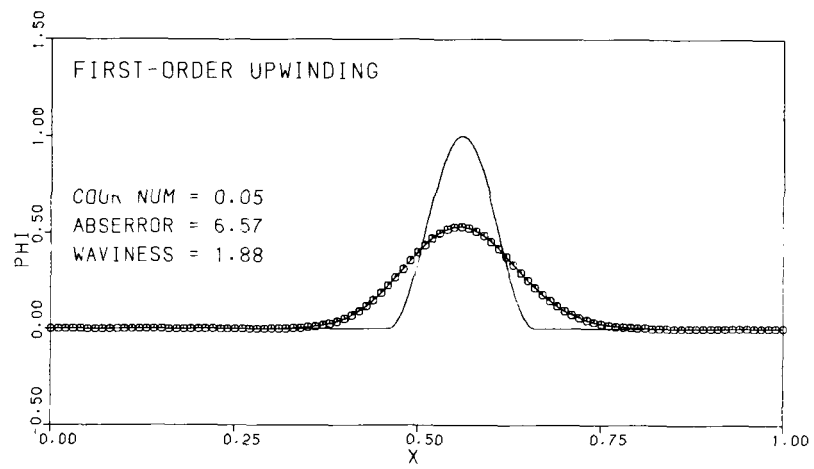
(a) c = 0.05.

FIGURE 3. - RESULTS FOR FIRST-ORDER UPWINDING.
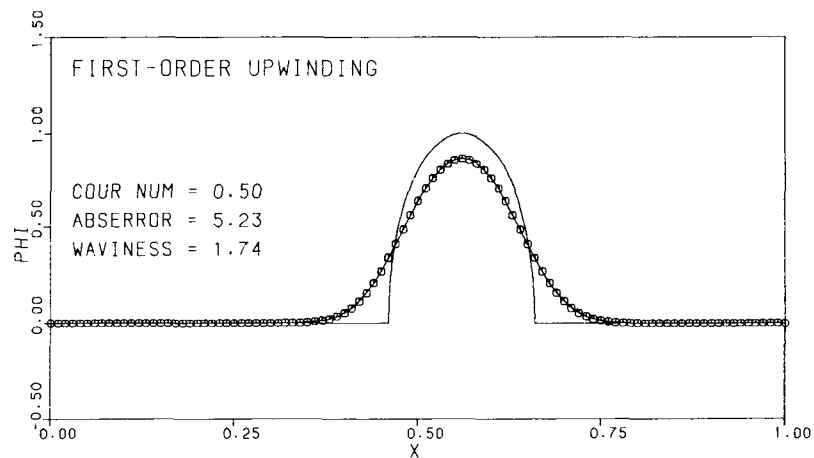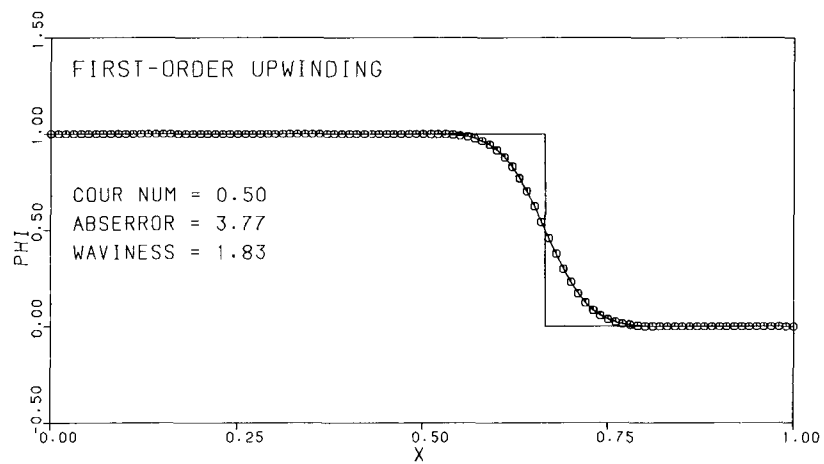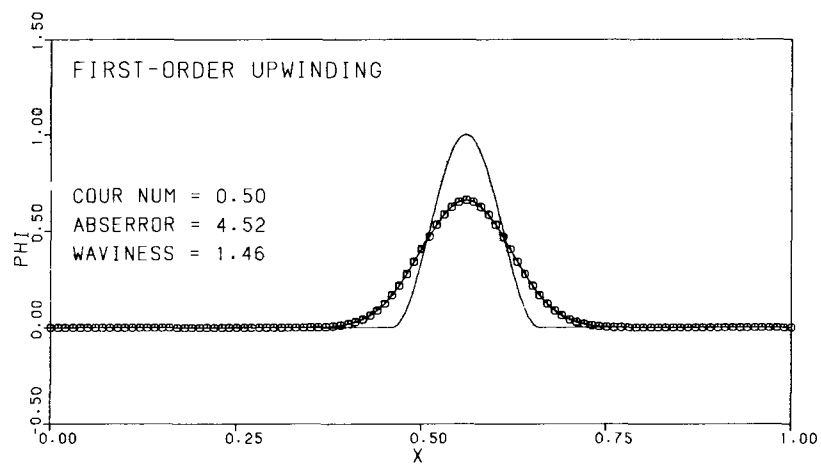
(b) c = 0.5.
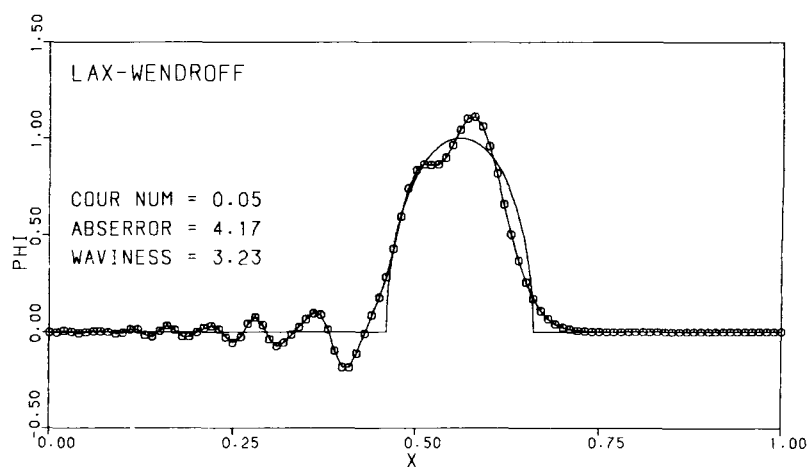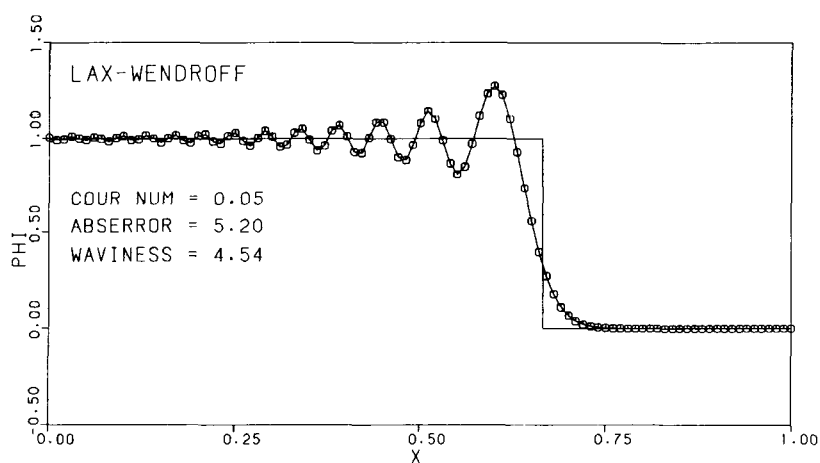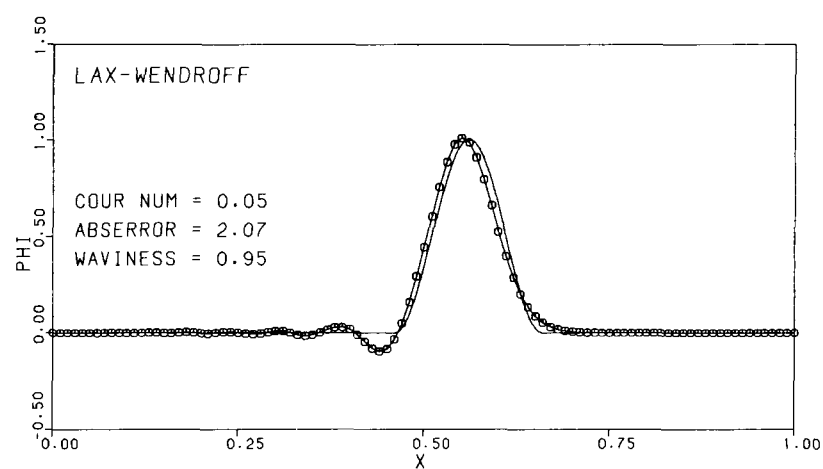
FIGURE 3. - CONCLUDED.

(a) c = 0.05.

FIGURE 4. - RESULTS FOR THE LAX-WENDROFF METHOD (SECOND-ORDER CENTRAL).

48
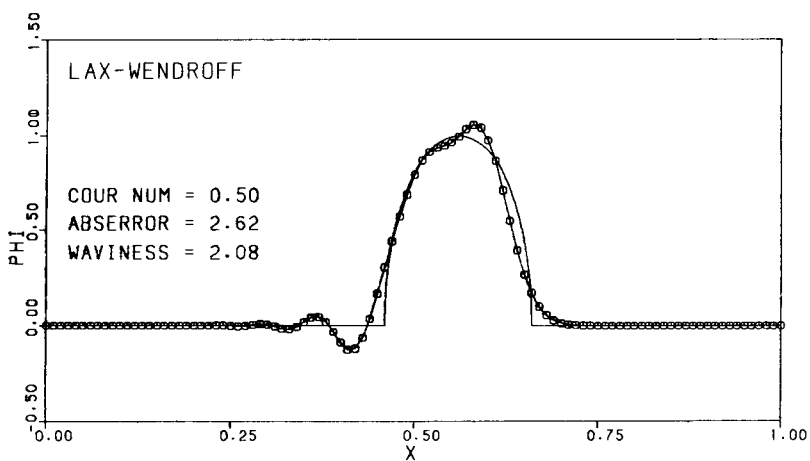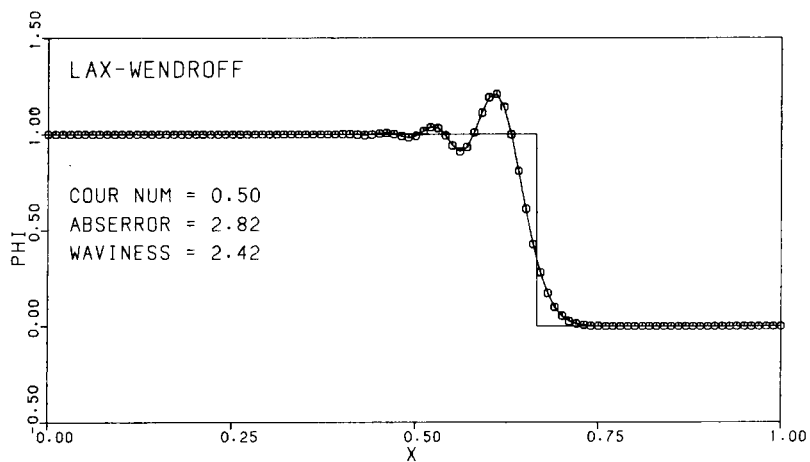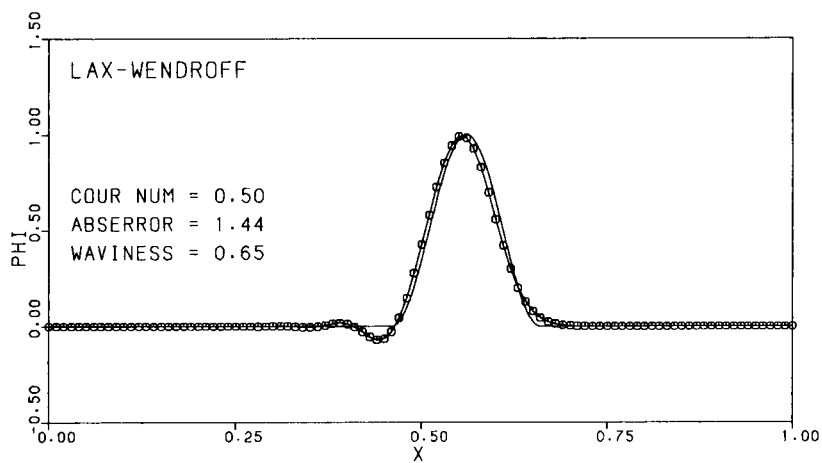
(b) c = 0.5.

FIGURE 4. - CONCLUDED.

49
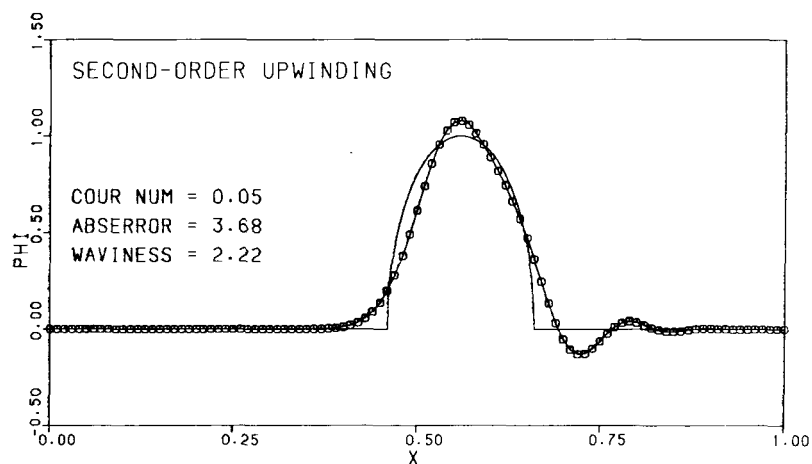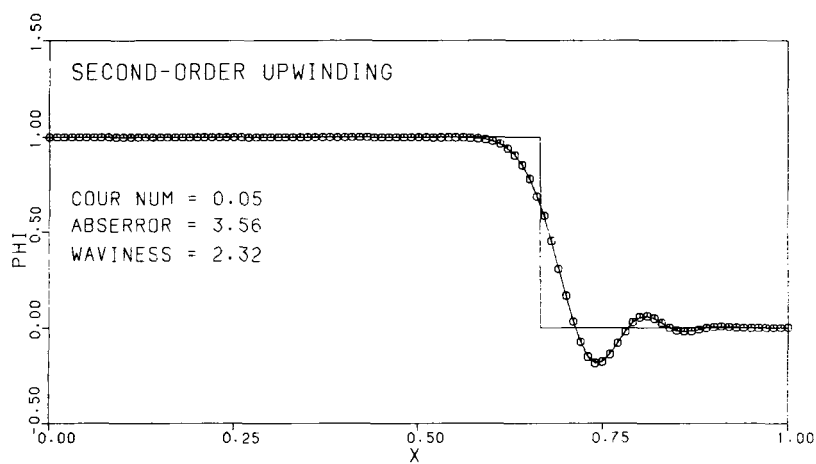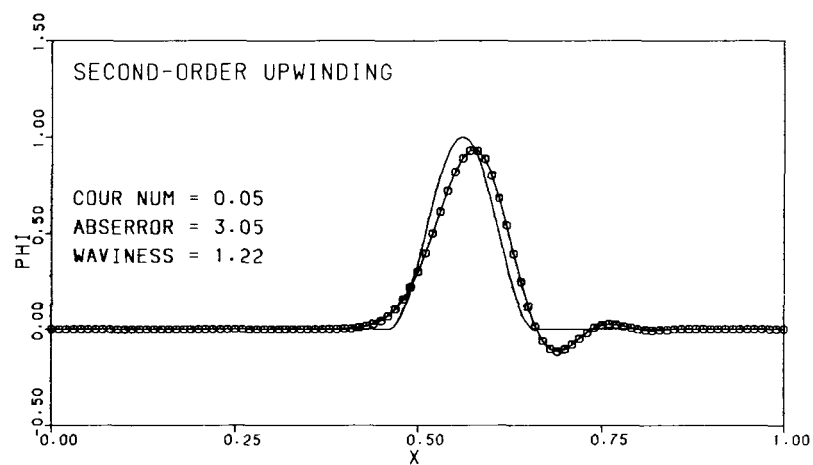
(a) c = 0.05.

FIGURE 5. - RESULTS FOR SECOND-ORDER UPWINDING.

(b) c = 0.5.

FIGURE 5. - CONCLUDED.

FROMM'S METHOD

COUR NUM = 0.05
ABSERROR = 0.85
WAVINESS = 0.39

FROMM'S METHOD

COUR NUM = 0.05
ABSERROR = 1.51
WAVINESS = 1.89

FROMM'S METHOD

COUR NUM = 0.05
ABSERROR = 1.70
WAVINESS = 1.51
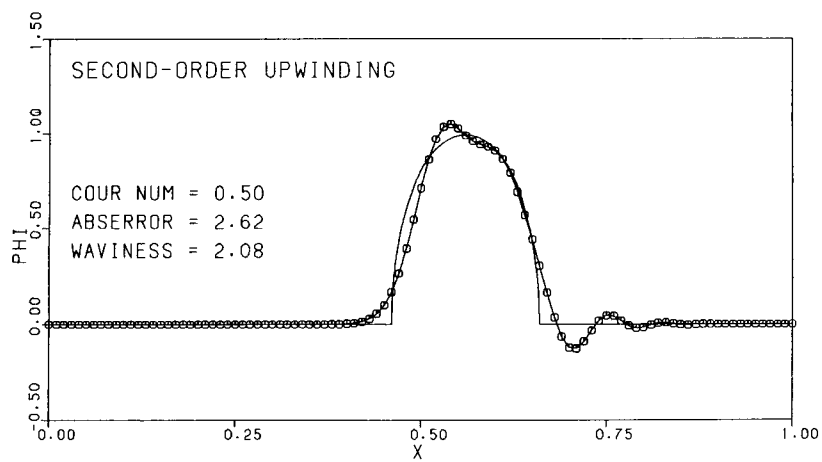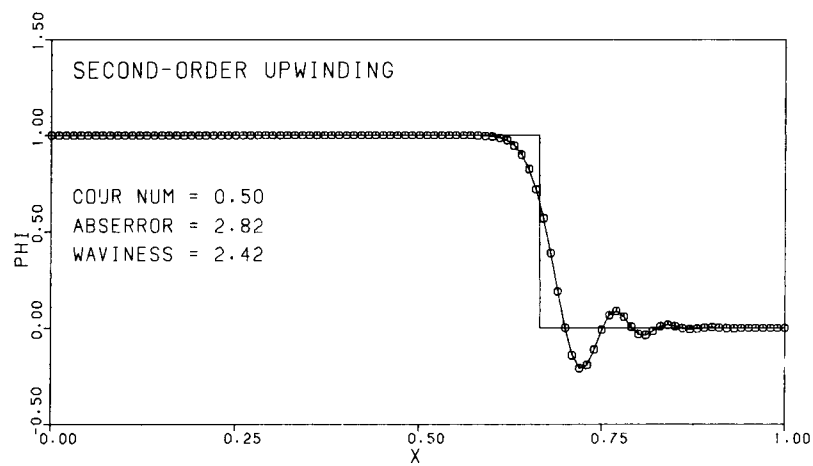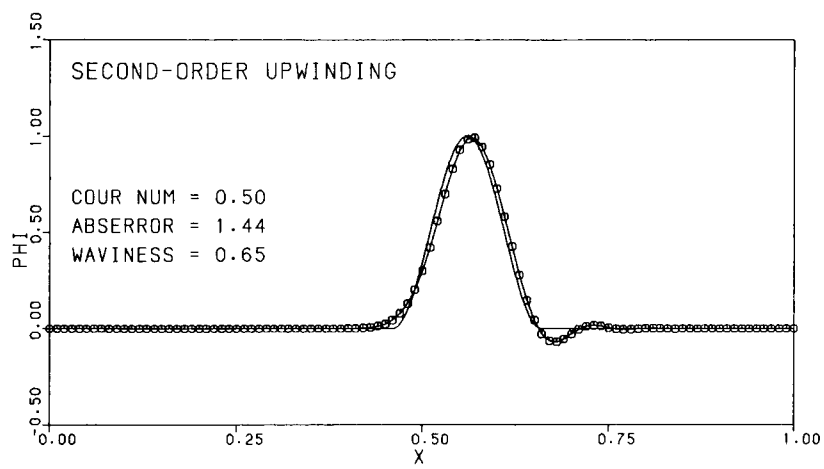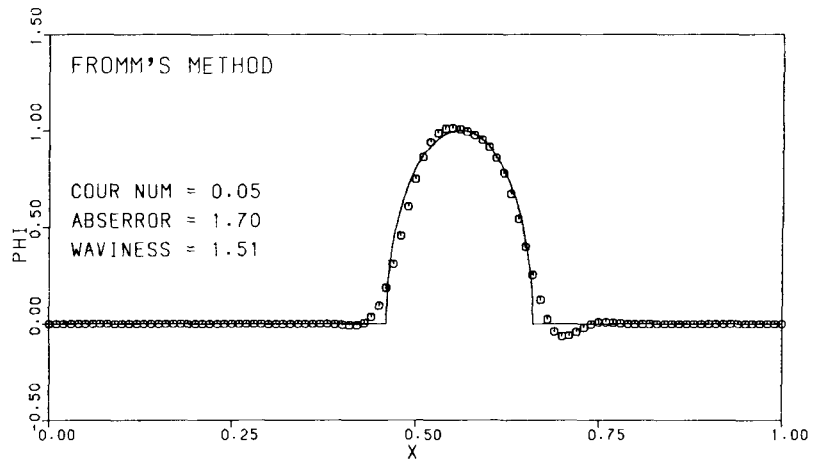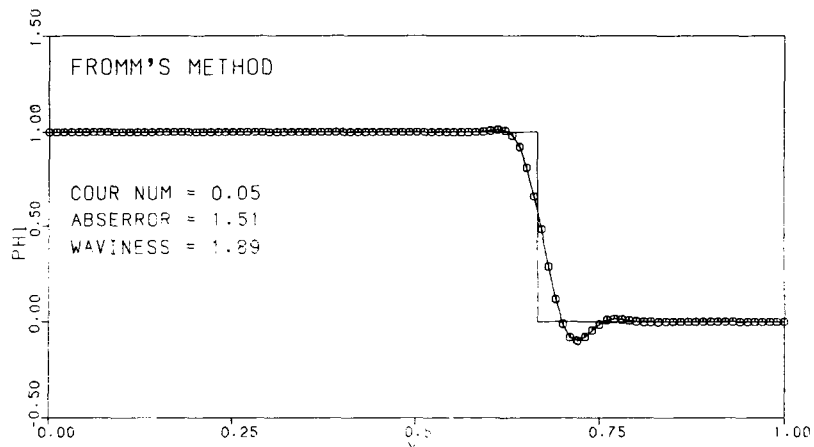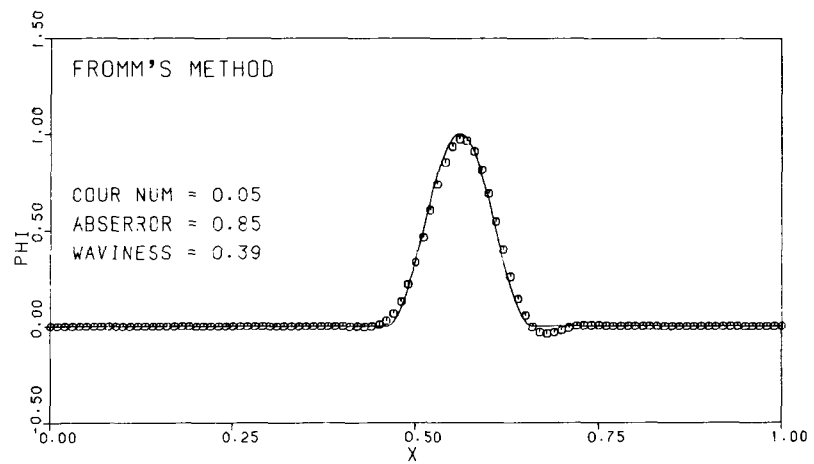
(a) c = 0.05.

FIGURE 6. - RESULTS FOR FROMM'S METHOD.
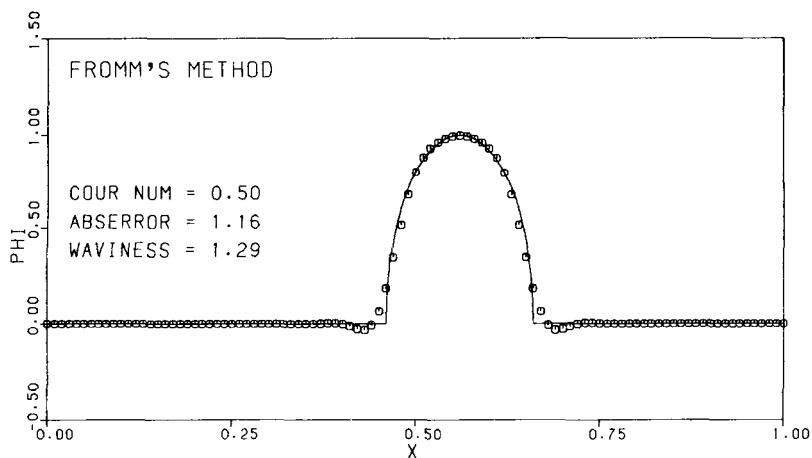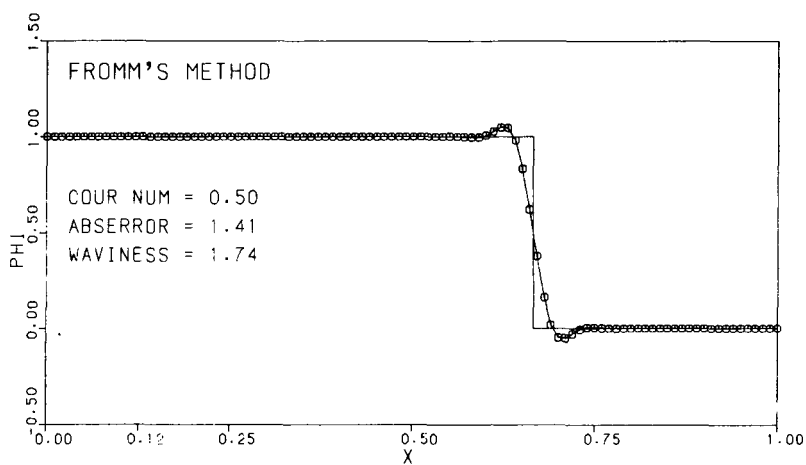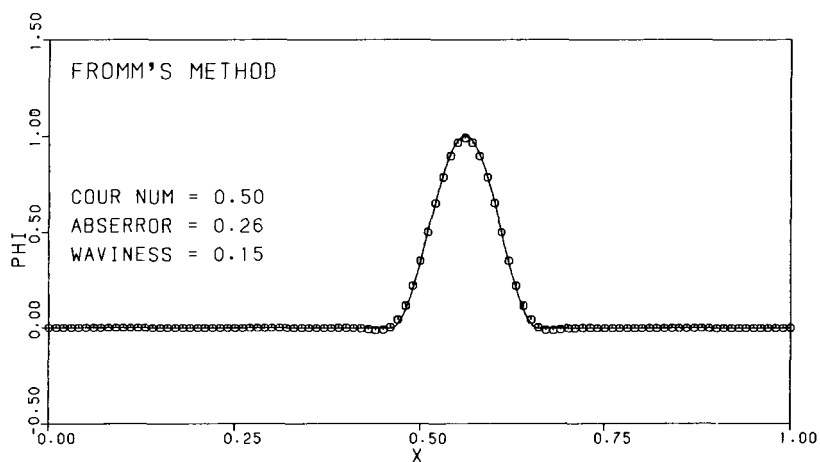
(b) c = 0.5.

FIGURE 6. - CONCLUDED.
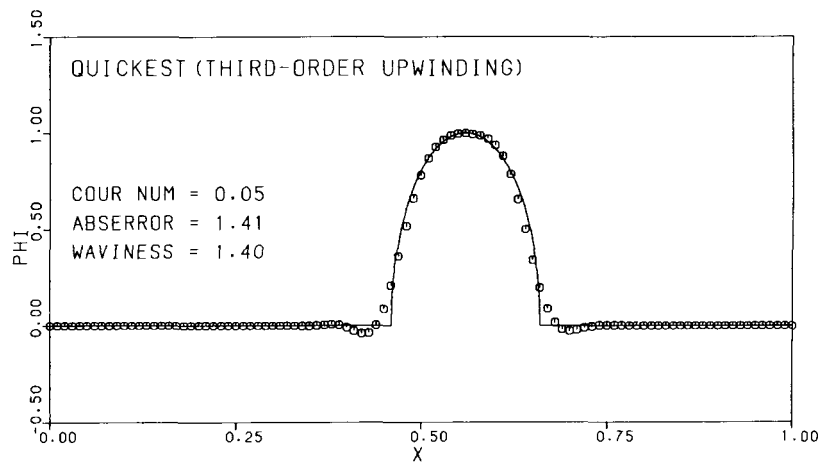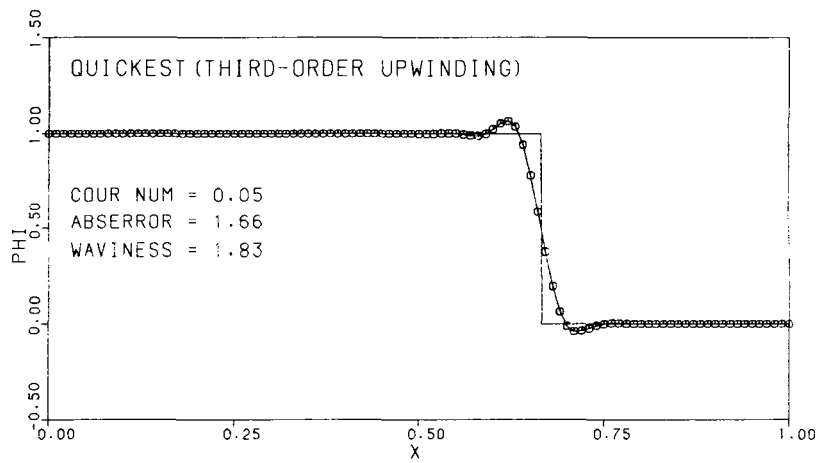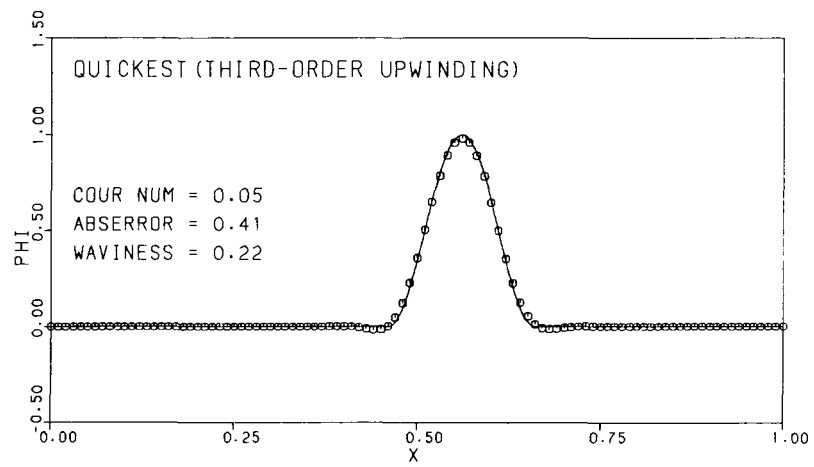
(a) c = 0.05.

FIGURE 7. – RESULTS FOR QUICKEST (THIRD-ORDER UPWINDING).

54
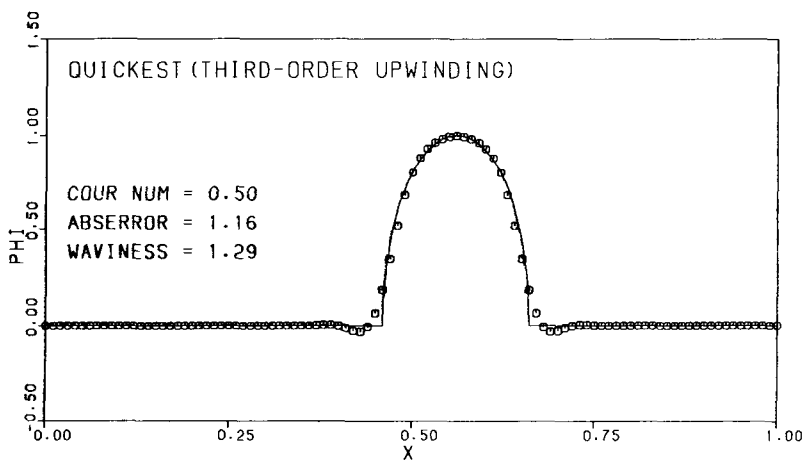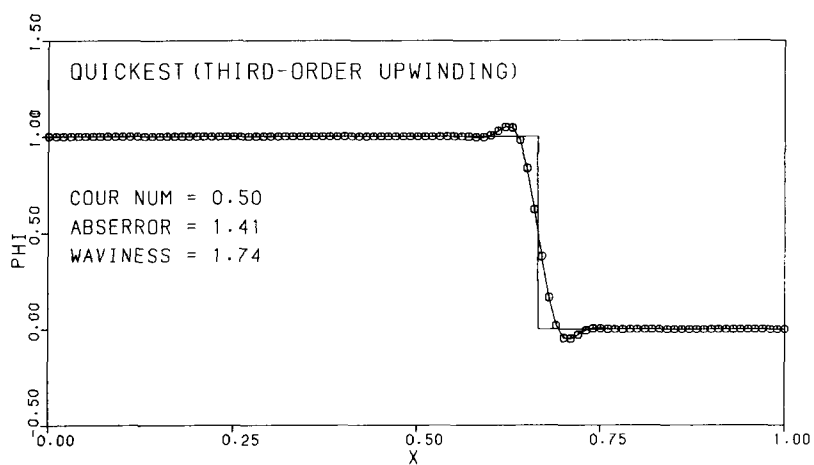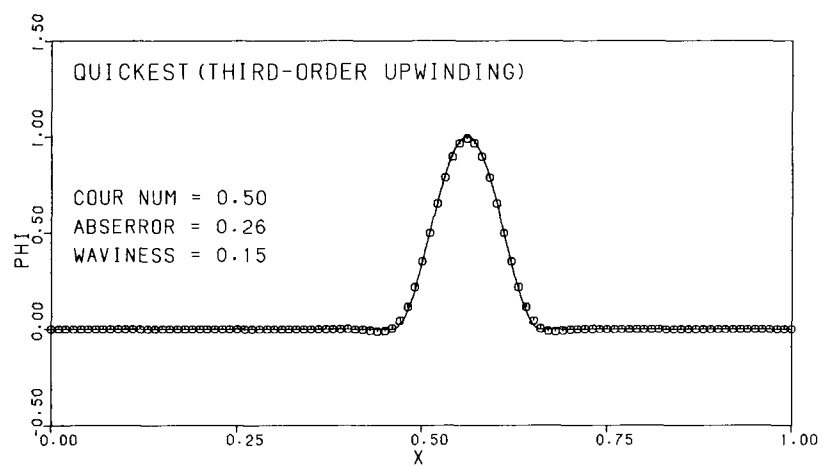
(b) c = 0.5.

FIGURE 7. - CONCLUDED.
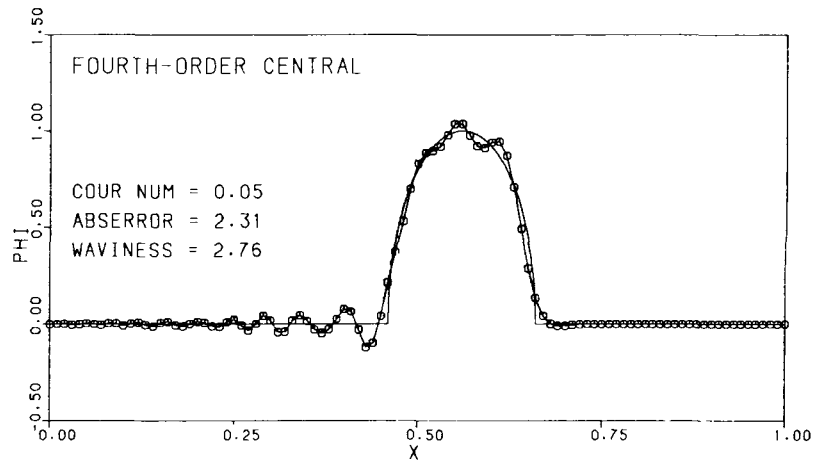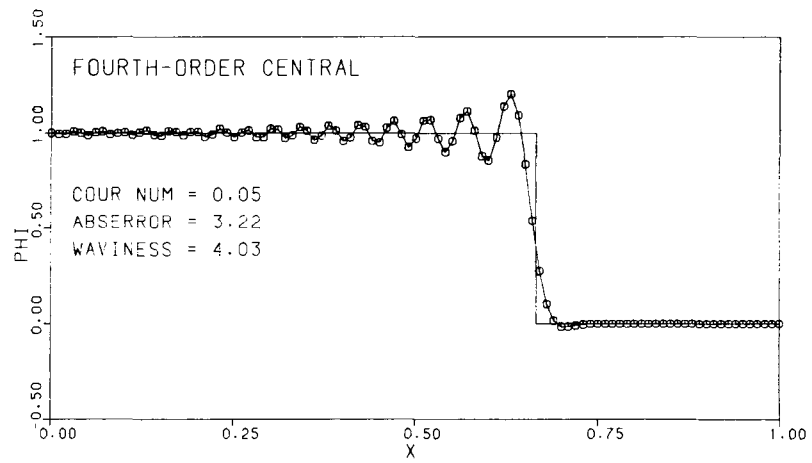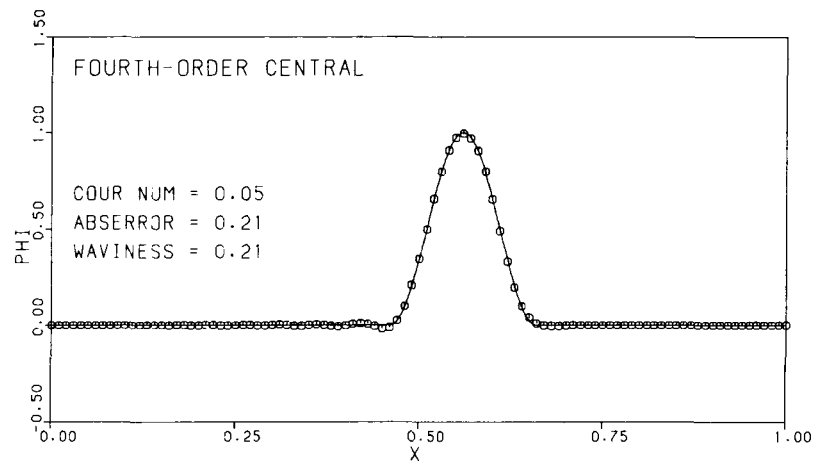
(a) c = 0.05.

FIGURE 8. - RESULTS FOR FOURTH-ORDER CENTRAL.
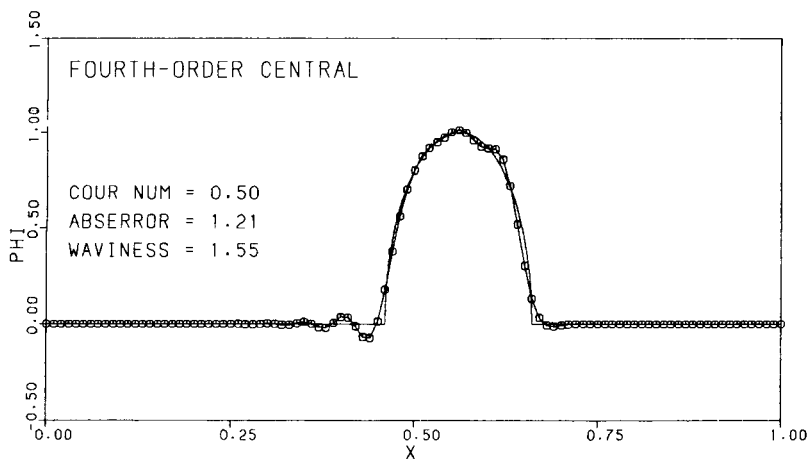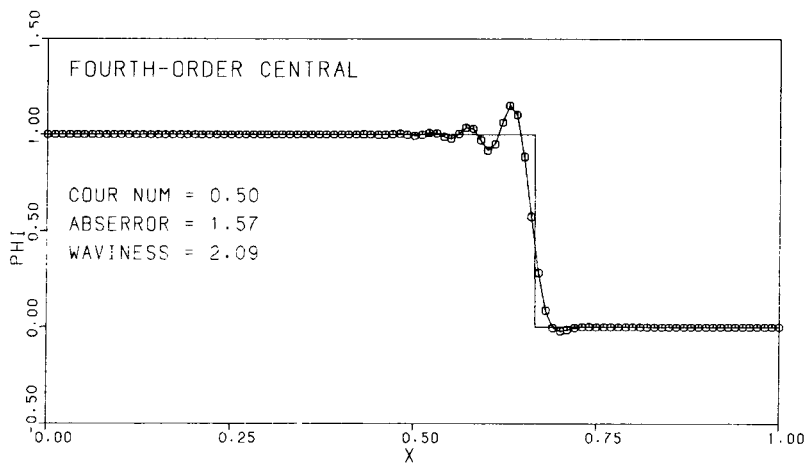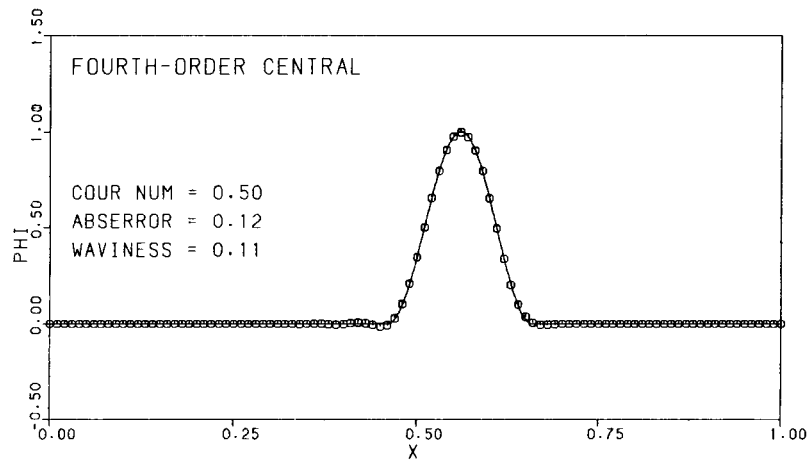
(b) c = 0.5
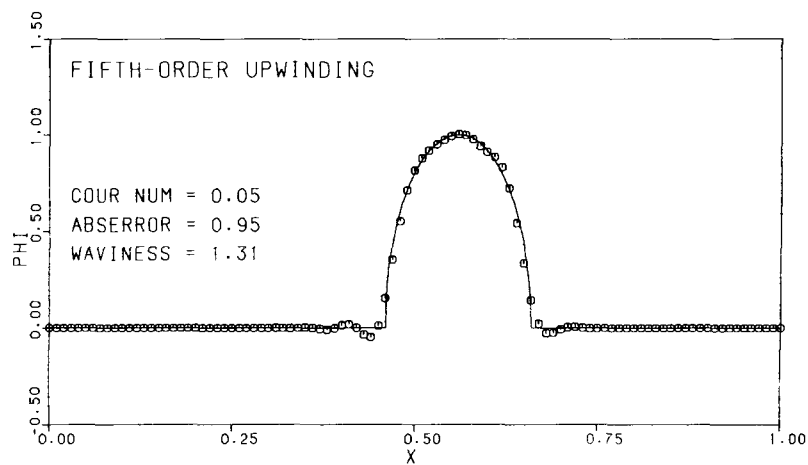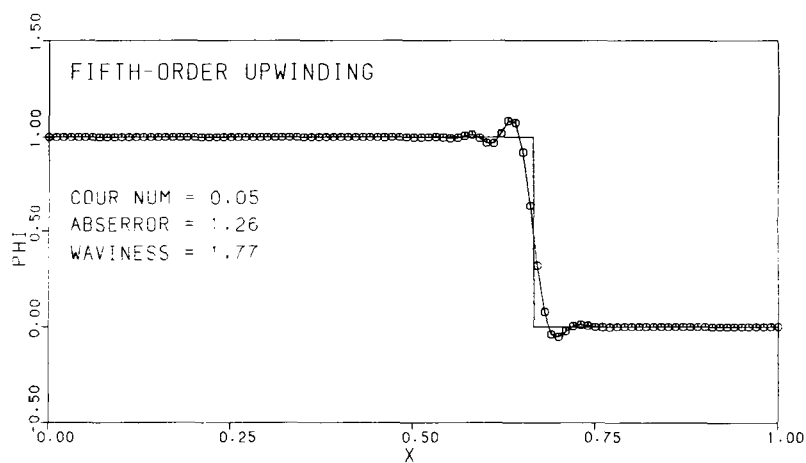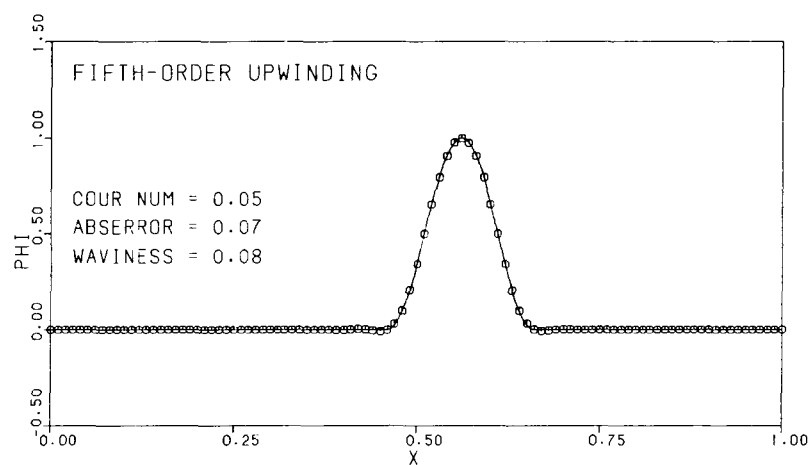
FIGURE 8. - CONCLUDED.

(a) c = 0.05.

FIGURE 9. - RESULTS FOR FIFTH-ORDER UPWINDING.

FIFTH-ORDER UPWINDING

COUR NUM = 0.50
ABSERROR = 0.05
WAVINESS = 0.06

FIFTH-ORDER UPWINDING

COUR NUM = 0.50
ABSERROR = 1.07
WAVINESS = 1.68

FIFTH-ORDER UPWINDING

COUR NUM = 0.50
ABSERROR = 0.81
WAVINESS = 1.22
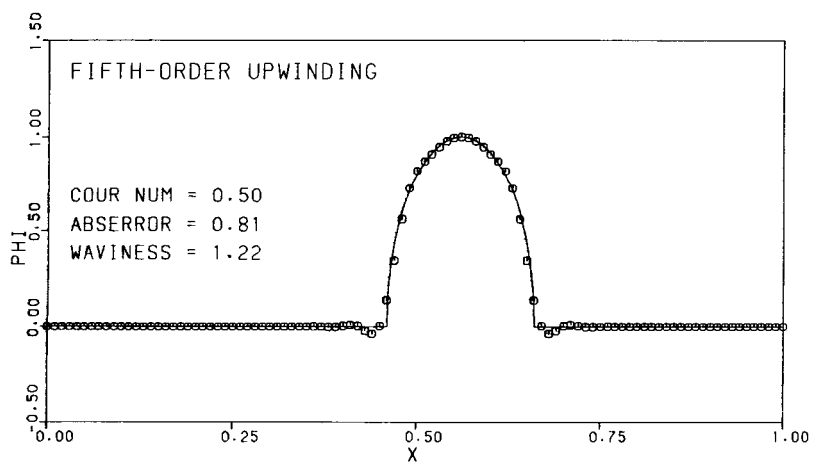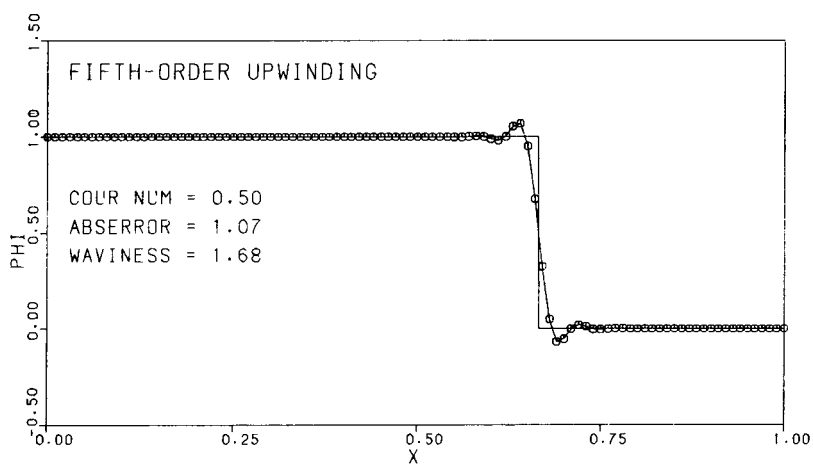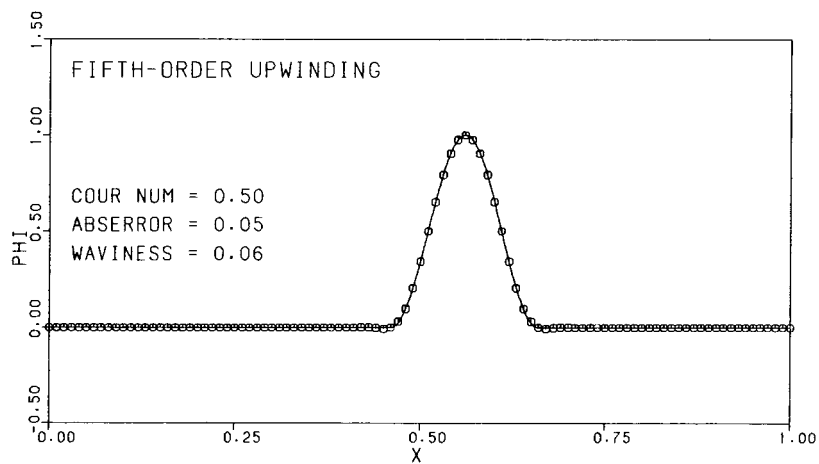
(b) c = 0.5.
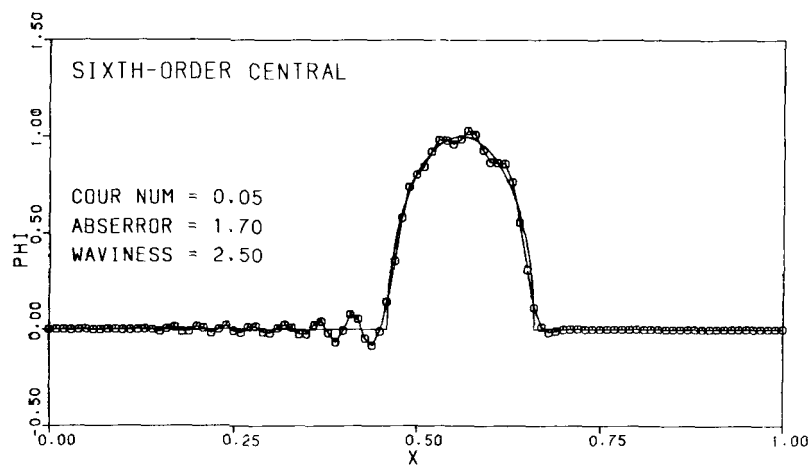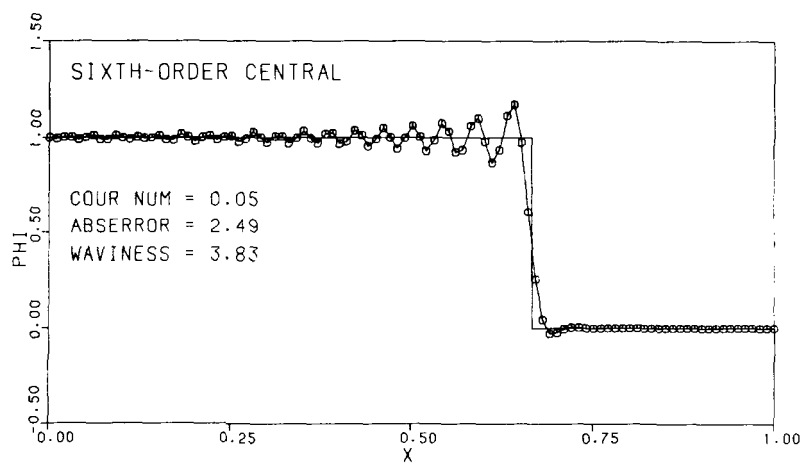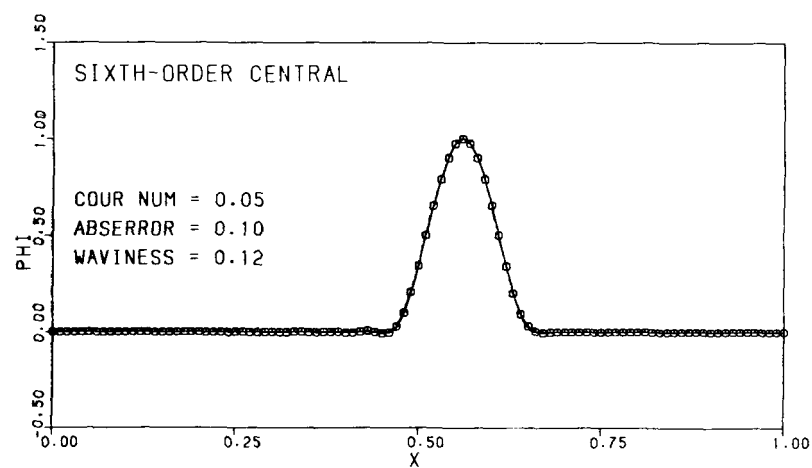
FIGURE 9. - CONCLUDED.

(a) c = 0.05.

FIGURE 10. - RESULTS FOR SIXTH-ORDER CENTRAL.
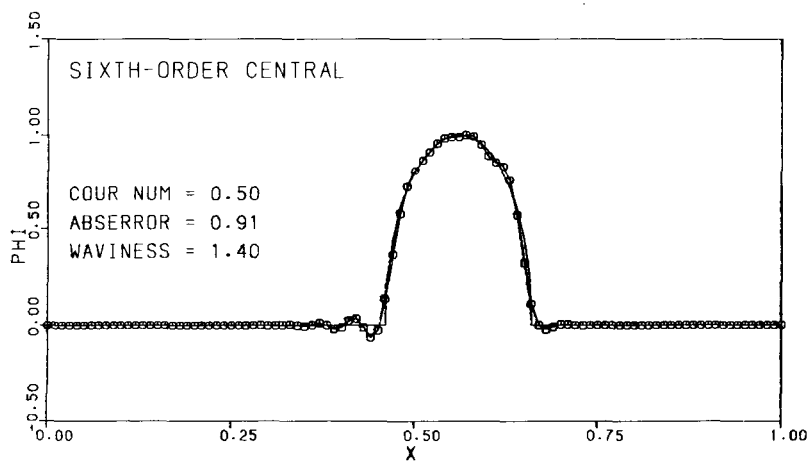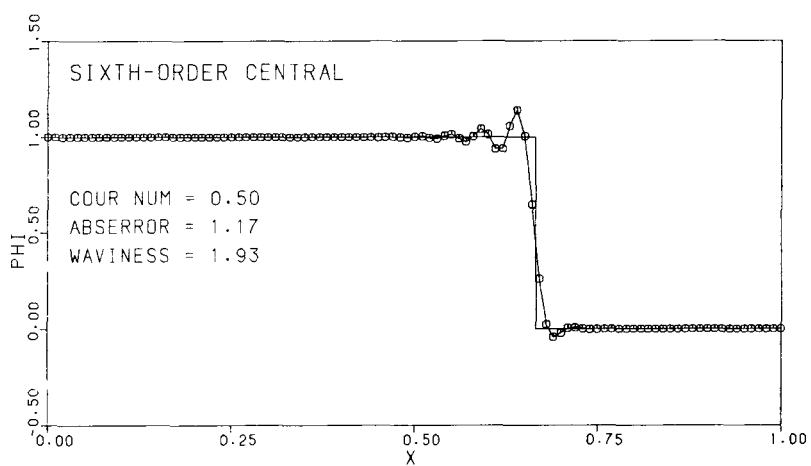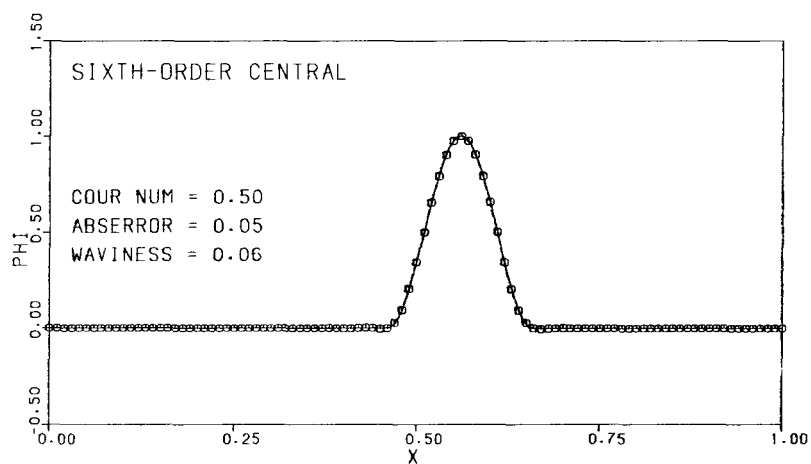
(b) c = 0.5.

FIGURE 10. - CONCLUDED.
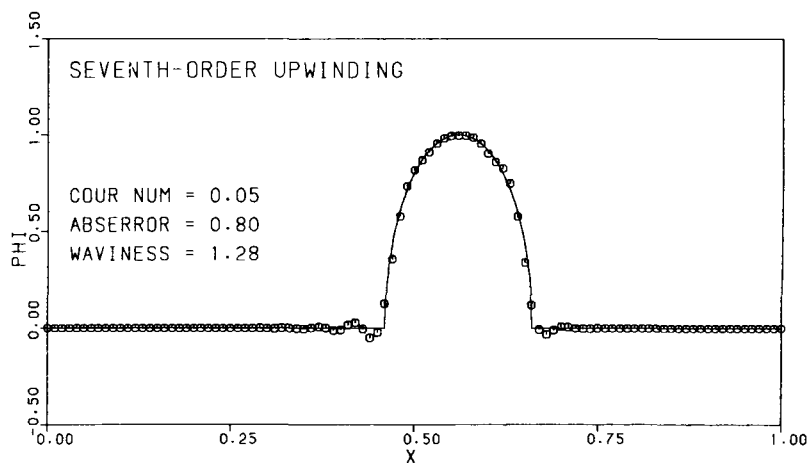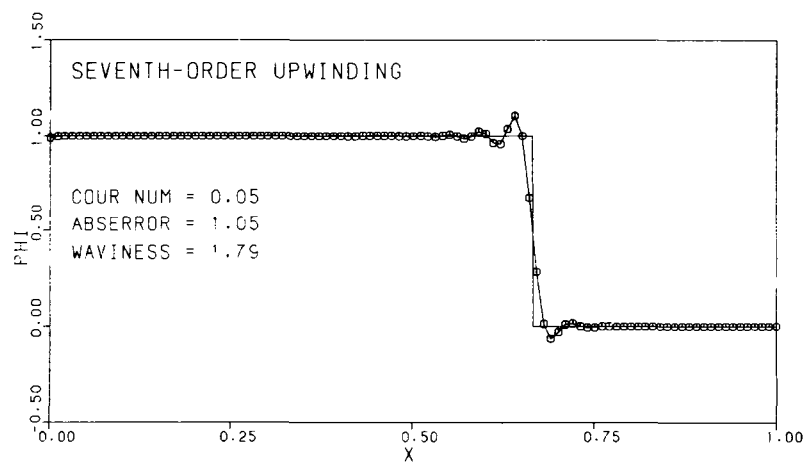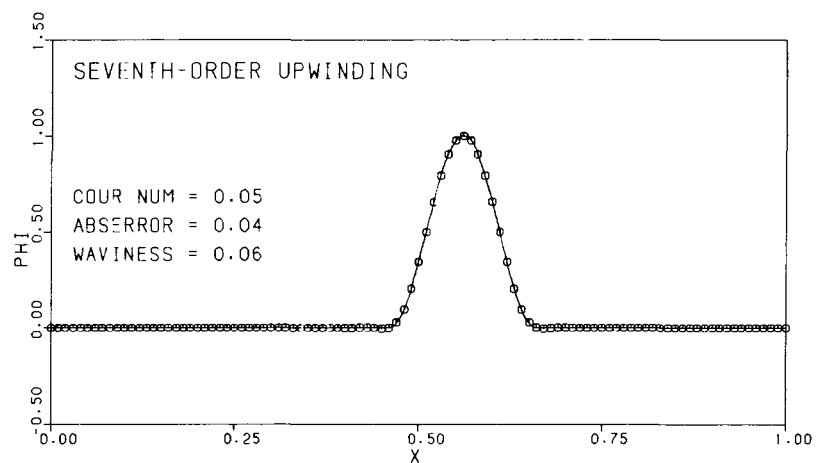
(a) c = 0.05.

FIGURE 11. - RESULTS FOR SEVENTH-ORDER UPWINDING.
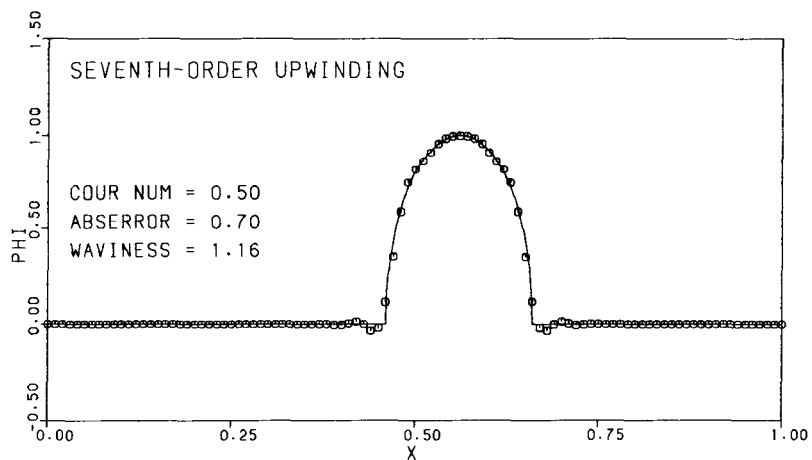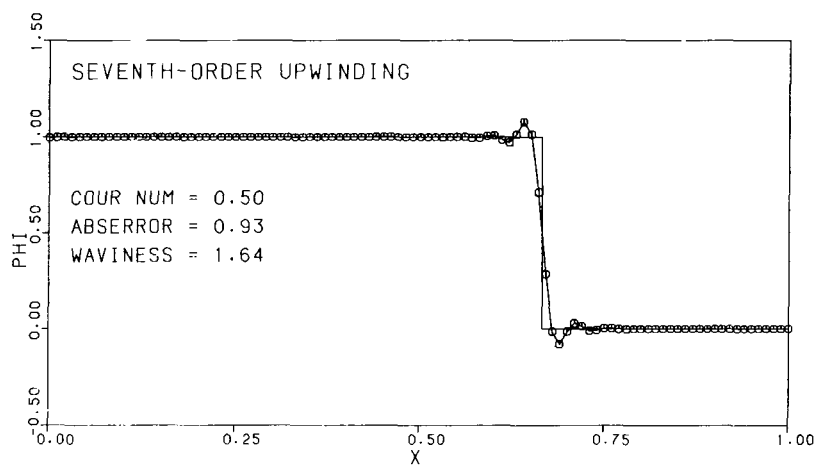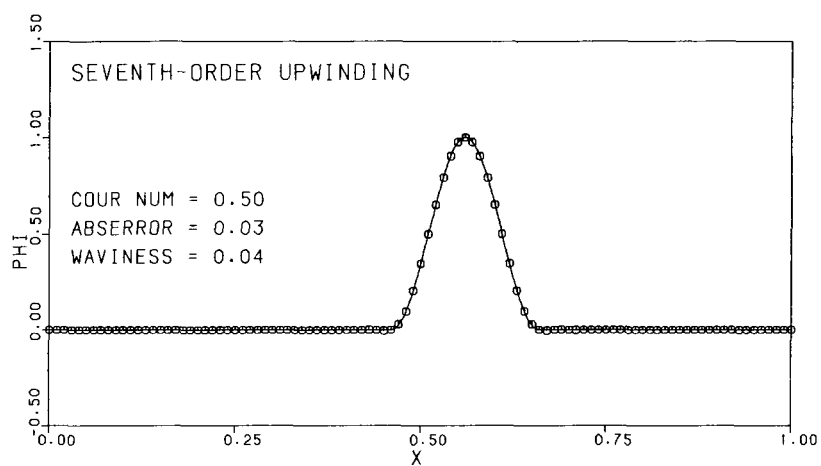
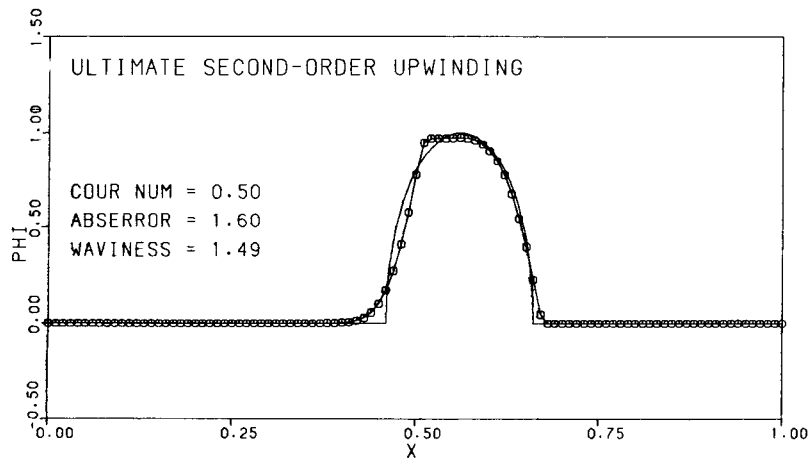(b) c = 0.5.

FIGURE 11. - CONCLUDED.
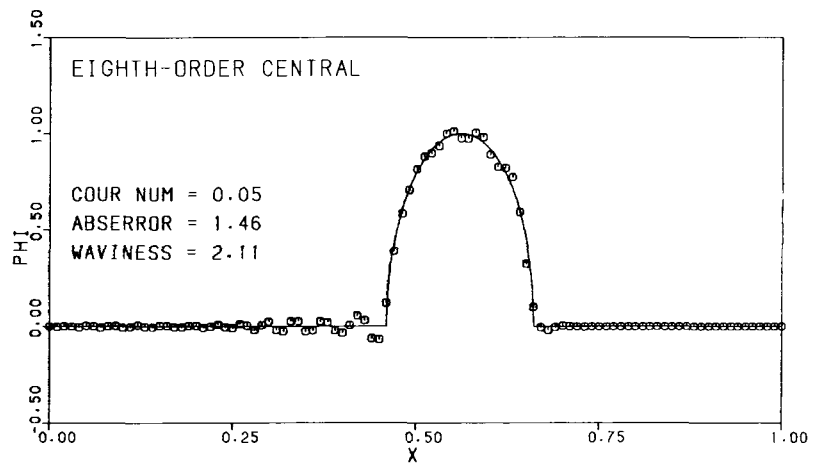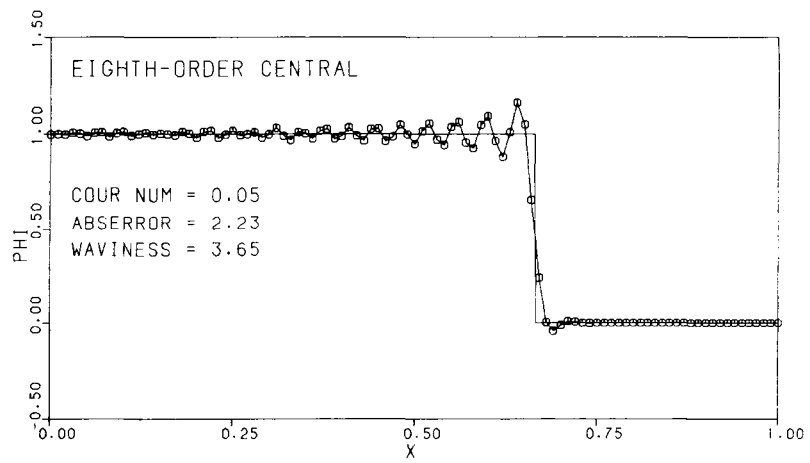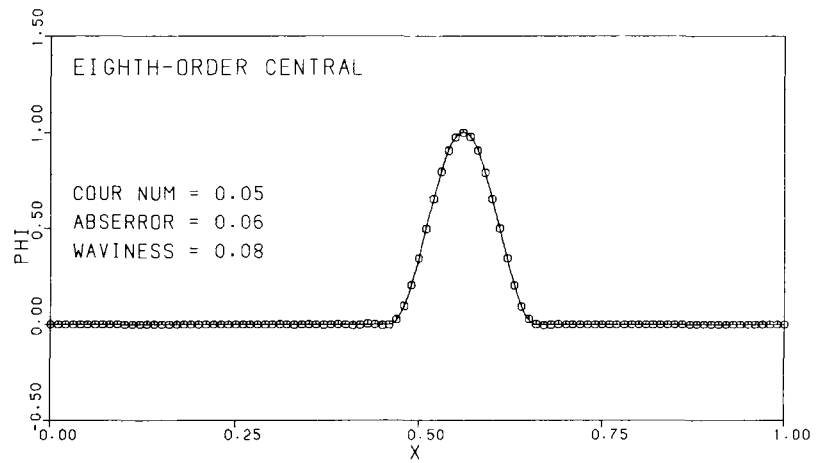
(a) c = 0.05.

FIGURE 12. - RESULTS FOR EIGHTH-ORDER CENTRAL.

64
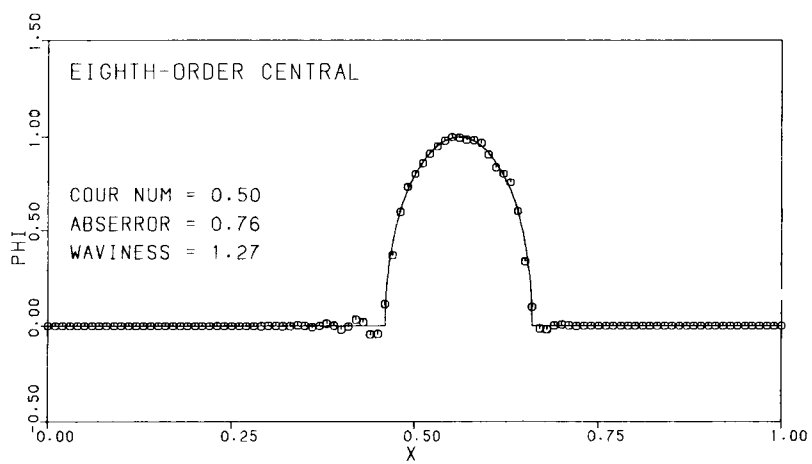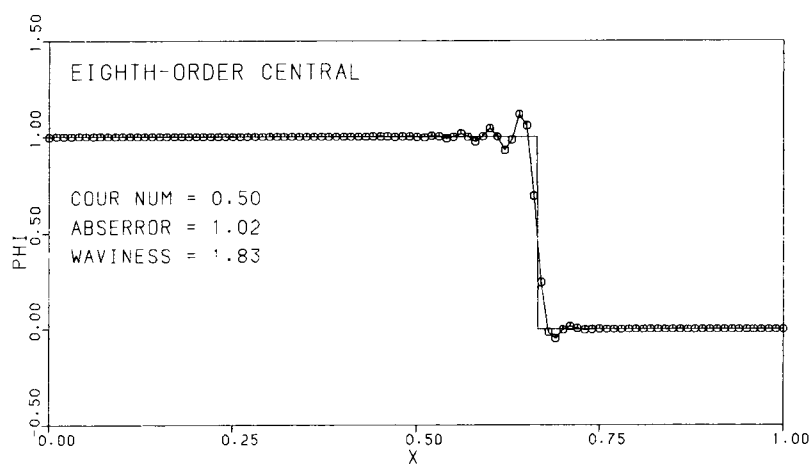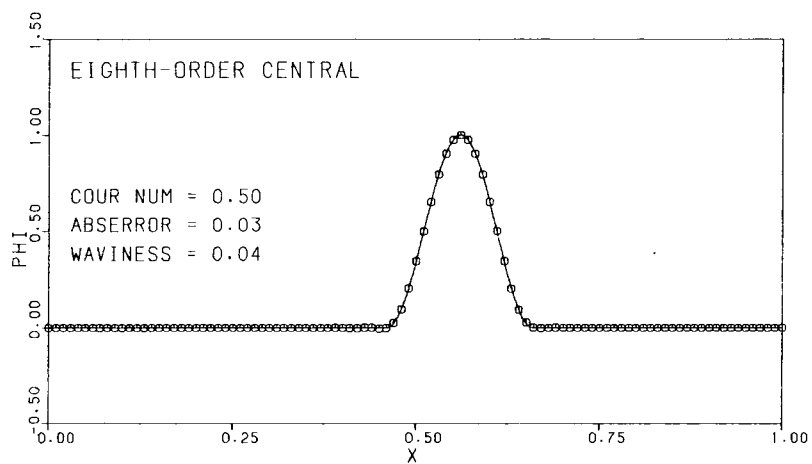
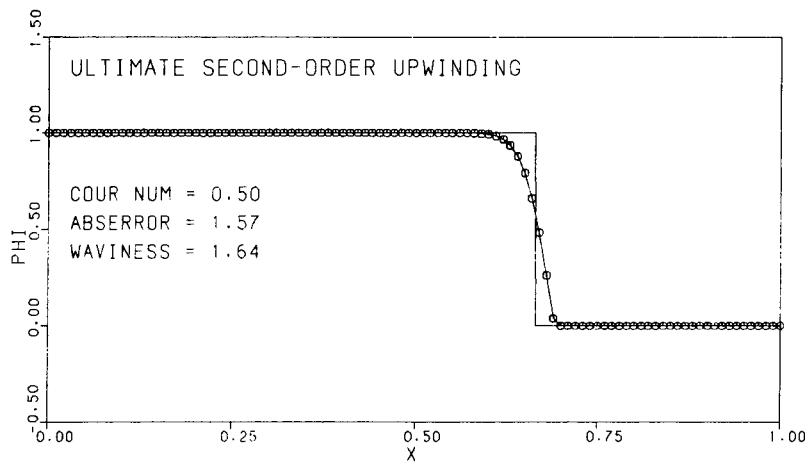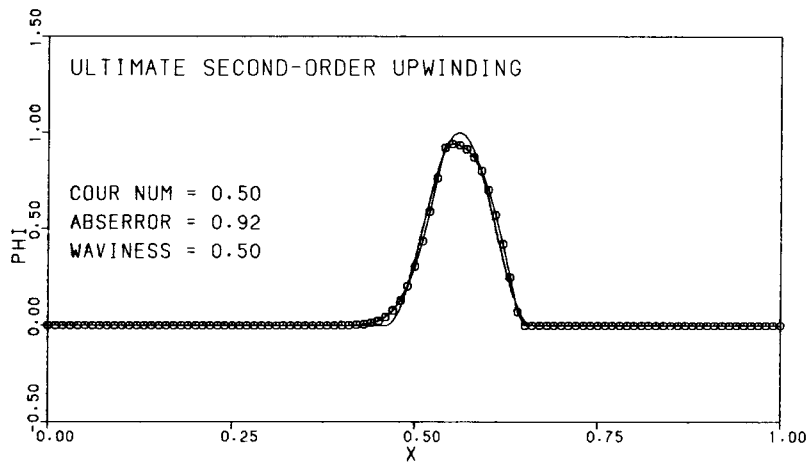(b) c = 0.5.

FIGURE 12. - CONCLUDED.

(a) $u_f > 0$. (b) $u_f < 0$.
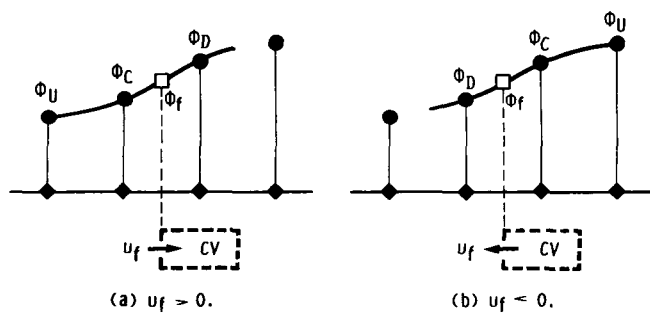
FIGURE 13. – DEFINITION OF UPSTREAM (U), DOWNSTREAM (D), AND CENTRAL
(C) NODES, DEPENDING ON SGN(u_f).
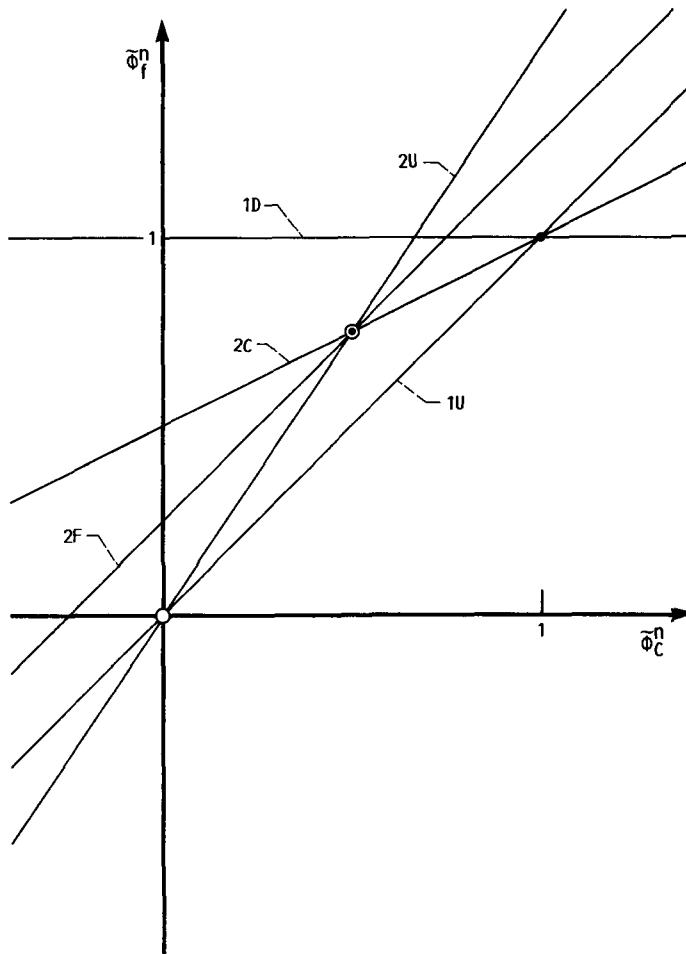
FIGURE 14. - NORMALIZED VARIABLE DIAGRAM SHOWING $\widetilde{\Phi}_f^n$ AS A FUNCTION OF $\widetilde{\Phi}_C^n$ FOR FIRST-ORDER UPWINDING (1U). LAX-WENDROFF (2C), SECOND-ORDER UP-WINDING (2U), FROMM'S METHOD (2F), AND FIRST-ORDER DOWNWINDING (1D).
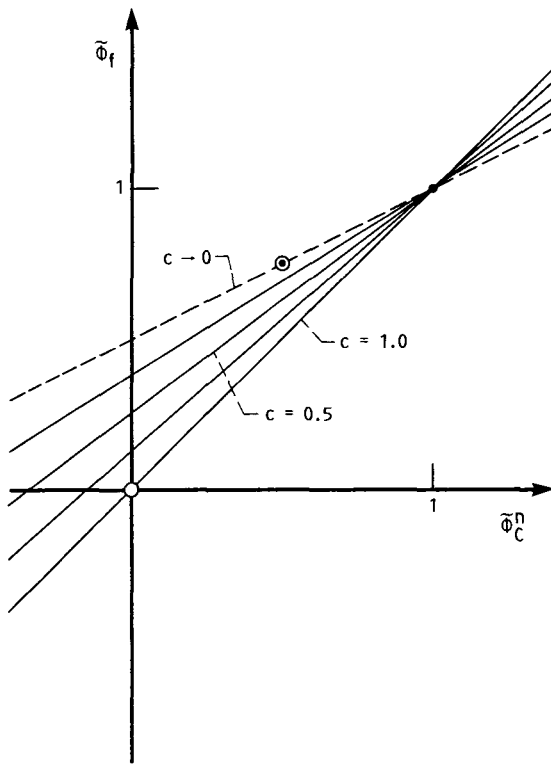
FIGURE 15. - NORMALIZED VARIABLE DIAGRAM (NVD) FOR THE
LAX-WENDROFF METHOD; $\widetilde{\Phi}_f$ AS A FUNCTION OF $\widetilde{\Phi}_C^n$ FOR
$c \to 0$, $c = 0.25$, 0.5, 0.75, AND 1.
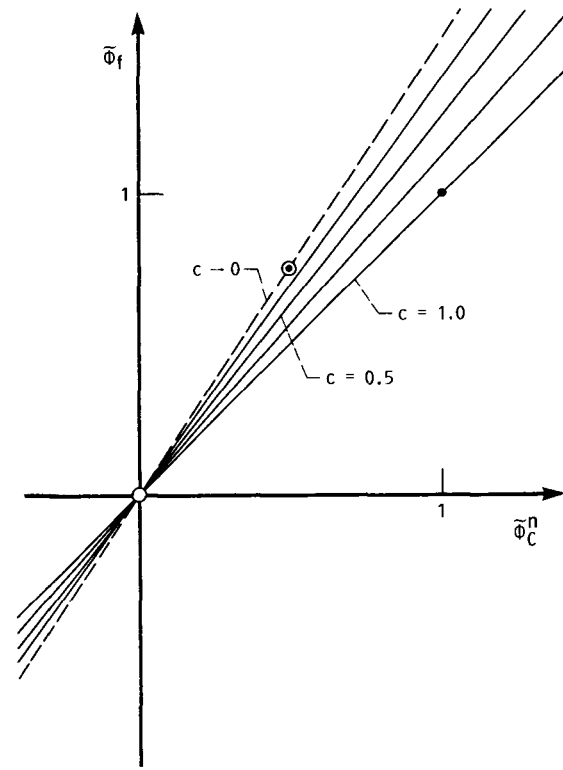
FIGURE 16. - NVD FOR SECOND-ORDER UPWINDING; $\widetilde{\Phi}_f$ AS A
FUNCTION OF $\widetilde{\Phi}_C^n$ FOR $c \to 0$, $c = 0.25$, 0.5, 0.75,
AND 1.
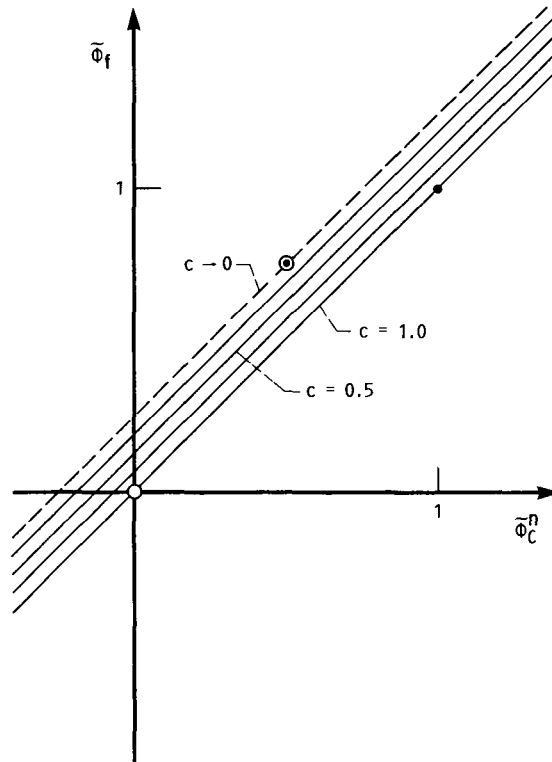
FIGURE 17. - NVD FOR FROMM'S METHOD; $\widetilde{\Phi}_f$ AS A FUNCTION OF
$\widetilde{\Phi}_C^n$ FOR $c \to 0$, $c = 0.25$, 0.5, 0.75, AND 1.
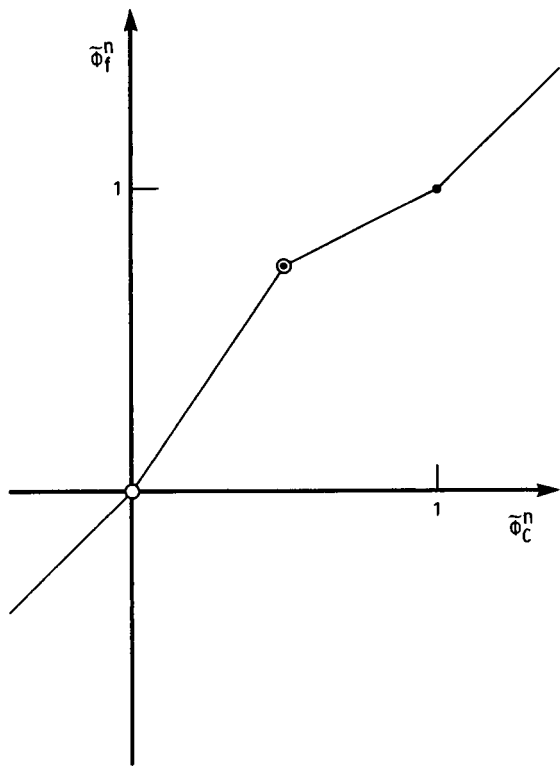
(a) $\widetilde{\Phi}_f^n$ AS A FUNCTION OF $\widetilde{\Phi}_C^n$.
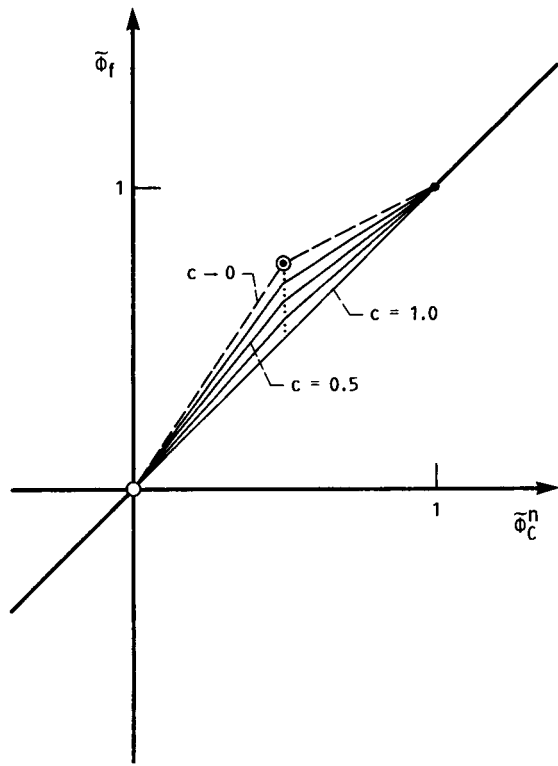
(b) $\widetilde{\Phi}_f$ AS A FUNCTION OF $\widetilde{\Phi}_C^n$ AND c.

FIGURE 18. - NVDs FOR THE MINMOD SCHEME.
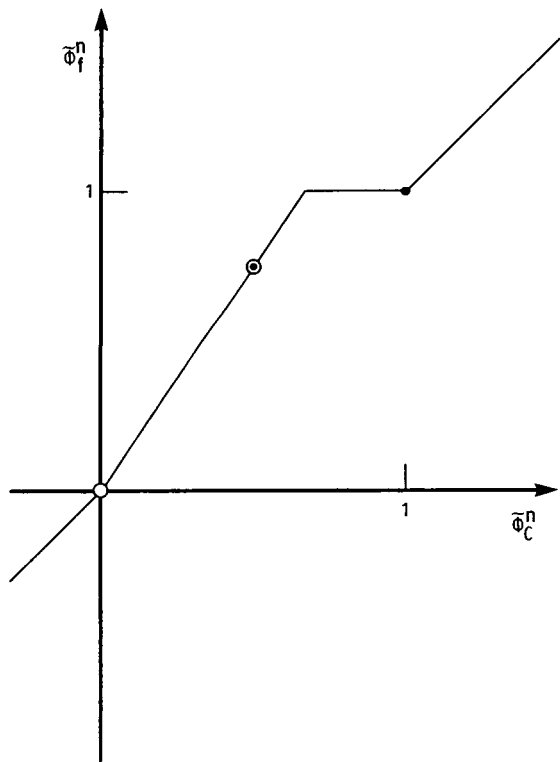
(a) $\widetilde{\Phi}_f^n$ AS A FUNCTION OF $\widetilde{\Phi}_C^n$.
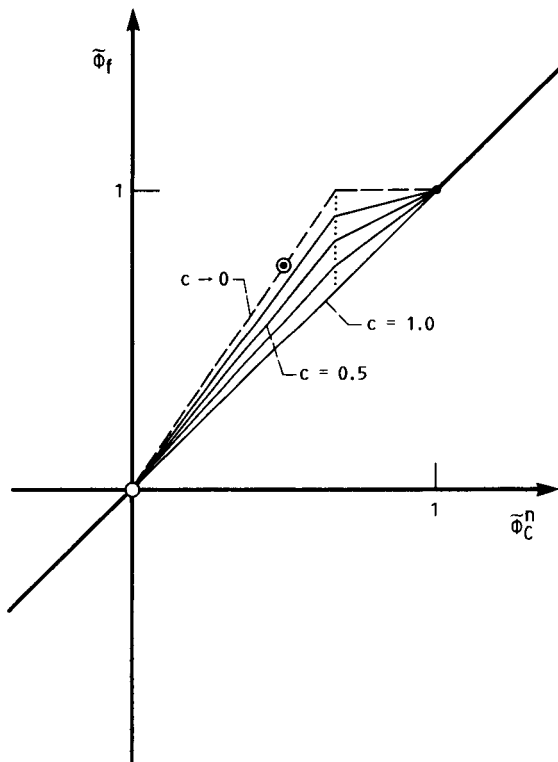
(b) $\widetilde{\Phi}_f$ AS A FUNCTION OF $\widetilde{\Phi}_C^n$ AND c.

FIGURE 19. - NVDs FOR THE CHAKRAVARTHY-OSHER SCHEME.
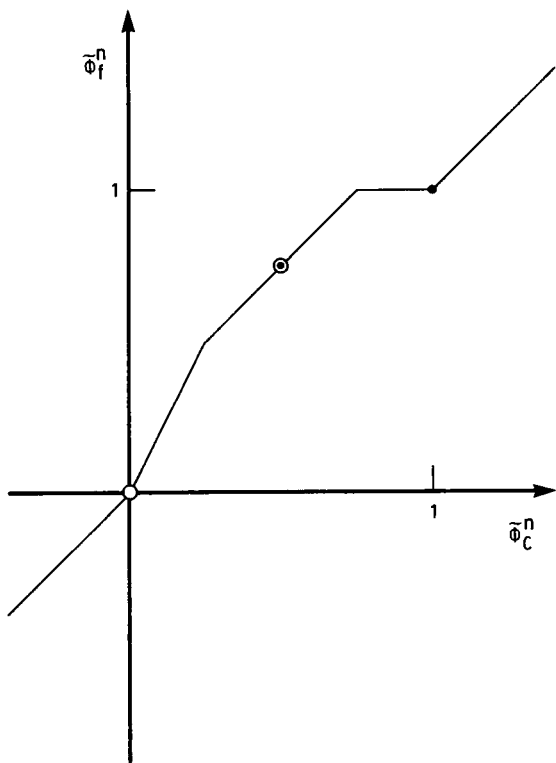
(a) $\widetilde{\Phi}_f^n$ AS A FUNCTION OF $\widetilde{\Phi}_C^n$.
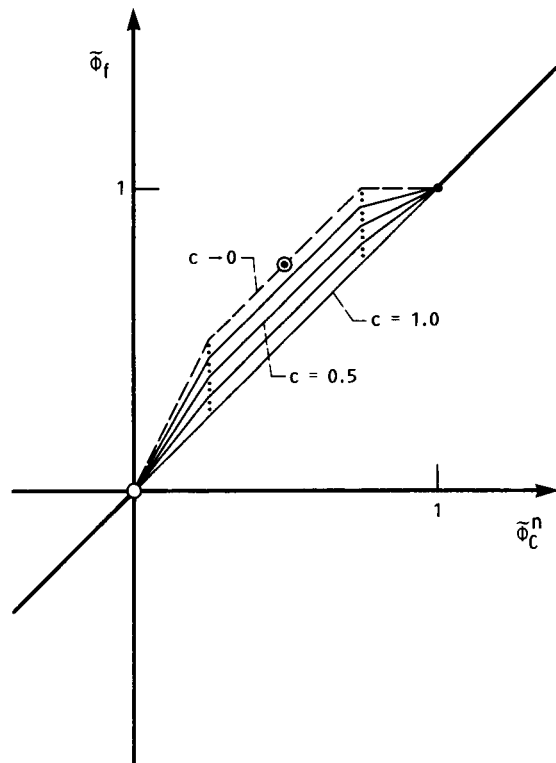
(b) $\widetilde{\Phi}_f$ AS A FUNCTION OF $\widetilde{\Phi}_C^n$ AND c.

FIGURE 20. - NVDs FOR VAN LEER'S MUSCL.
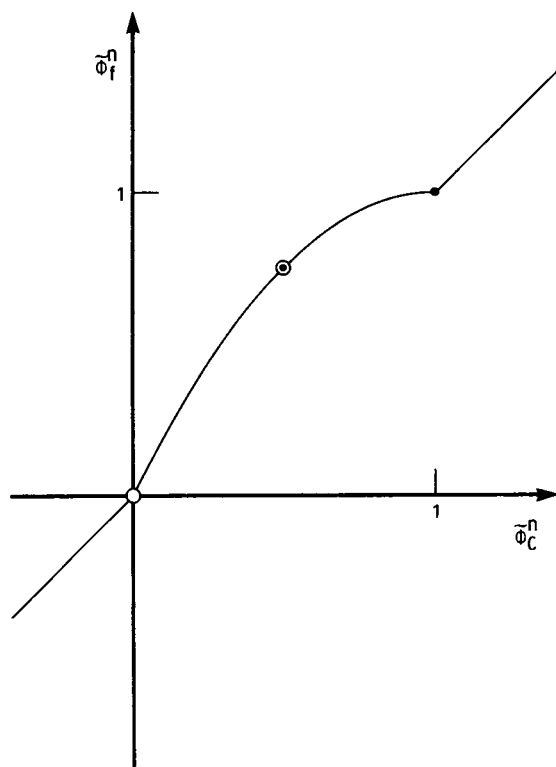
(a) $\widetilde{\Phi}_f^n$ AS A FUNCTION OF $\widetilde{\Phi}_C^n$.
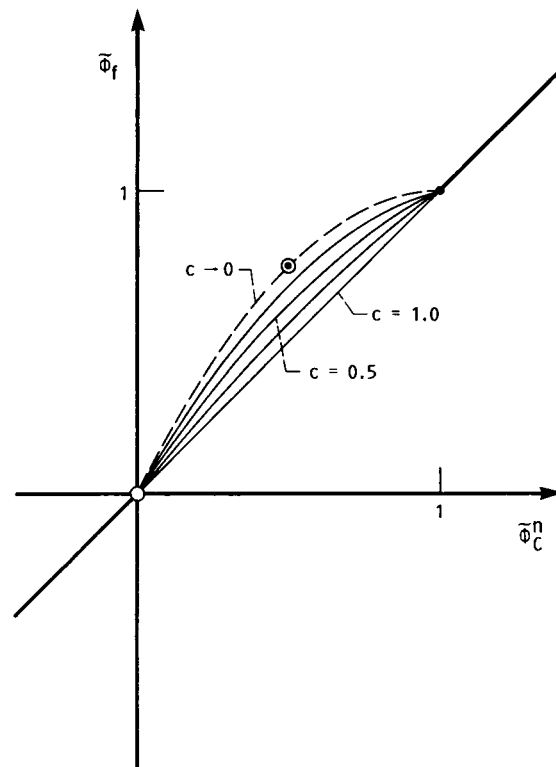
(b) $\widetilde{\Phi}_f$ AS A FUNCTION OF $\widetilde{\Phi}_C^n$ AND c.

FIGURE 21. - NVDs FOR VAN LEER'S CLAM.
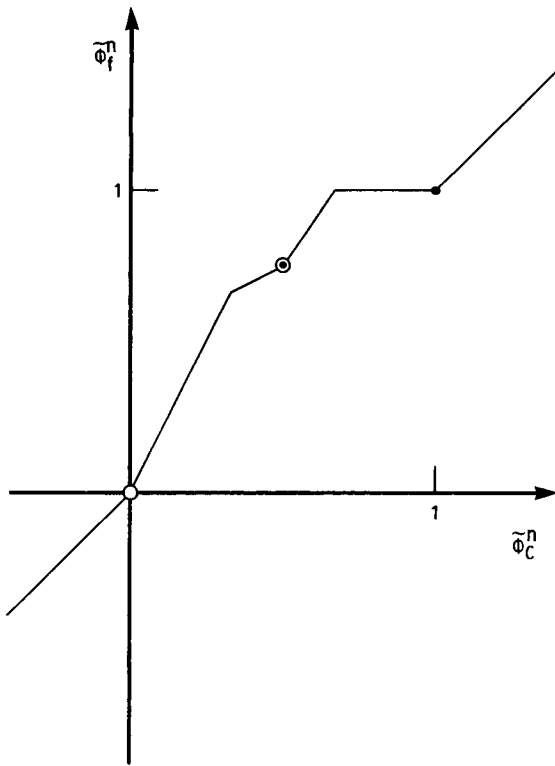
(a) $\widetilde{\Phi}_f^n$ AS A FUNCTION OF $\widetilde{\Phi}_C^n$.
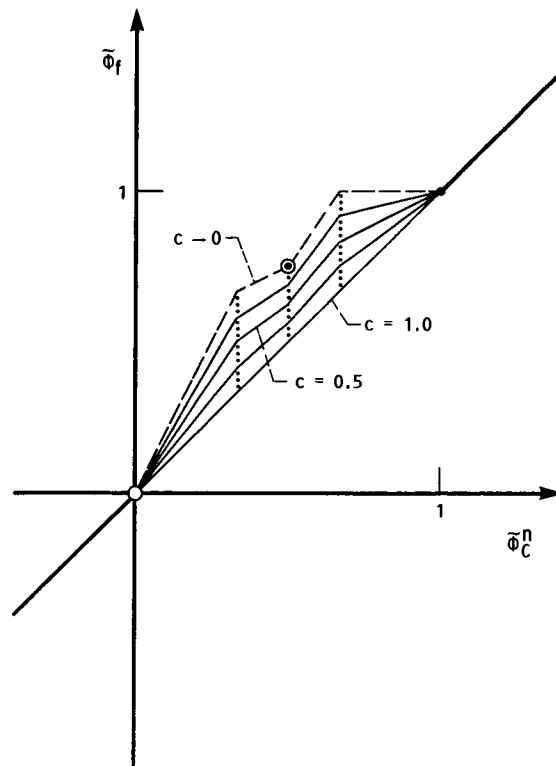
(b) $\widetilde{\Phi}_f$ AS A FUNCTION OF $\widetilde{\Phi}_C^n$ AND c.

FIGURE 22. - NVDs FOR ROE'S SUPERBEE.
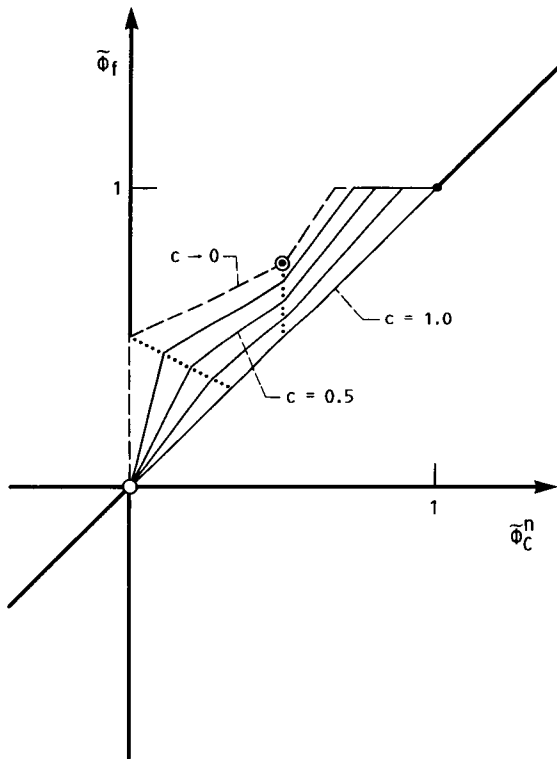
(a) SUPER-C.
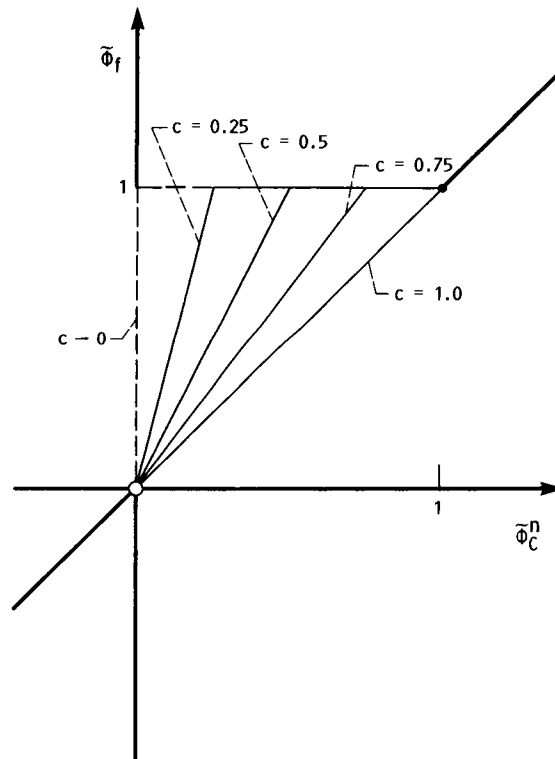
(b) HYPER-C.

FIGURE 23. - NVDs IN THE $\left(\widetilde{\Phi}_C^n, \widetilde{\Phi}_f\right)$ PLANE.
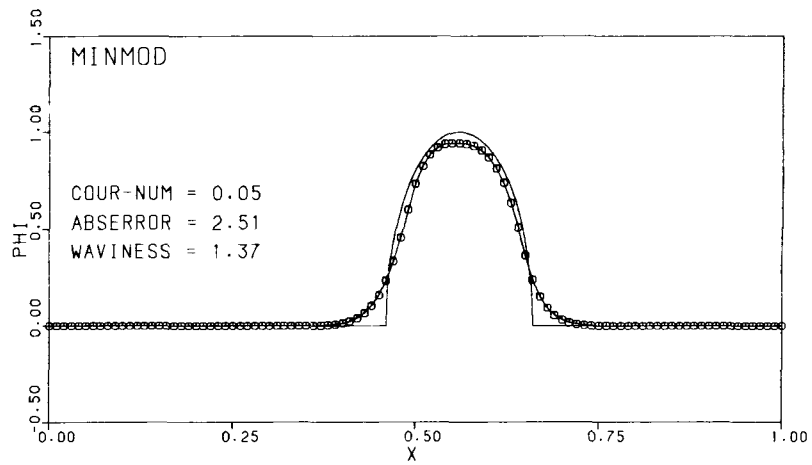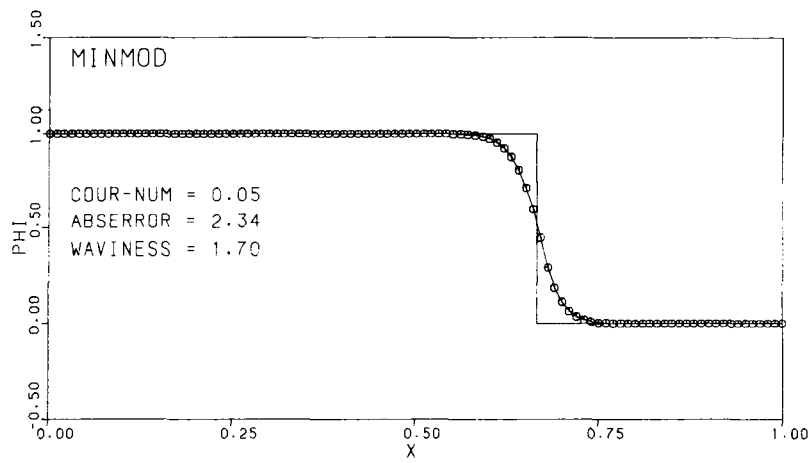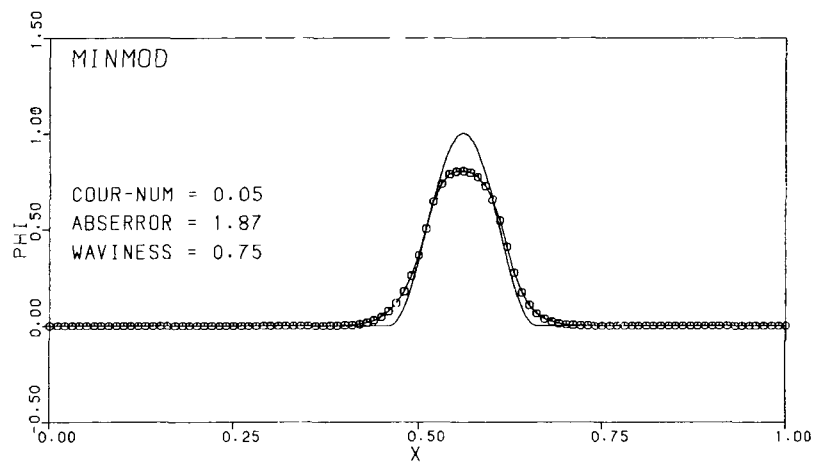
(a) c = 0.05.

FIGURE 24. - RESULTS FOR THE MINMOD SCHEME.
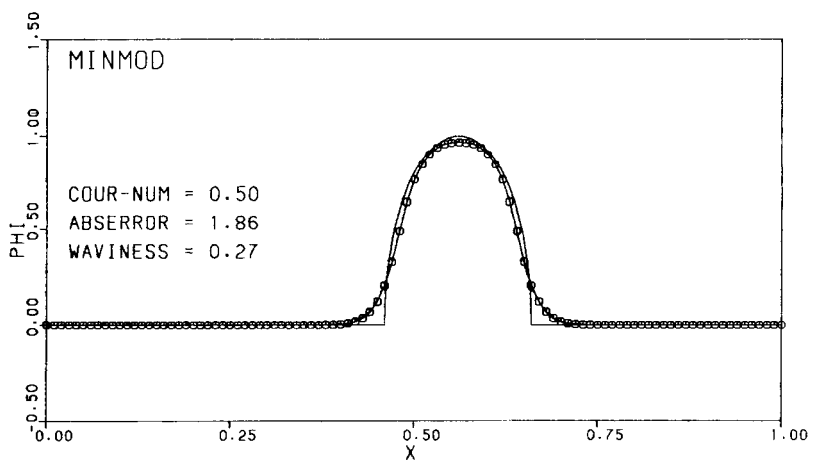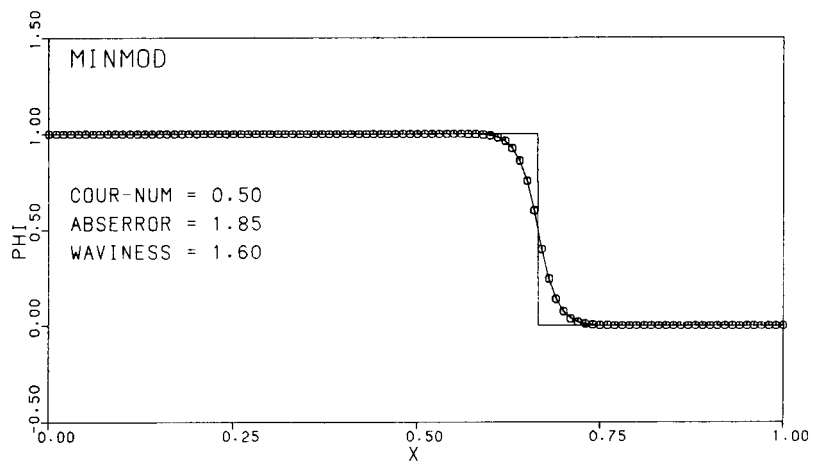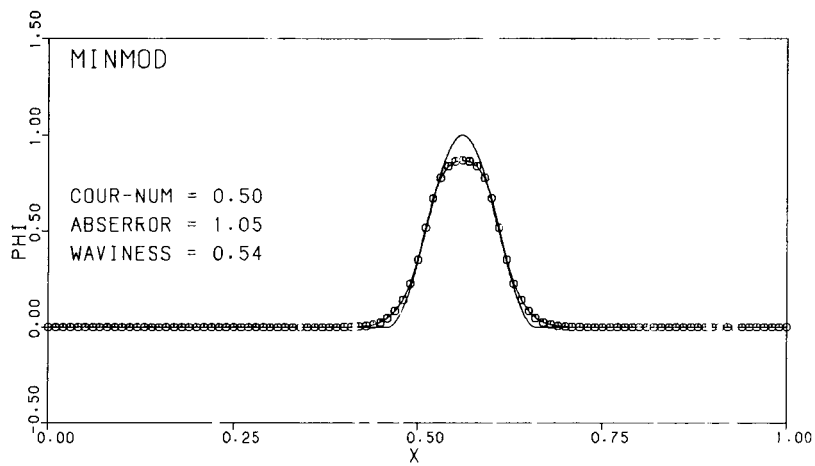
(b) c = 0.5.

FIGURE 24. - CONCLUDED.
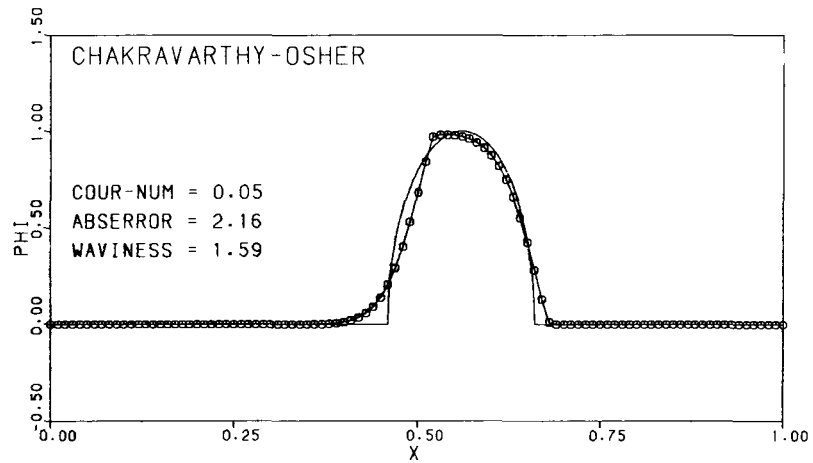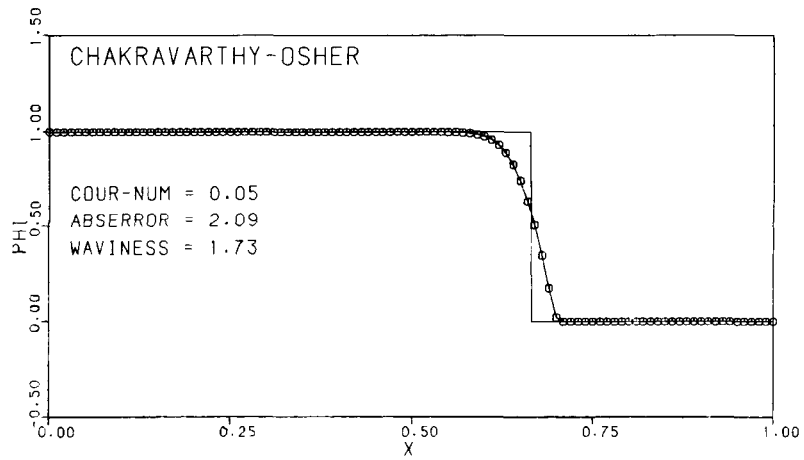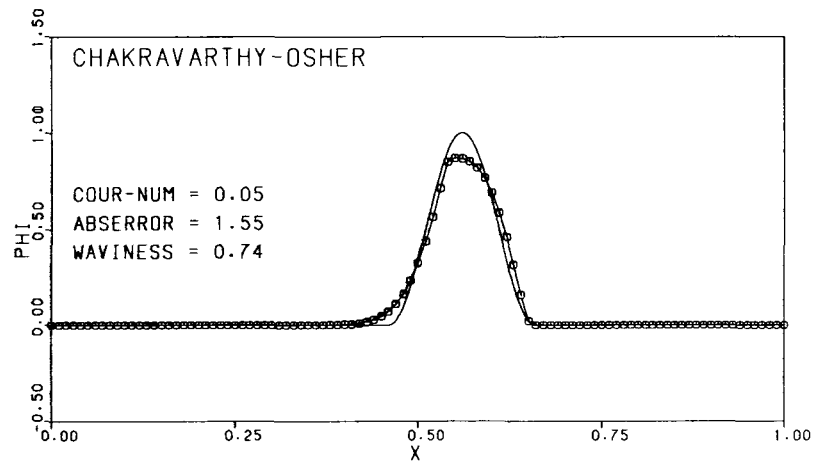
(a) c = 0.05.

FIGURE 25. - RESULTS FOR THE CHAKRAVARTHY-OSHER SCHEME.
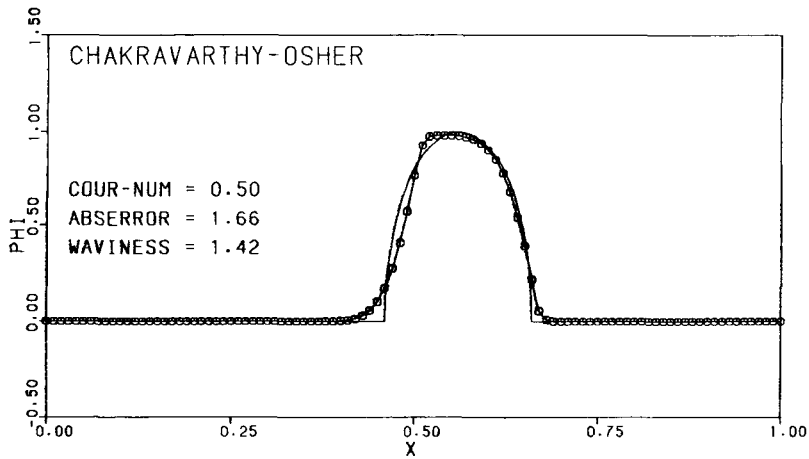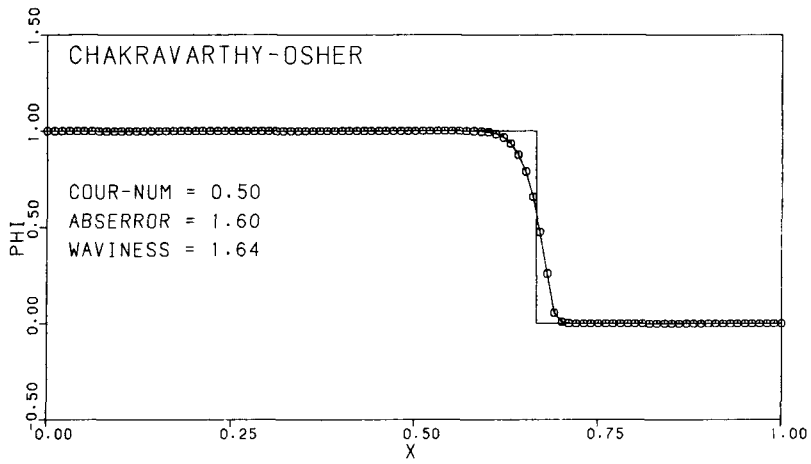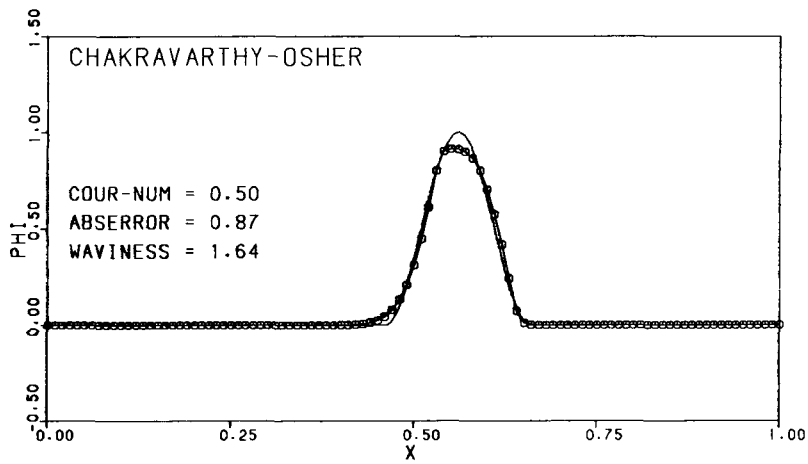
(b) c = 0.5.

FIGURE 25. - CONCLUDED.
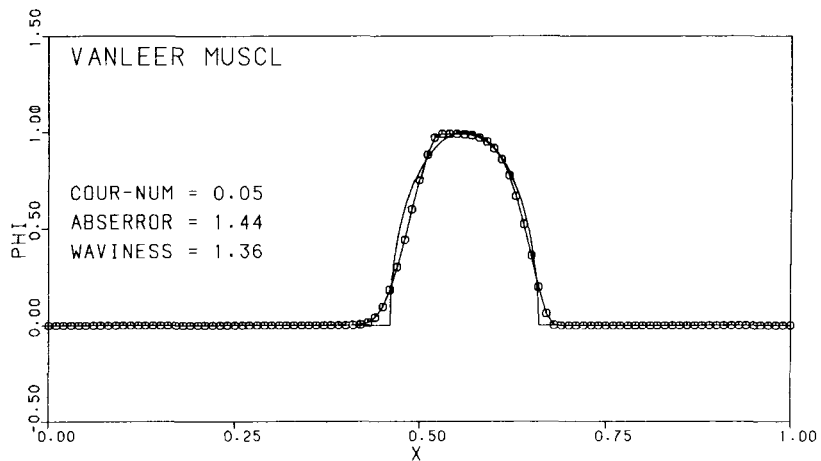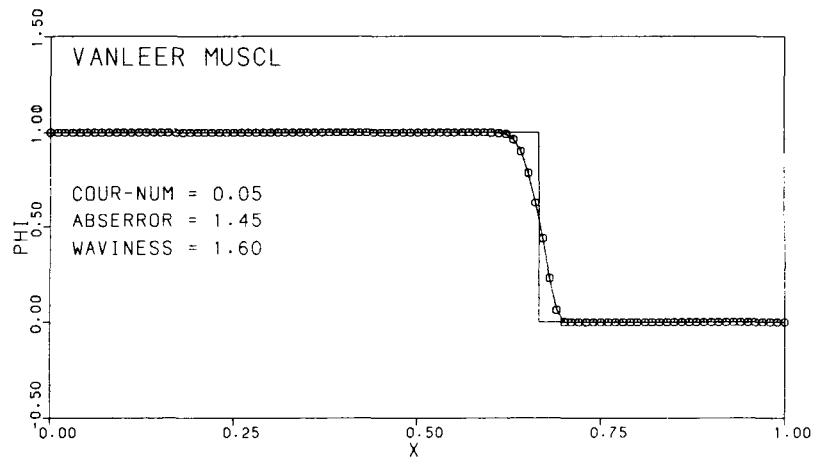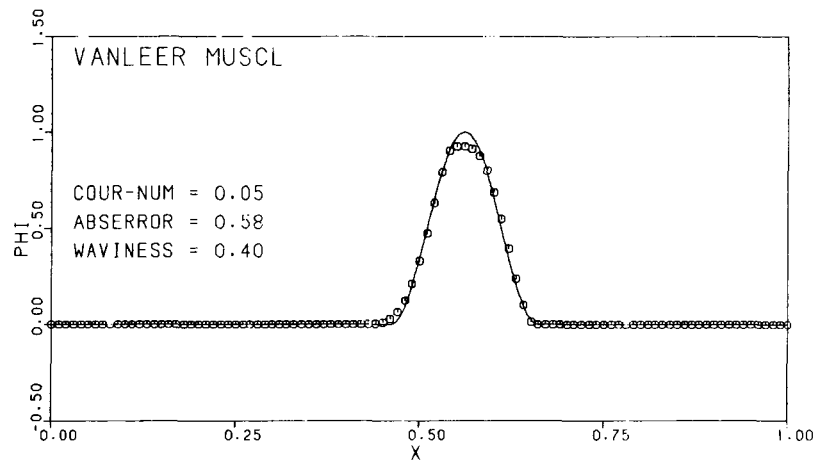
(a) c = 0.05.

FIGURE 26. - RESULTS FOR VAN LEER'S MUSCL.
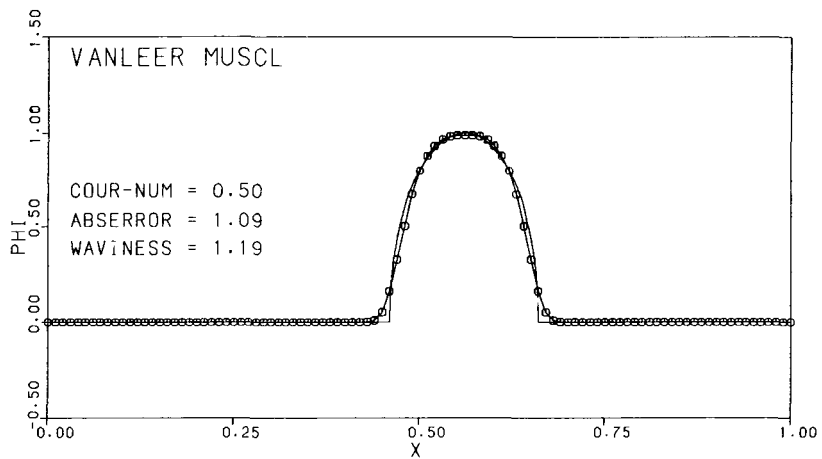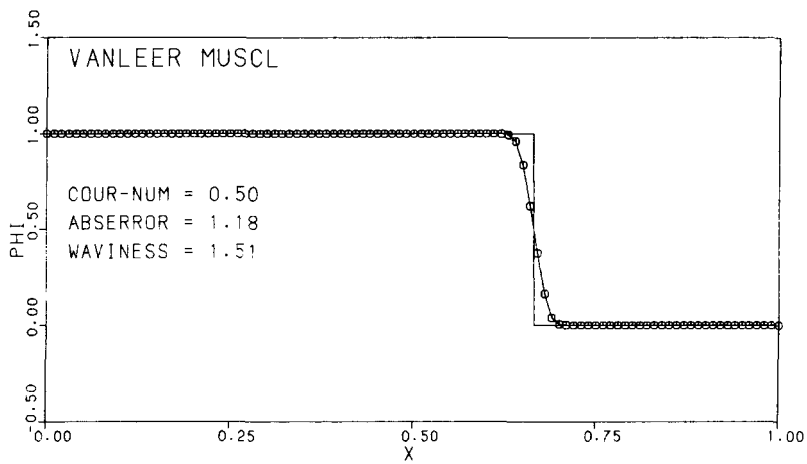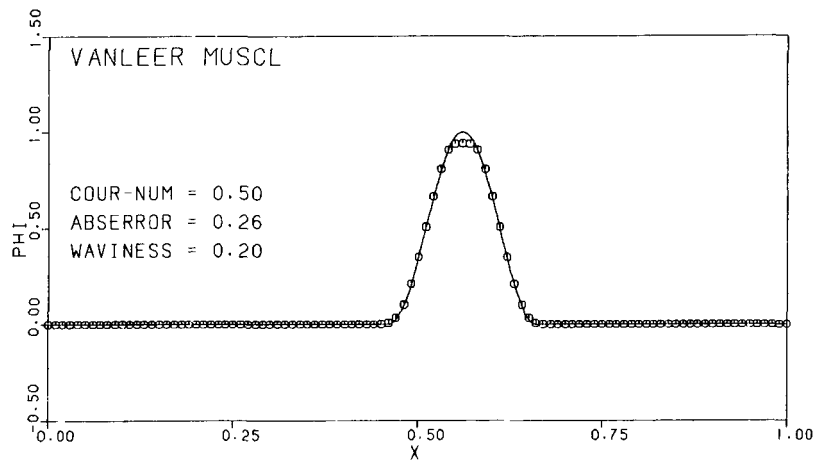
(b) c = 0.5.

FIGURE 26. - CONCLUDED.
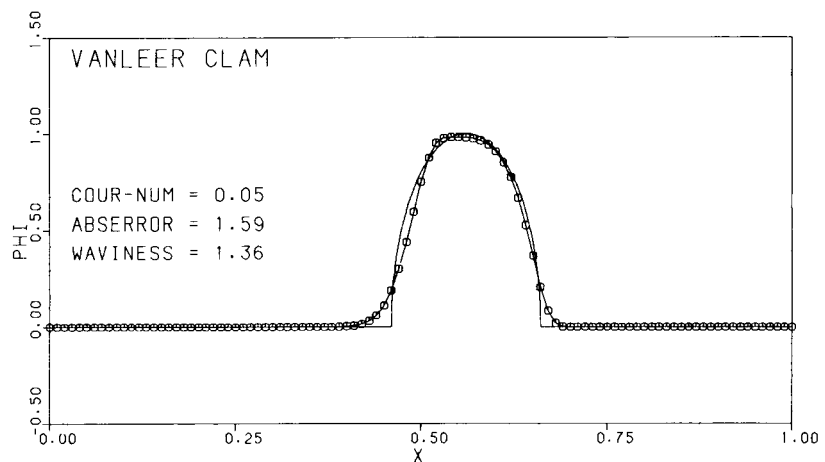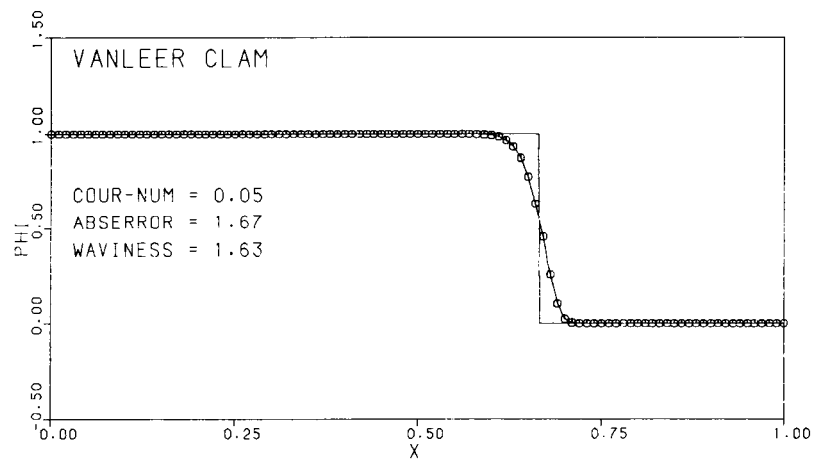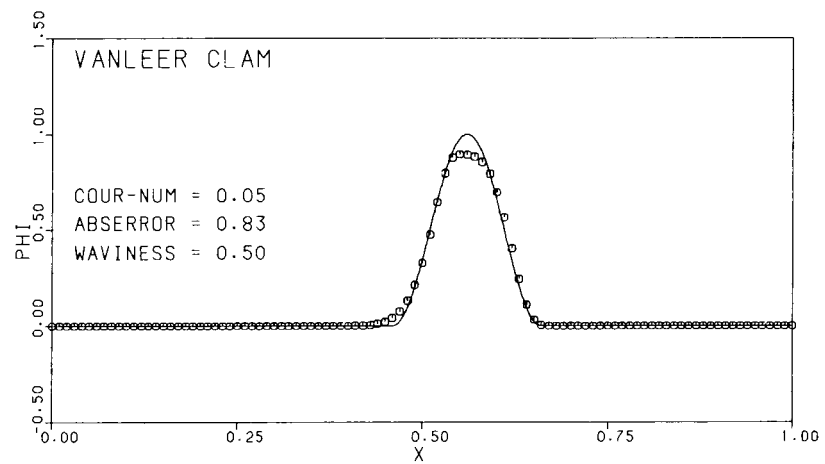
(a) c = 0.05.

FIGURE 27. – RESULTS FOR VAN LEER'S CLAM.
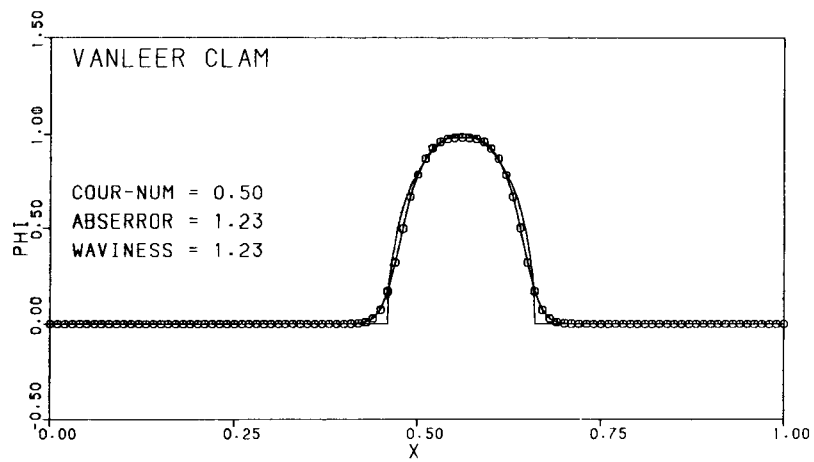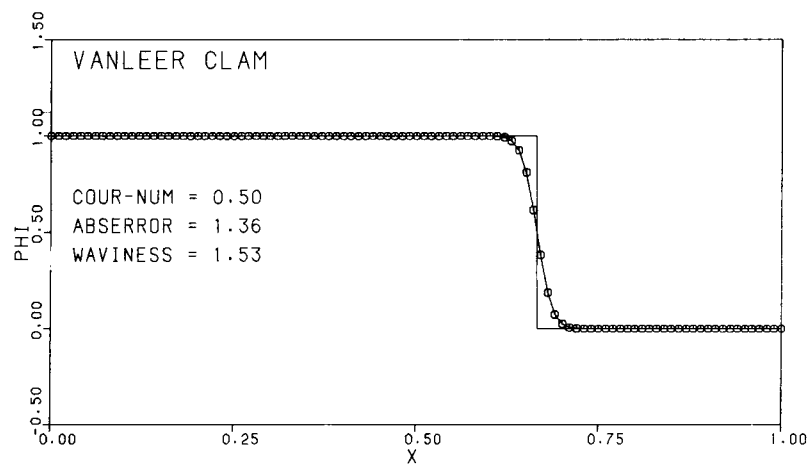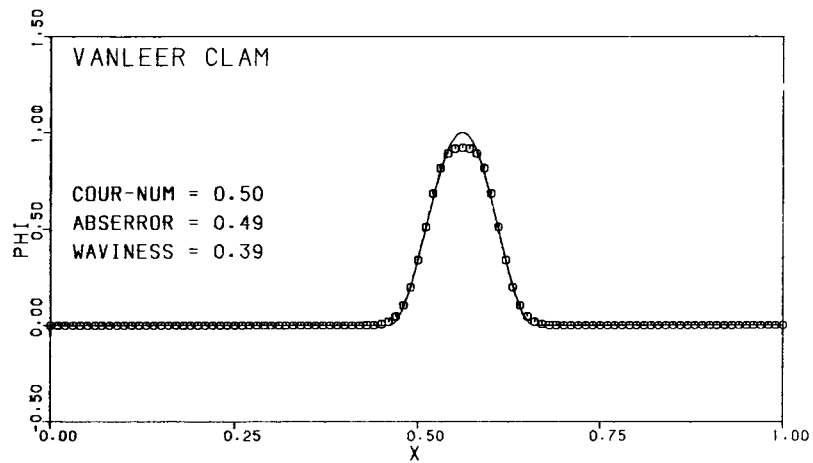
(b) c = 0.5.

FIGURE 27. - CONCLUDED.
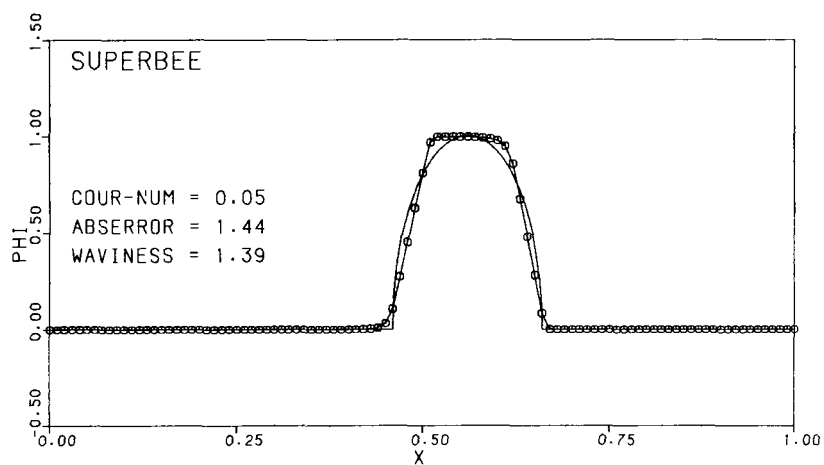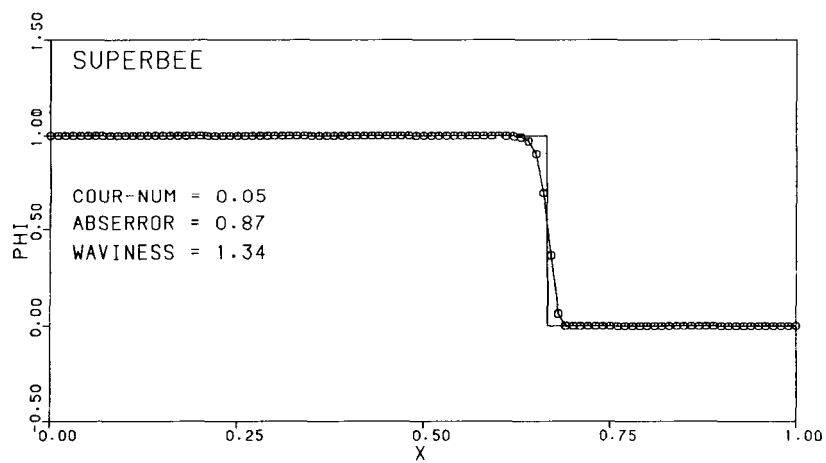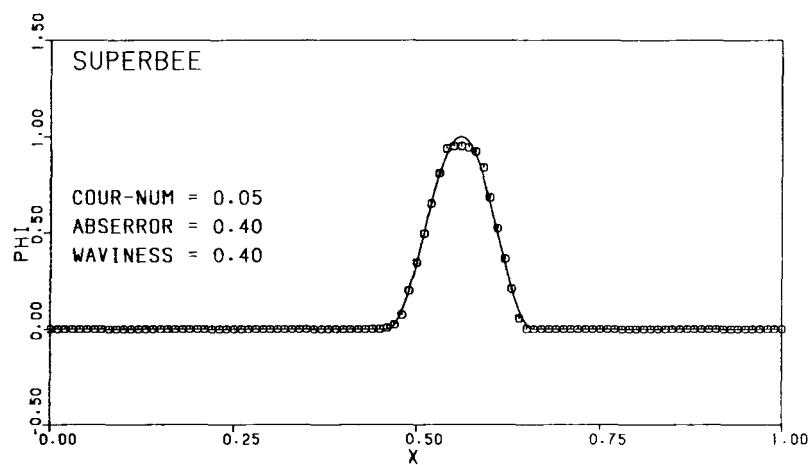
(a) c = 0.05.

FIGURE 28. - RESULTS FOR ROE'S SUPERBEE SCHEME.
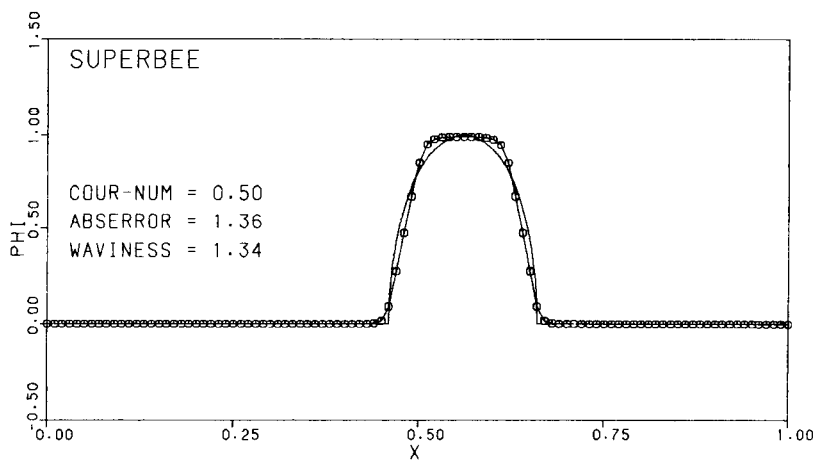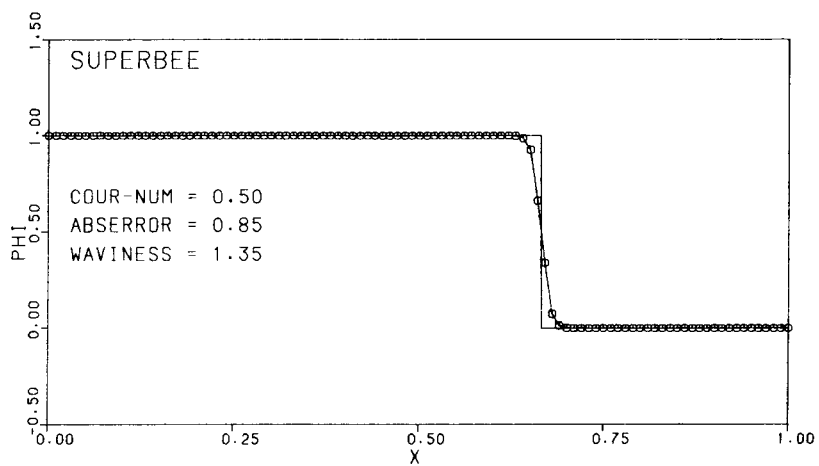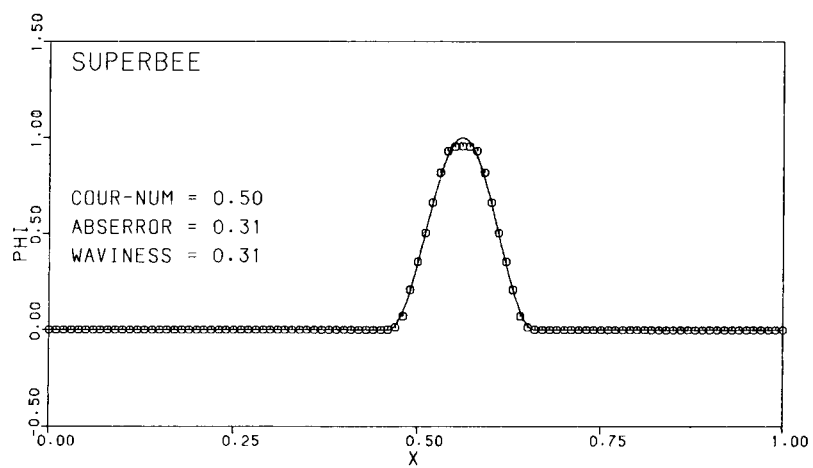
(b) c = 0.5.

FIGURE 28. - CONCLUDED.
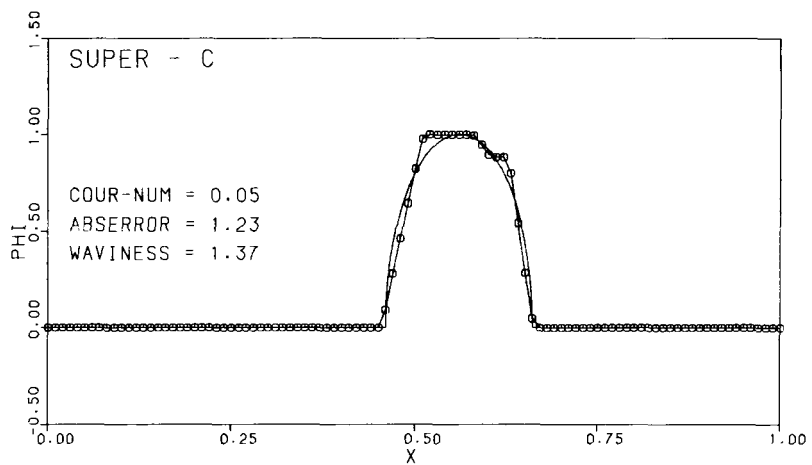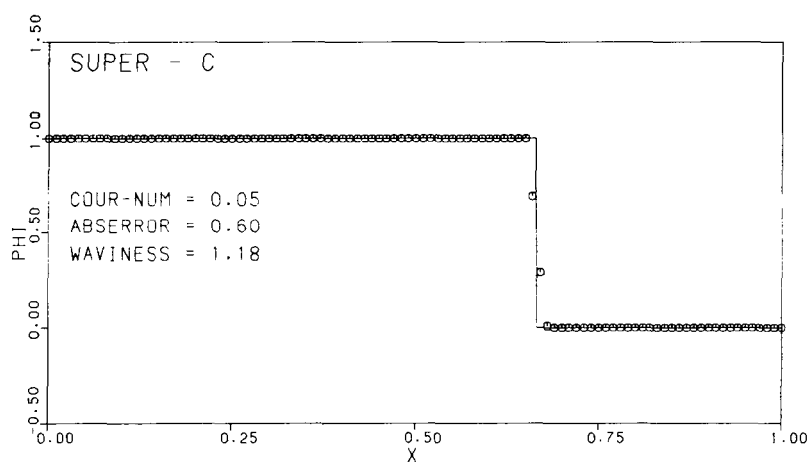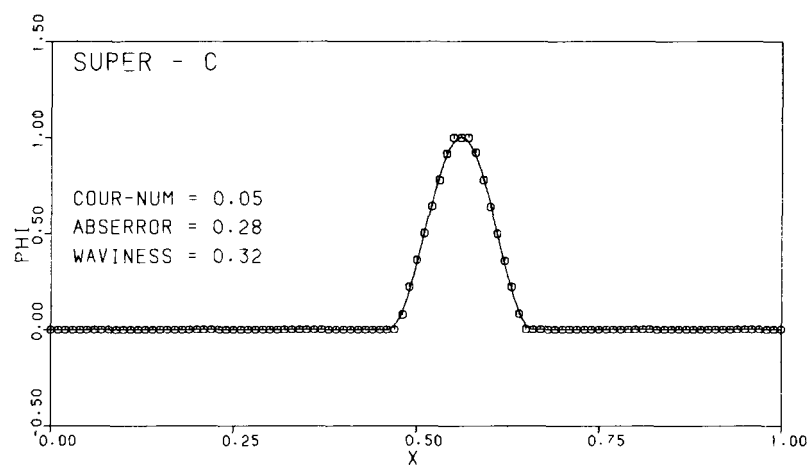
(a) c = 0.05.

FIGURE 29. - RESULTS FOR THE SUPER-C SCHEME.
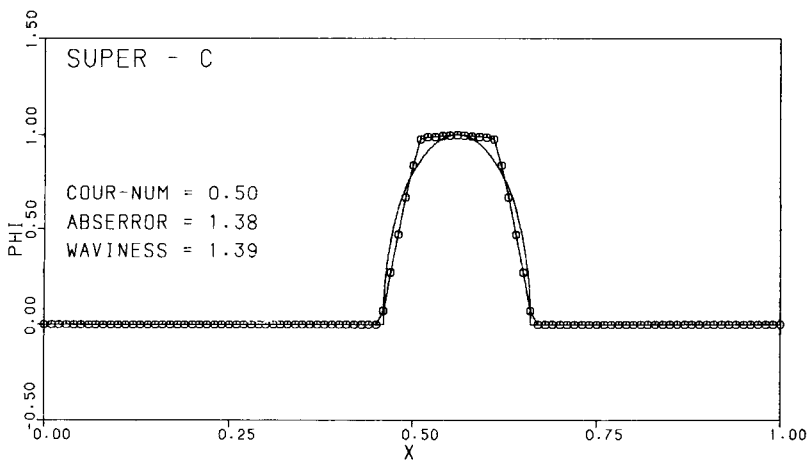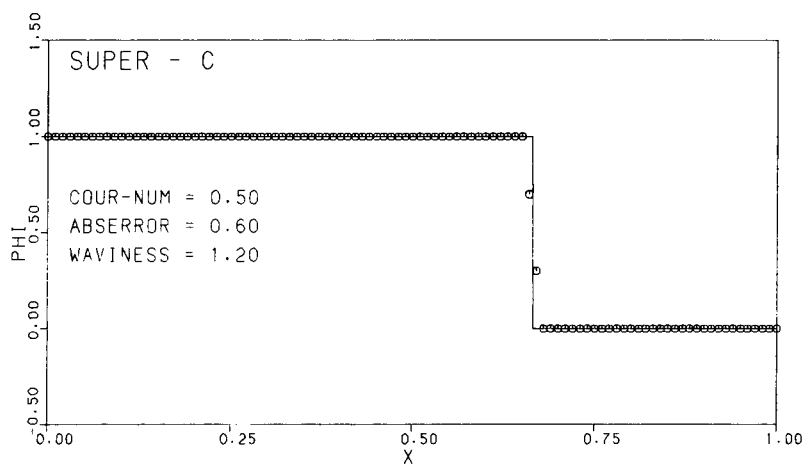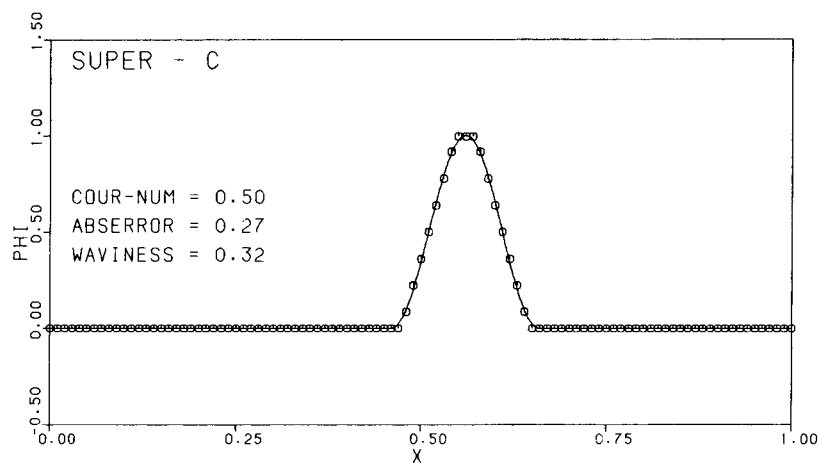
(b) c = 0.5.

FIGURE 29. – CONCLUDED.
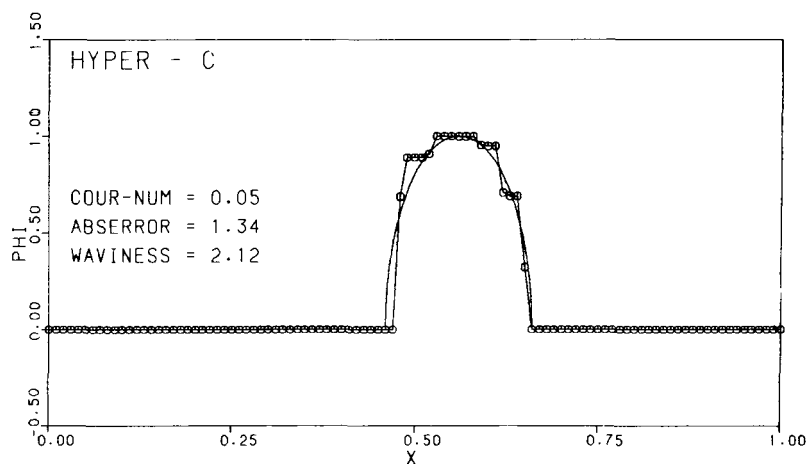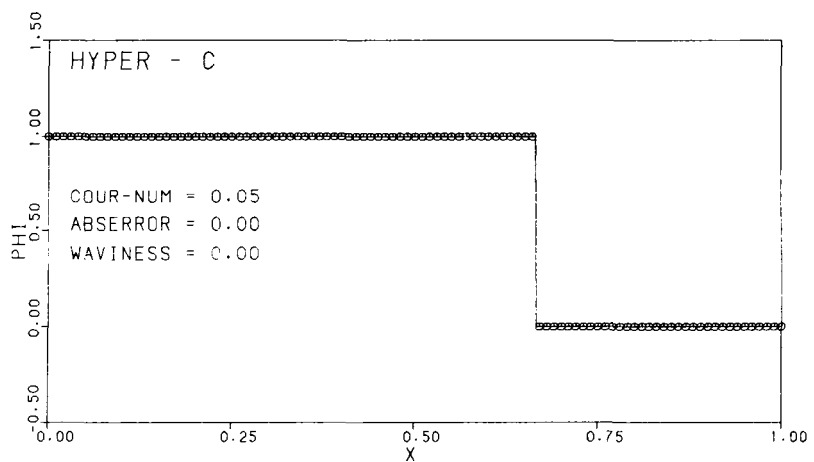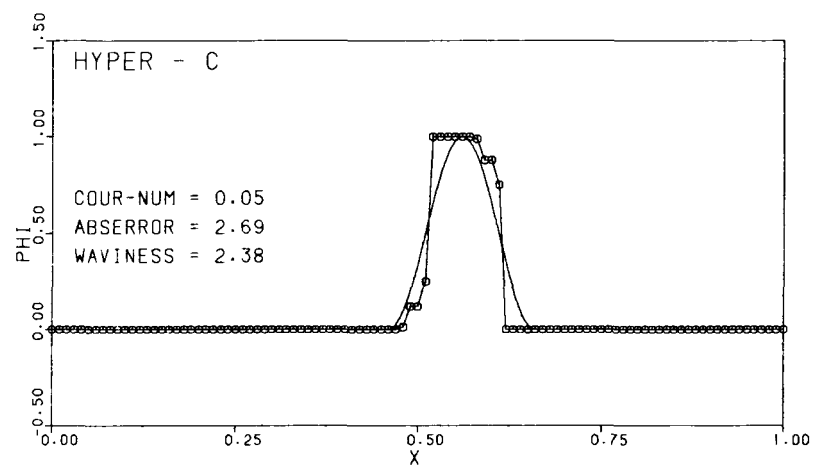
(a) c = 0.05.

FIGURE 30. - RESULTS FOR HYPER-C (LIMITED FIRST-ORDER DOWNWINDING).

HYPER - C

COUR-NUM = 0.50
ABSERROR = 2.69
WAVINESS = 2.76

HYPER - C

COUR-NUM = 0.50
ABSERROR = 0.00
WAVINESS = 0.00

HYPER - C

COUR-NUM = 0.50
ABSERROR = 3.10
WAVINESS = 2.89
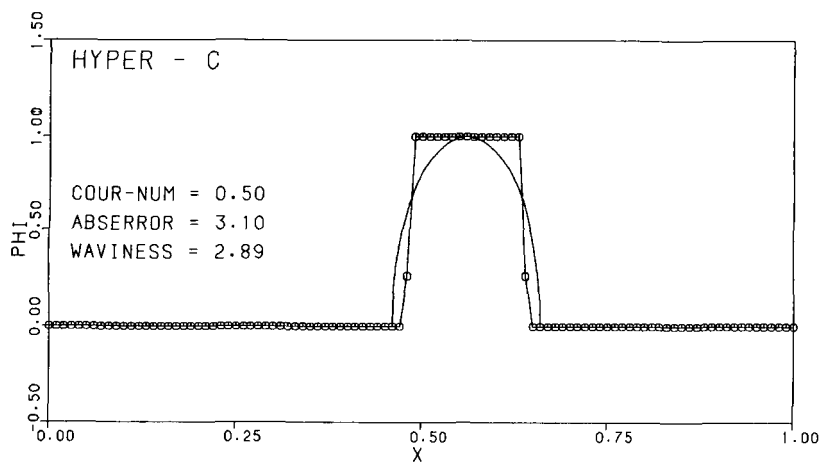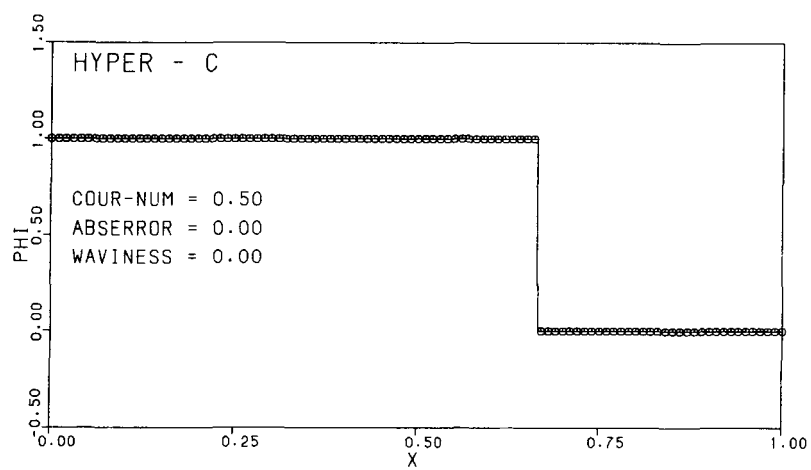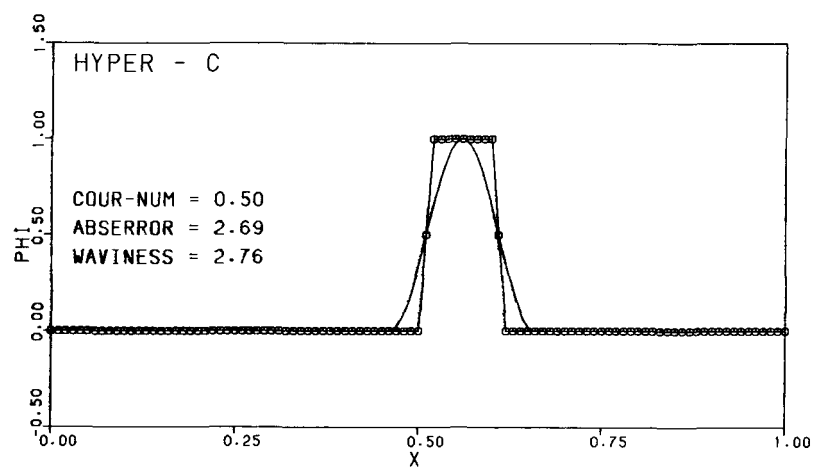
(b) c = 0.5.

FIGURE 30. - CONCLUDED.
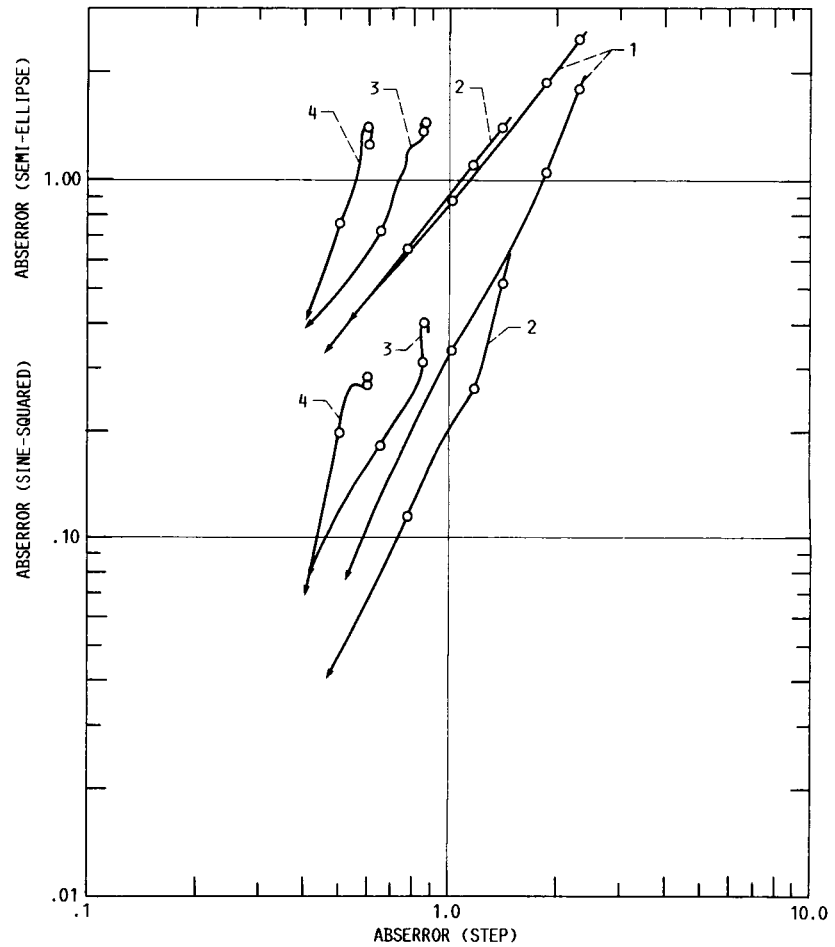
FIGURE 31. – ABSERROR FOR THE SEMI-ELLIPSE PROFILE (UPPER CURVES) AND SINE-
SQUARED PROFILE (LOWER CURVES) PLOTTED ON A LOG-LOG SCALE AGAINST ABSERROR
FOR THE STEP, WITH COURANT NUMBER AS A PARAMETER RANGING FROM 0.01 TO
0.978, WITH VALUES SHOWN AT 0.1, 0.5, AND 0.9. CURVES SHOW RESULTS FOR:
(1) MINMOD, (2) MUSCL, (3) SUPERBEE, AND (4) SUPER-C. ARROWS SHOW DI-
RECTION OF INCREASING COURANT NUMBER.
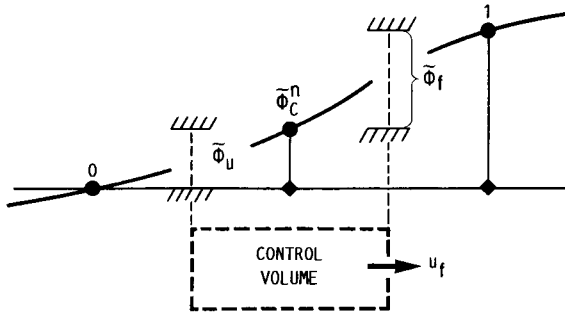
FIGURE 32. - NORMALIZED NODE VALUES FOR LOCALLY MONOTONIC
BEHAVIOR. HATCHING SHOWS NECESSARY CONDITIONS ON THE
FACE VALUE OF INTEREST, $\widetilde{\Phi}_f$, AND ON THAT OF THE CORRE-
SPONDING UPSTREAM FACE VALUE, $\widetilde{\Phi}_u$.
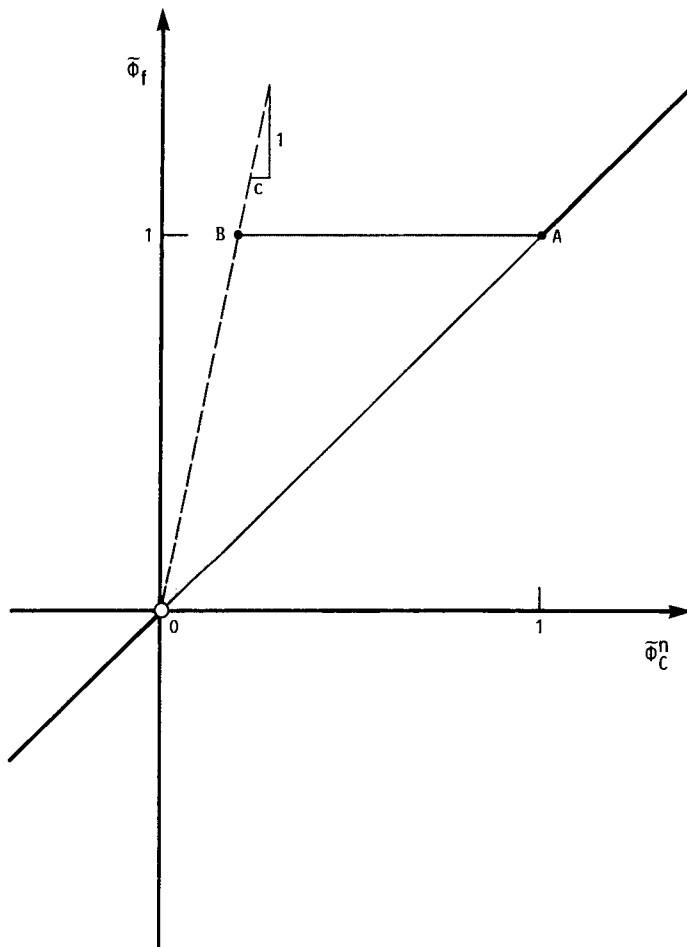
FIGURE 33. - NORMALIZED VARIABLE DIAGRAM SHOWING THE ULTIMATE STRATEGY.
THE DASHED BOUNDARY HAS A COURANT-NUMBER-DEPENDENT SLOPE OF 1/c.
THE CASE SHOWN IS FOR c = 0.2.
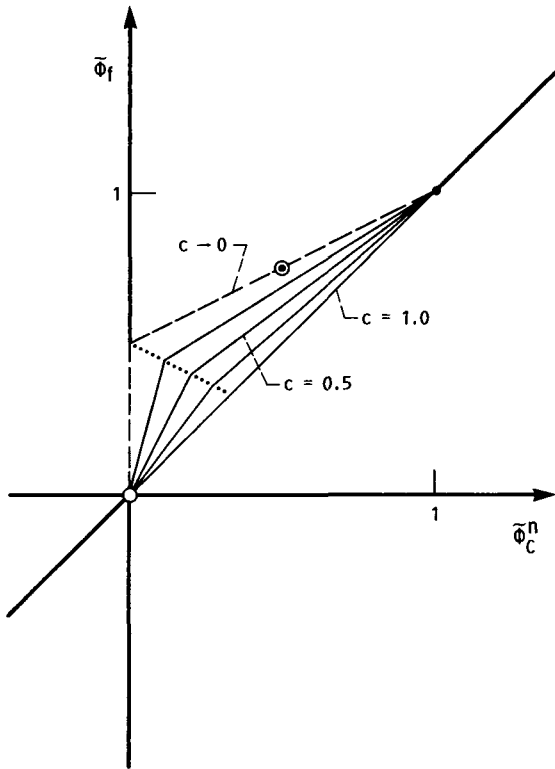
FIGURE 34. - NVD SHOWING $\widetilde{\Phi}_f$ AS A FUNCTION OF $\widetilde{\Phi}_C^n$ AND c FOR THE ULTIMATE LAX-WENDROFF METHOD.
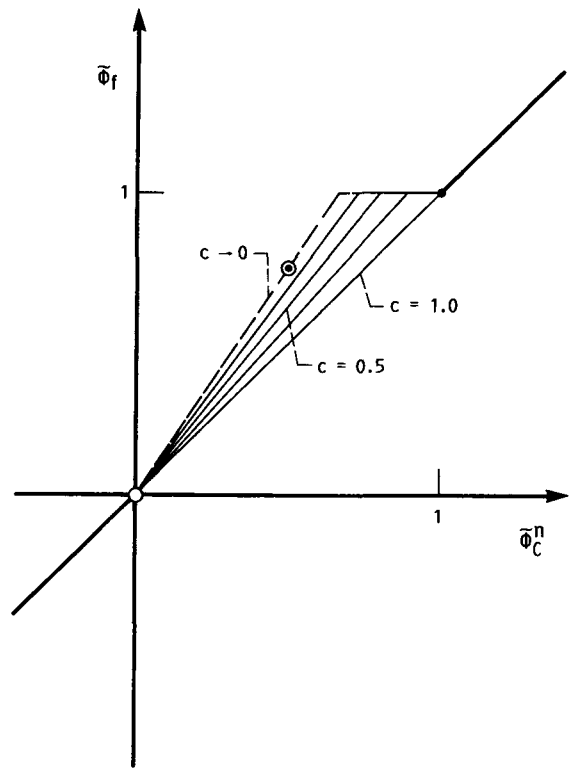
FIGURE 35. - NVD SHOWING $\widetilde{\Phi}_f$ AS A FUNCTION OF $\widetilde{\Phi}_C^n$ AND c FOR ULTIMATE SECOND-ORDER UPWINDING.
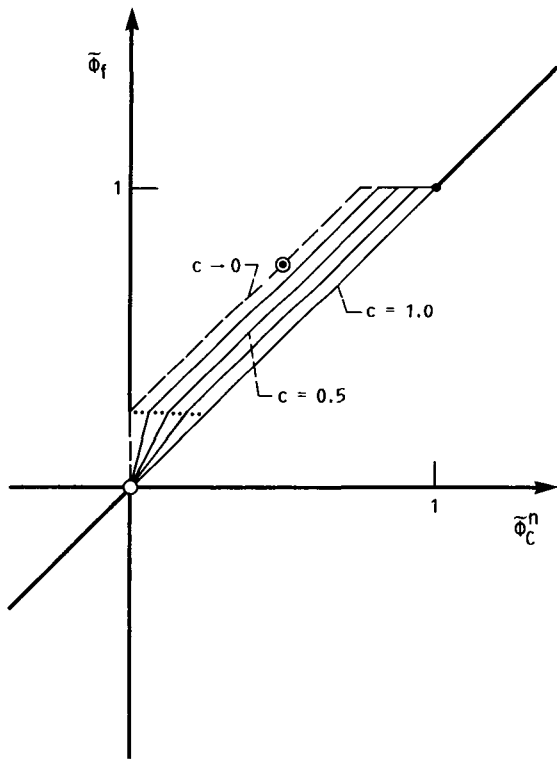
FIGURE 36. - NVD SHOWING $\widetilde{\Phi}_f$ AS A FUNCTION OF $\widetilde{\Phi}_C^n$ AND c FOR THE ULTIMATE FROMM SCHEME.
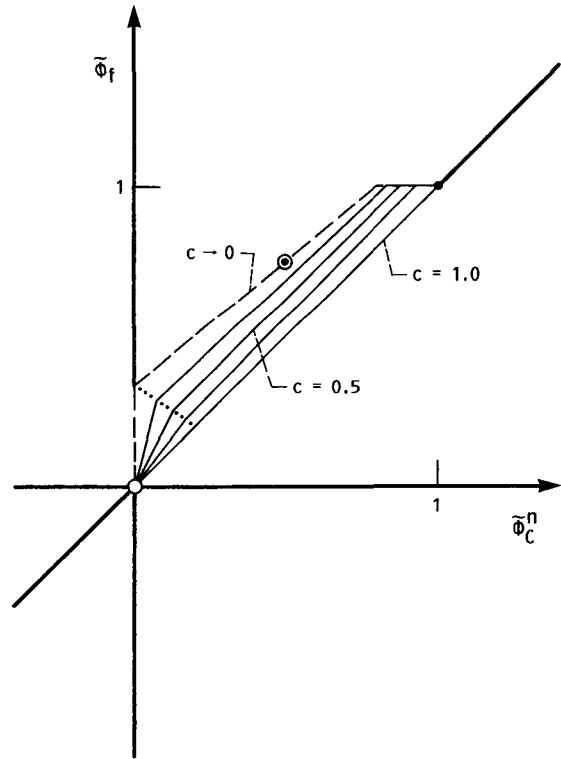
FIGURE 37. - NVD SHOWING $\widetilde{\Phi}_f$ AS A FUNCTION OF $\widetilde{\Phi}_C^n$ AND c FOR THE ULTIMATE QUICKEST METHOD.

89
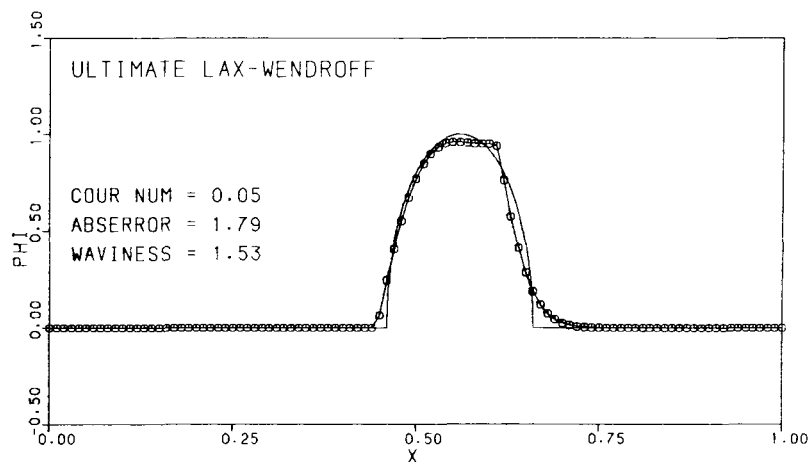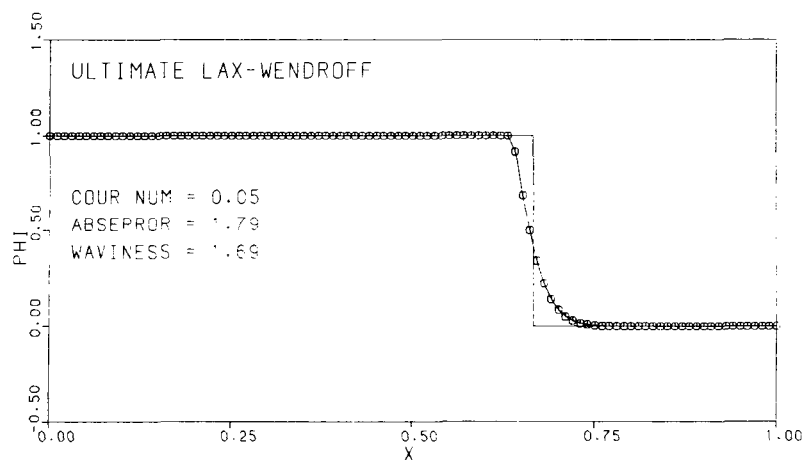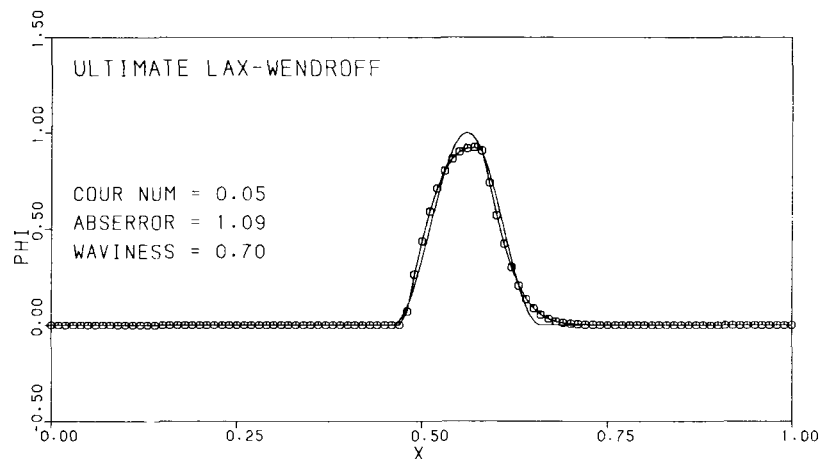
(a) c = 0.05.

FIGURE 38. - RESULTS FOR THE ULTIMATE LAX-WENDROFF METHOD.

ULTIMATE LAX-WENDROFF

COUR NUM = 0.50
ABSERROR = 0.88
WAVINESS = 0.60

ULTIMATE LAX-WENDROFF

COUR NUM = 0.50
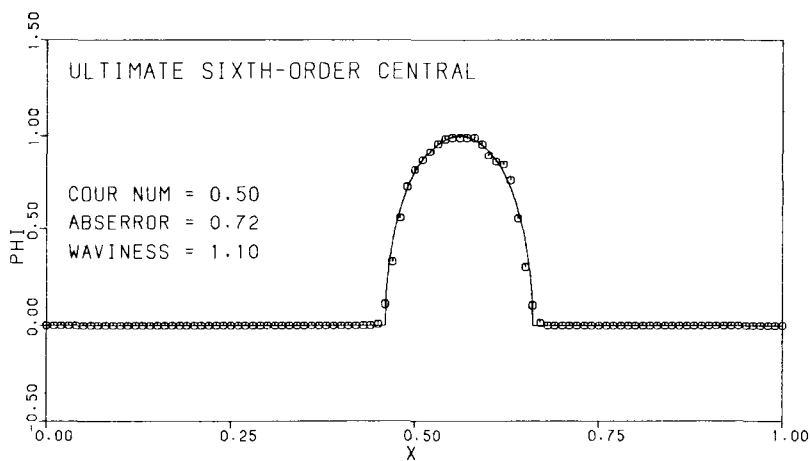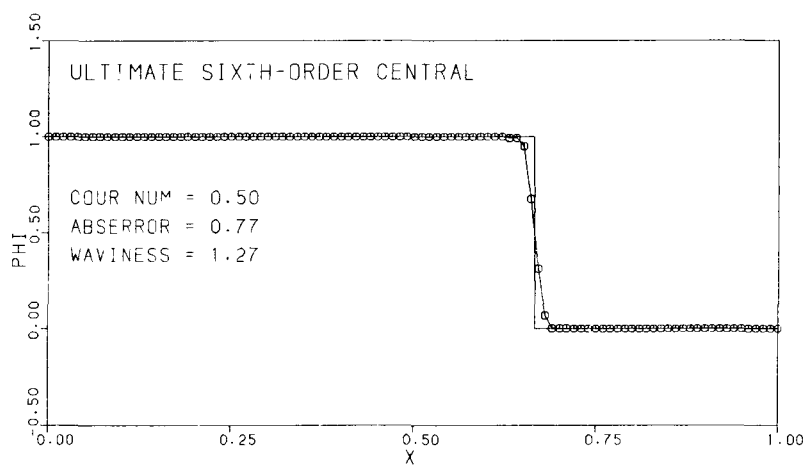ABSERROR = 1.57
WAVINESS = 1.64

ULTIMATE LAX-WENDROFF

COUR NUM = 0.50
ABSERROR = 1.63
WAVINESS = 1.47
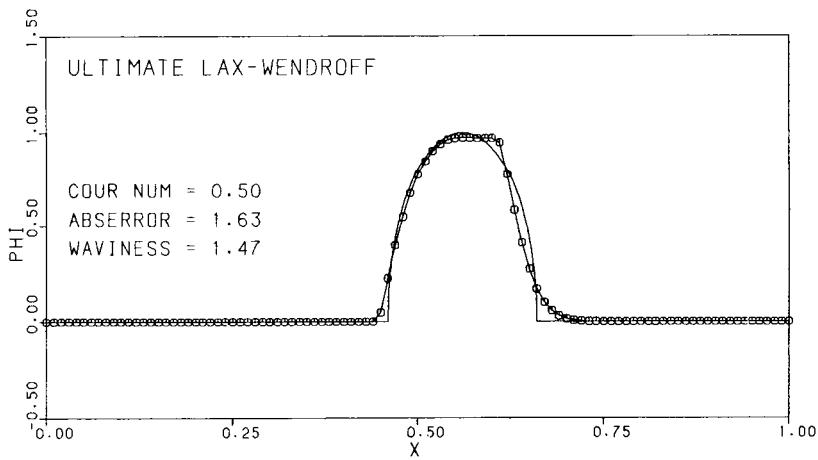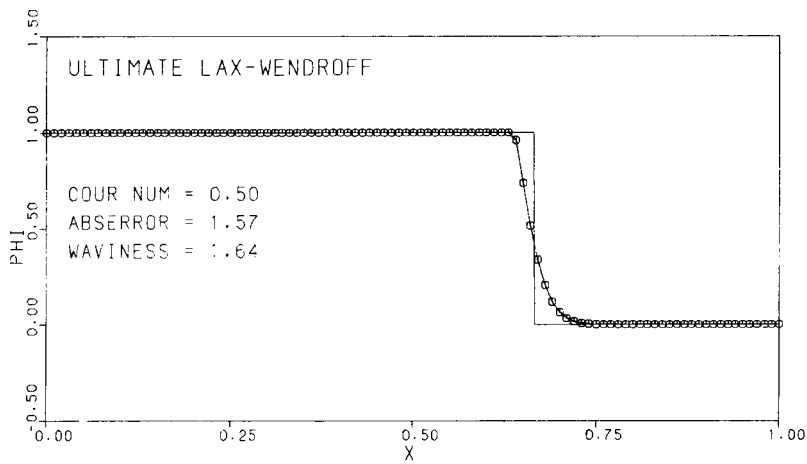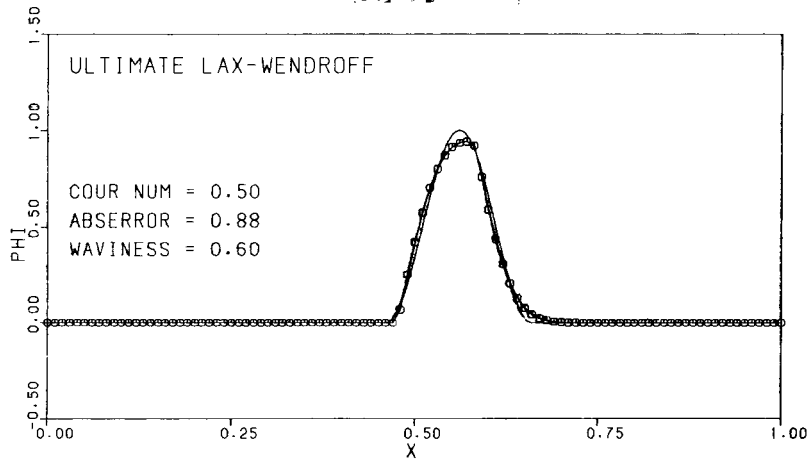
(b) c = 0.5.

FIGURE 38. - CONCLUDED.

ULTIMATE SECOND-ORDER UPWINDING

COUR NUM = 0.05
ABSERROR = 1.57
WAVINESS = 0.73

ULTIMATE SECOND-ORDER UPWINDING

COUR NUM = 0.05
ABSERROR = 2.09
WAVINESS = 1.73

ULTIMATE SECOND-ORDER UPWINDING

COUR NUM = 0.05
ABSERROR = 2.17
WAVINESS = 1.59
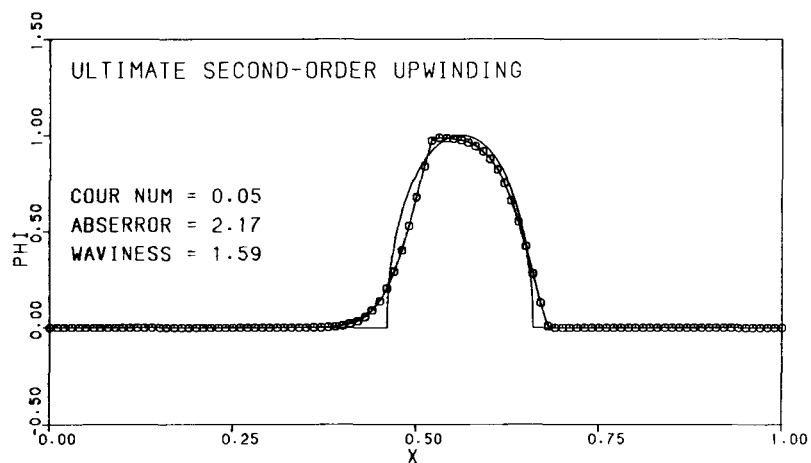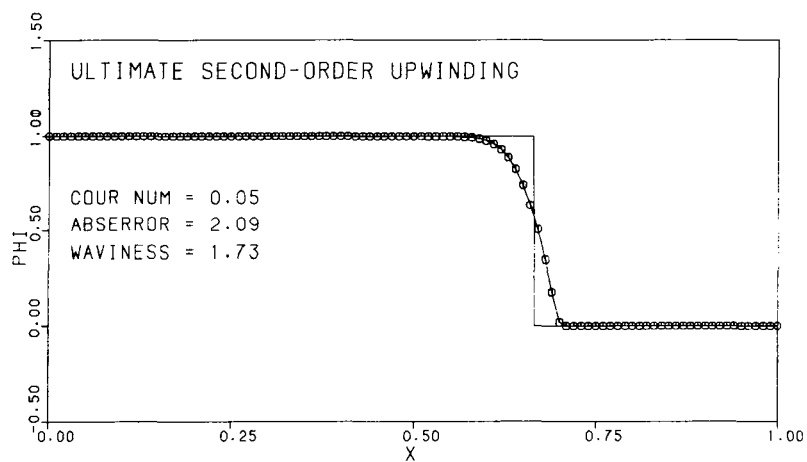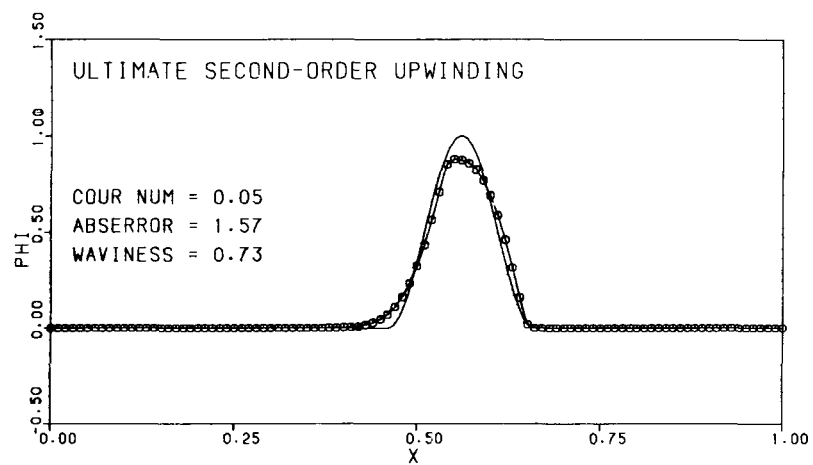
(a) c = 0.05.

FIGURE 39. - RESULTS FOR ULTIMATE SECOND-ORDER UPWINDING.

ULTIMATE SECOND-ORDER UPWINDING

COUR NUM = 0.50
ABSERROR = 0.92
WAVINESS = 0.50

ULTIMATE SECOND-ORDER UPWINDING

COUR NUM = 0.50
ABSERROR = 1.57
WAVINESS = 1.64

ULTIMATE SECOND-ORDER UPWINDING

COUR NUM = 0.50
ABSERROR = 1.60
WAVINESS = 1.49

(b) c = 0.5.

FIGURE 39. - CONCLUDED.

ULTIMATE FROMM

COUR NUM = 0.05
ABSERROR = 0.53
WAVINESS = 0.36

ULTIMATE FROMM

COUR NUM = 0.05
ABSERROR = 1.41
WAVINESS = 1.51

ULTIMATE FROMM

COUR NUM = 0.05
ABSERROR = 1.42
WAVINESS = 1.34
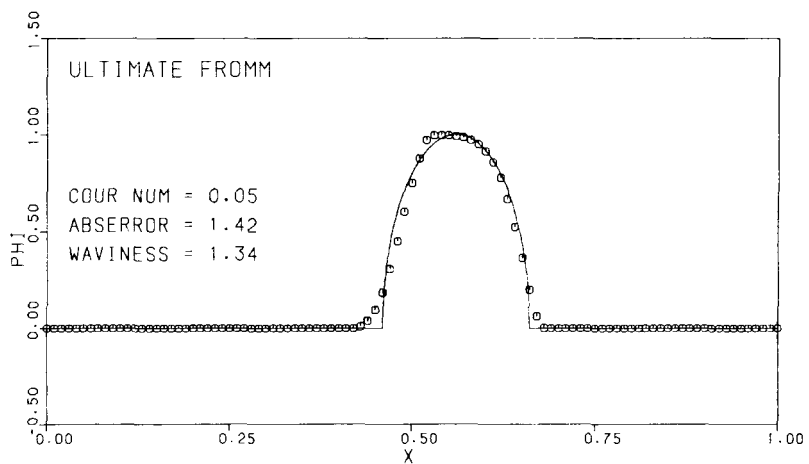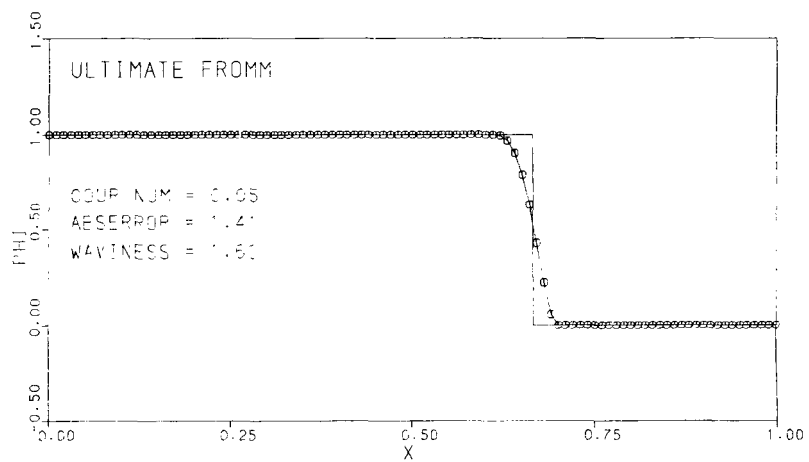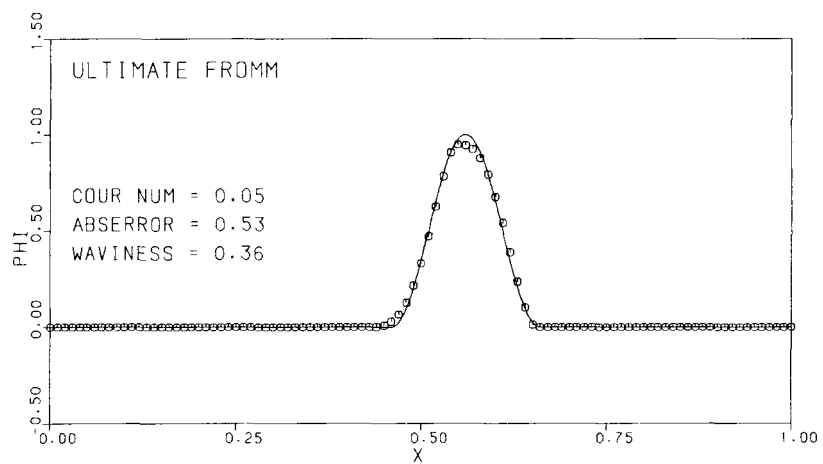
(a) c = 0.05.

FIGURE 40. – RESULTS FOR THE ULTIMATE FROMM SCHEME.

94
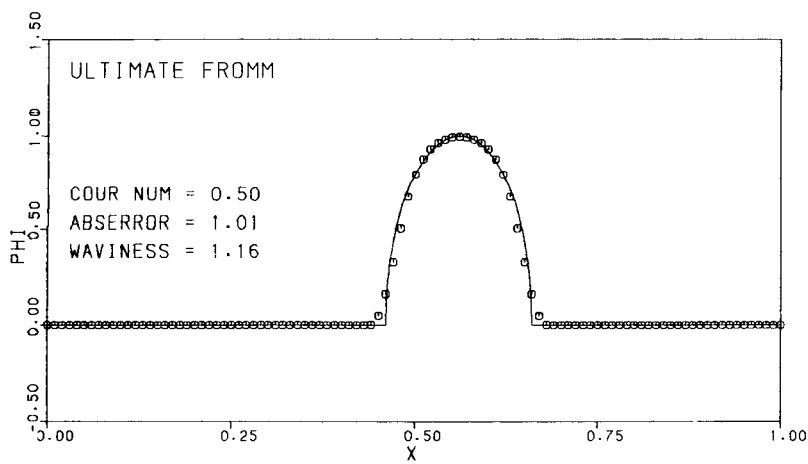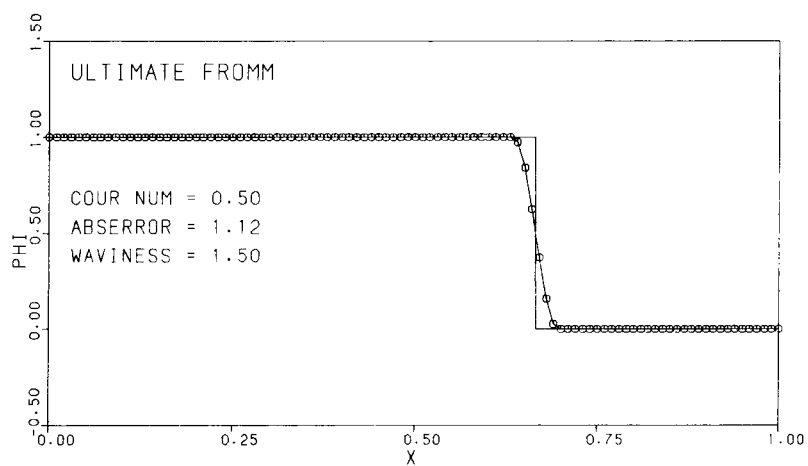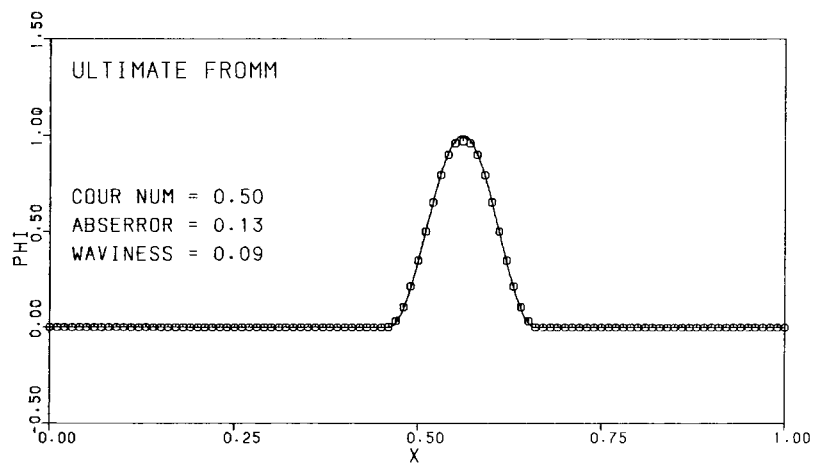
(b) c = 0.5.

FIGURE 40. – CONCLUDED.
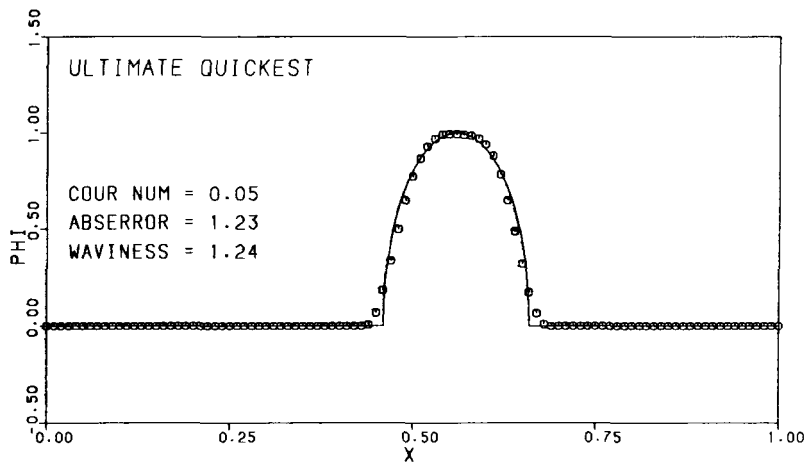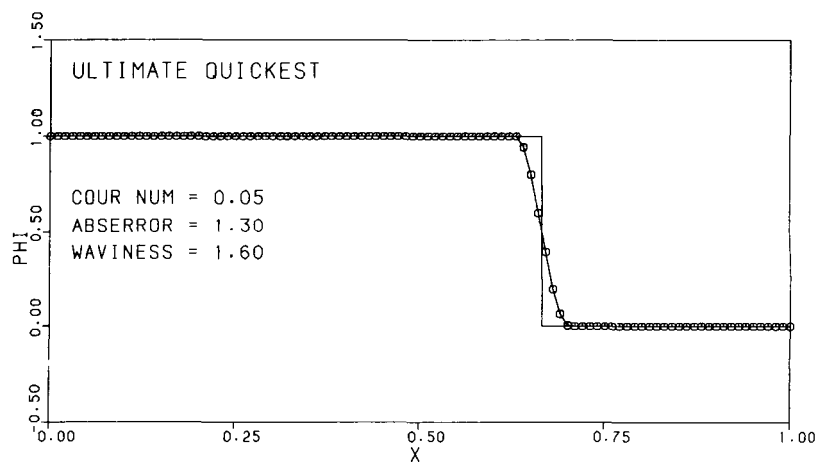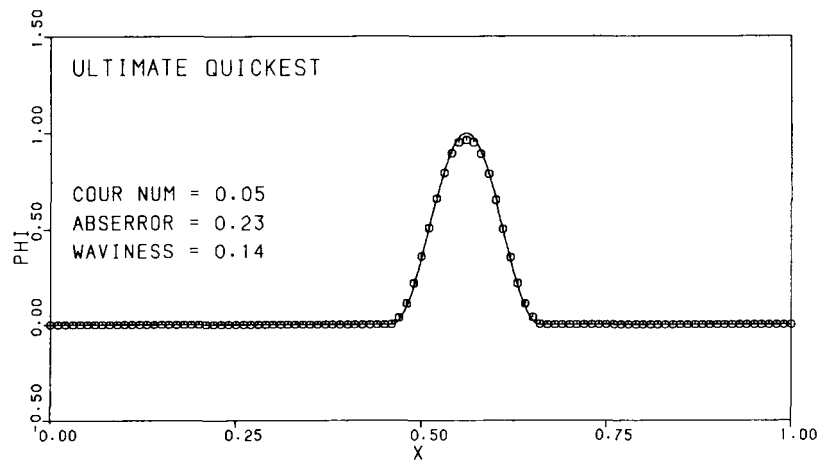
(a) c = 0.05.

FIGURE 41. - RESULTS FOR ULTIMATE QUICKEST.
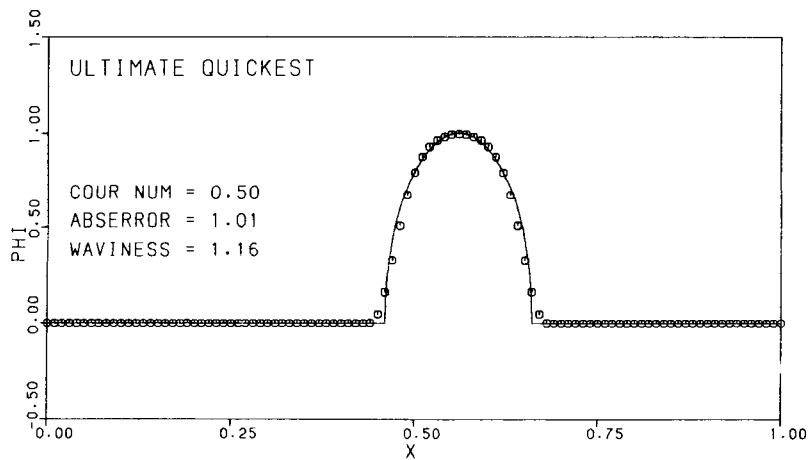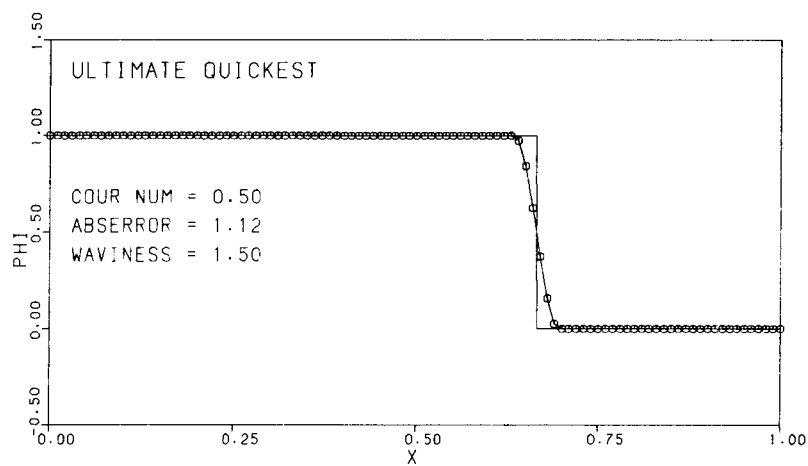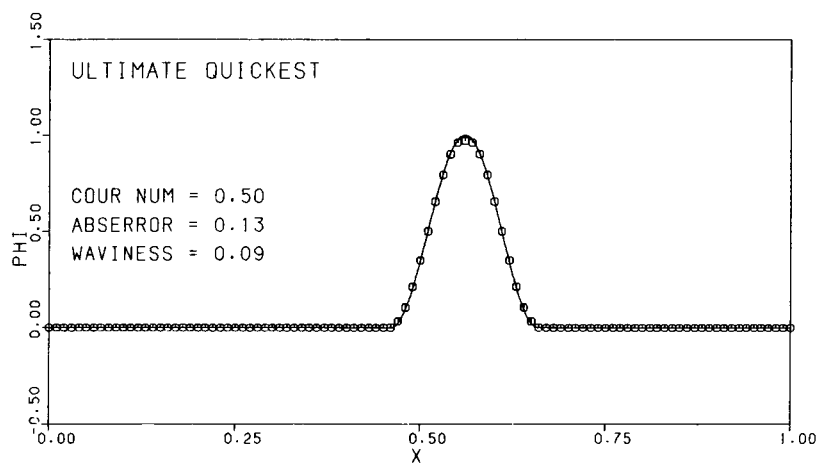
(b) c = 0.5.

FIGURE 41. - CONCLUDED.

ULTIMATE FOURTH-ORDER CENTRAL

COUR NUM = 0.05
ABSERROR = 0.20
WAVINESS = 0.20

ULTIMATE FOURTH-ORDER CENTRAL

COUR NUM = 0.05
ABSERROR = 1.01
WAVINESS = 1.45

ULTIMATE FOURTH-ORDER CENTRAL

COUR NUM = 0.05
ABSERROR = 1.04
WAVINESS = 1.29
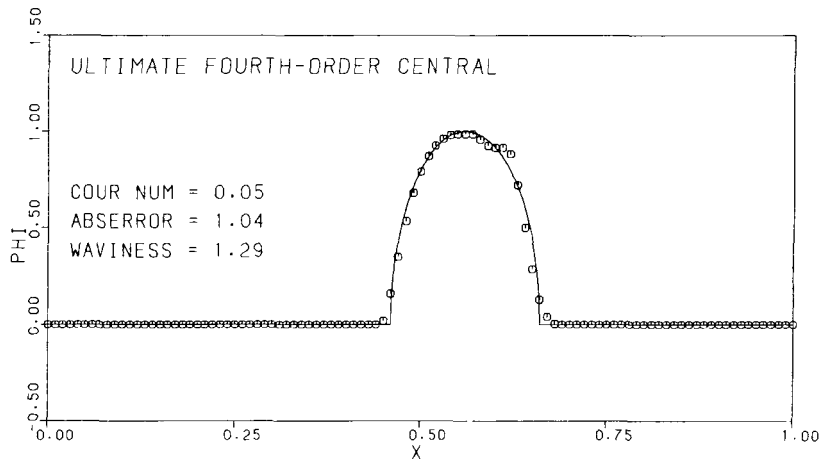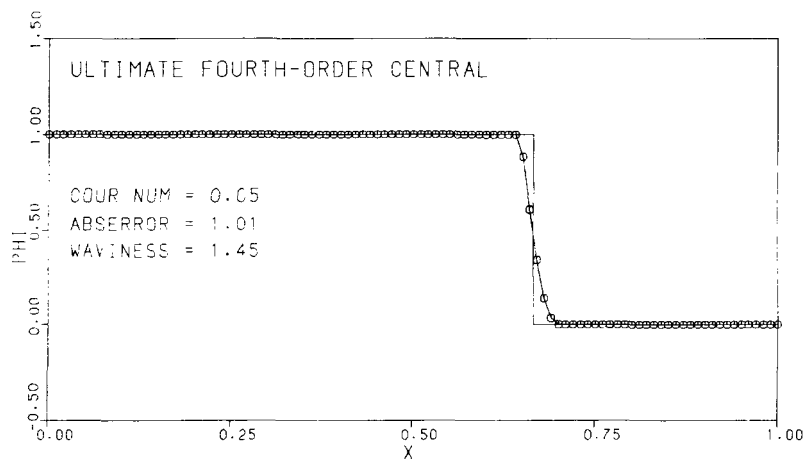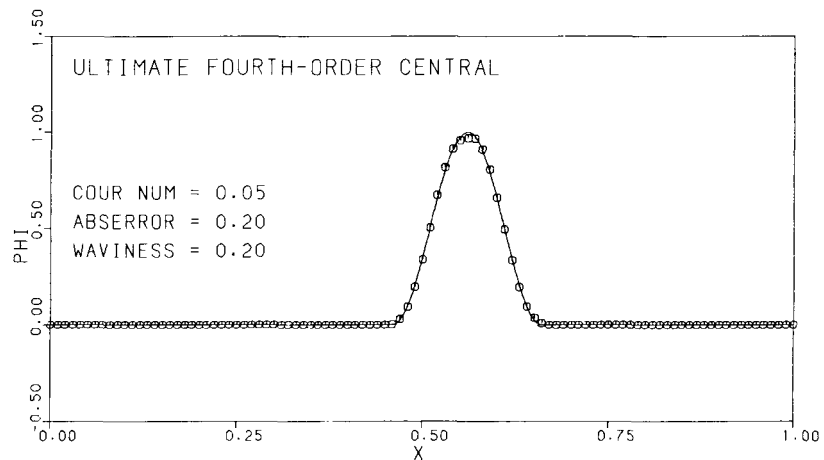
(a) c = 0.05.

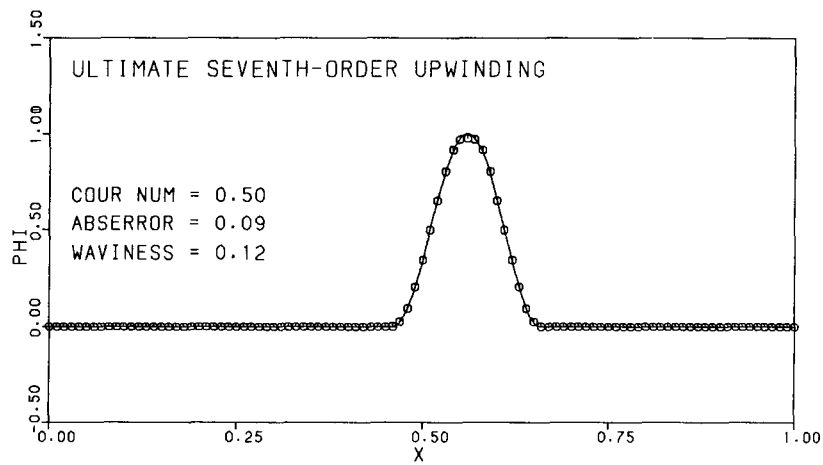FIGURE 42. - RESULTS FOR THE ULTIMATE FOURTH-ORDER CENTRAL SCHEME.

C - 2
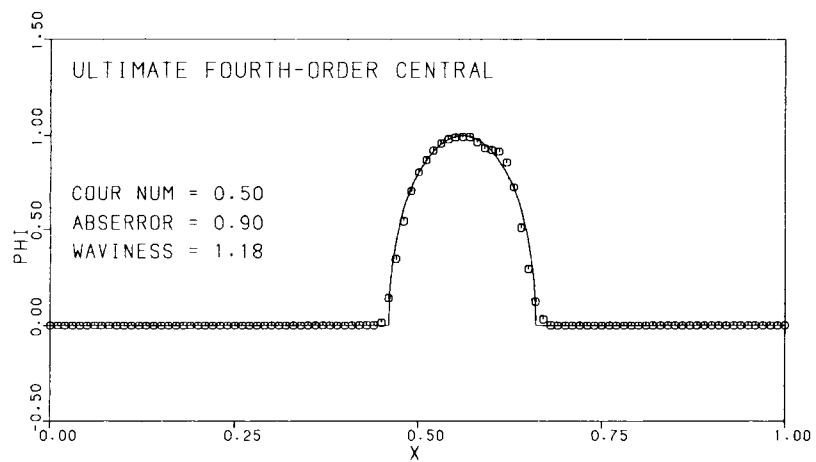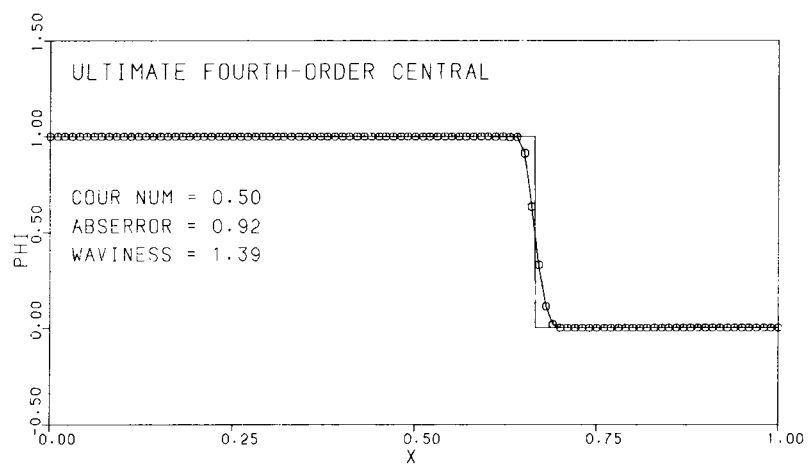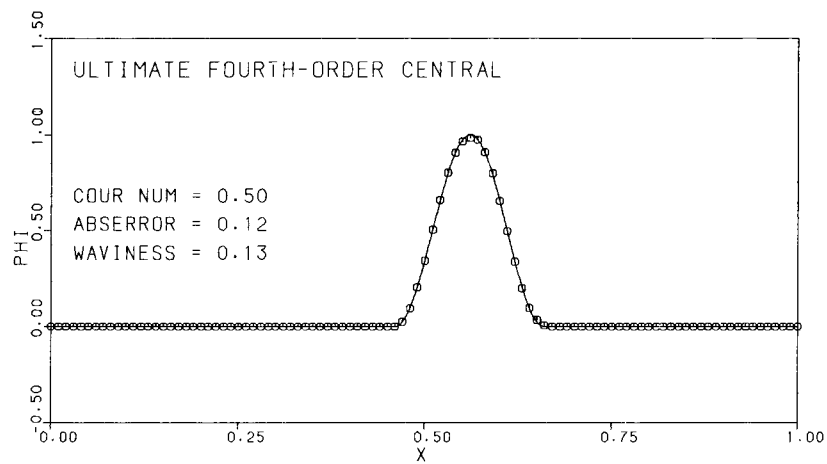
(b) c = 0.5.

FIGURE 42. - CONCLUDED.
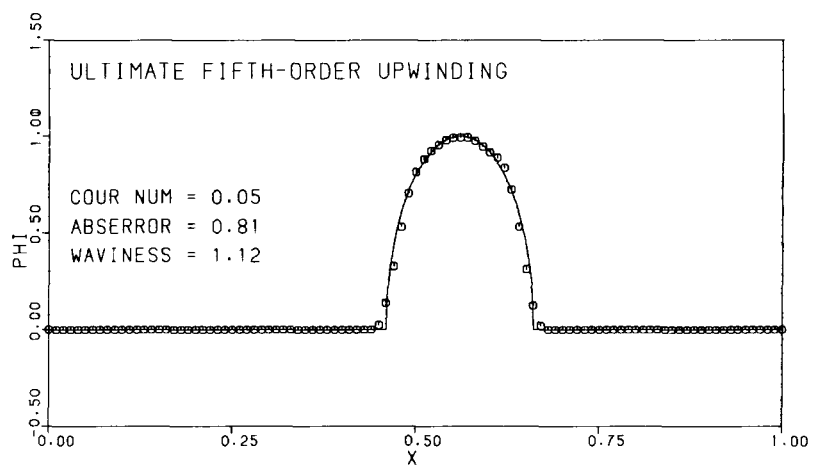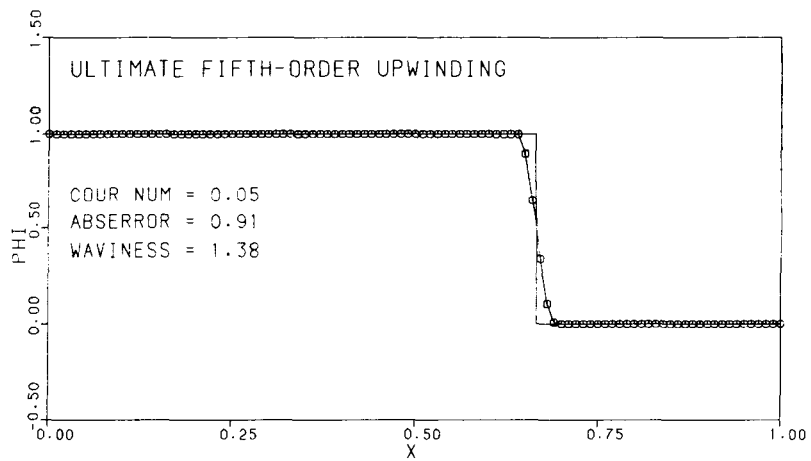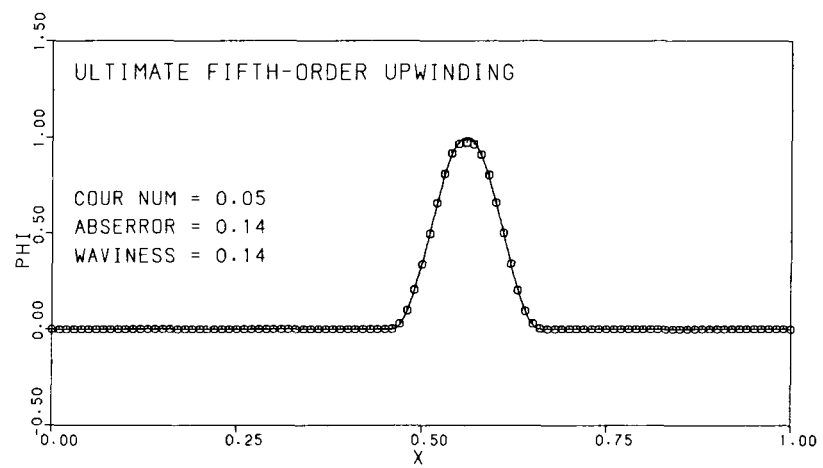
(a) c = 0.05.

FIGURE 43. - RESULTS FOR ULTIMATE FIFTH-ORDER UPWINDING.

ULTIMATE FIFTH-ORDER UPWINDING

COUR NUM = 0.50
ABSERROR = 0.09
WAVINESS = 0.09

ULTIMATE FIFTH-ORDER UPWINDING

COUR NUM = 0.50
ABSERROR = 0.83
WAVINESS = 1.32

ULTIMATE FIFTH-ORDER UPWINDING

COUR NUM = 0.50
ABSERROR = 0.72
WAVINESS = 1.07
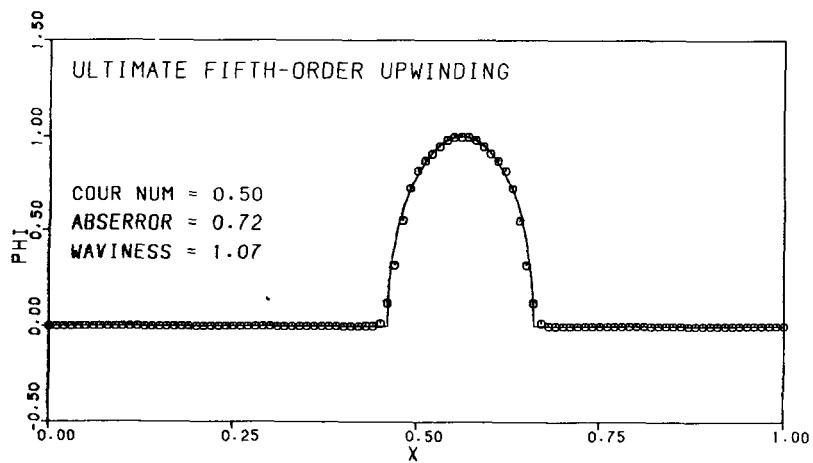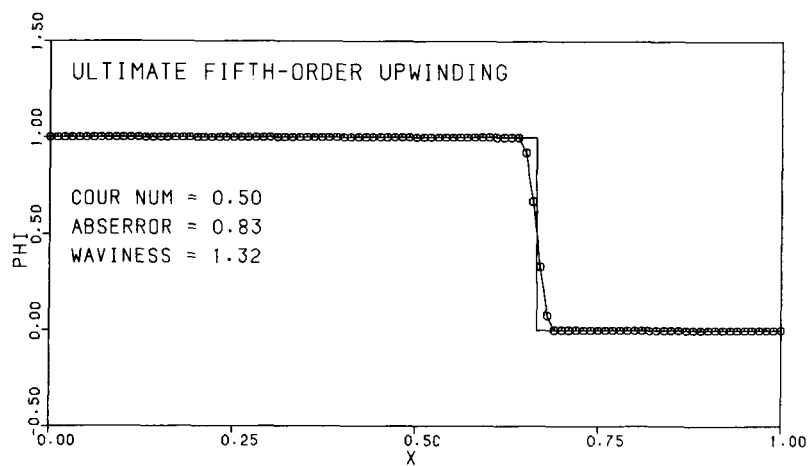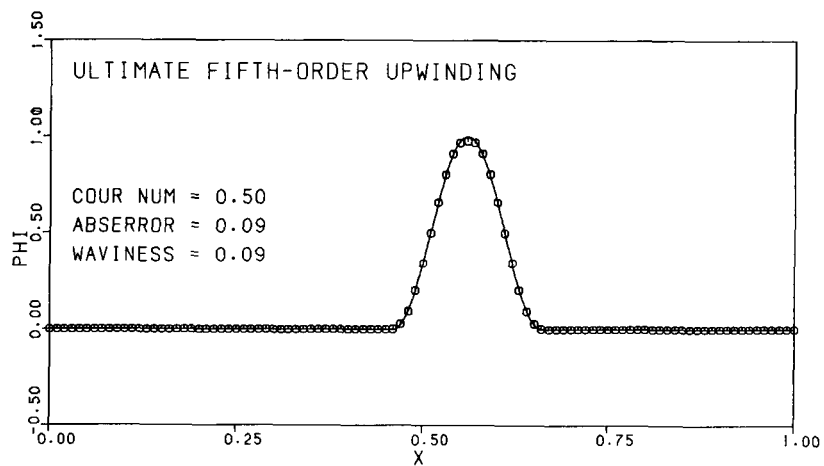
(b) c = 0.5.

FIGURE 43. – CONCLUDED.

ULTIMATE SIXTH-ORDER CENTRAL

COUR NUM = 0.05
ABSERROR = 0.16
WAVINESS = 0.17

ULTIMATE SIXTH-ORDER CENTRAL

COUR NUM = 0.05
ABSERROR = 0.82
WAVINESS = 1.32

ULTIMATE SIXTH-ORDER CENTRAL

COUR NUM = 0.05
ABSERROR = 0.83
WAVINESS = 1.18
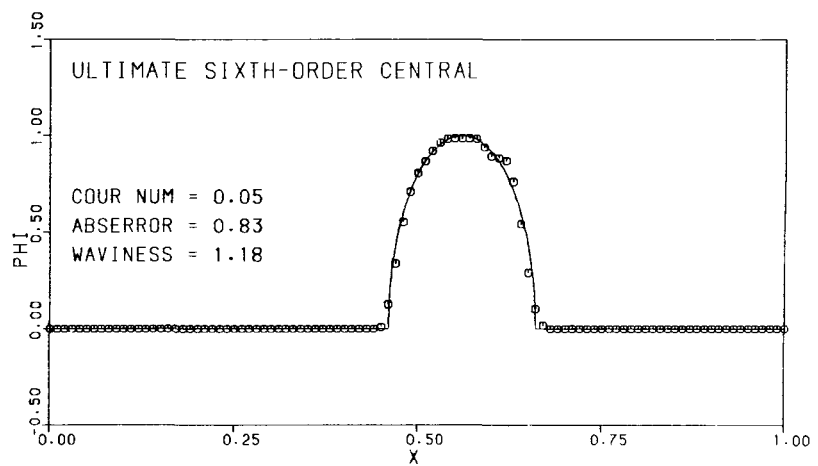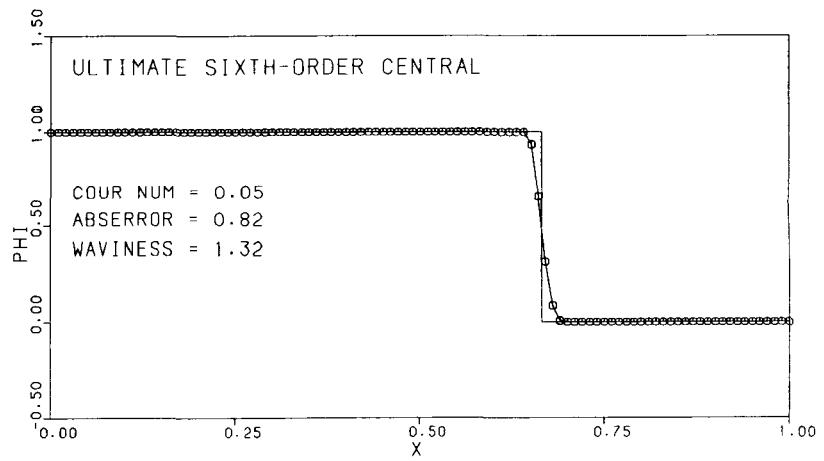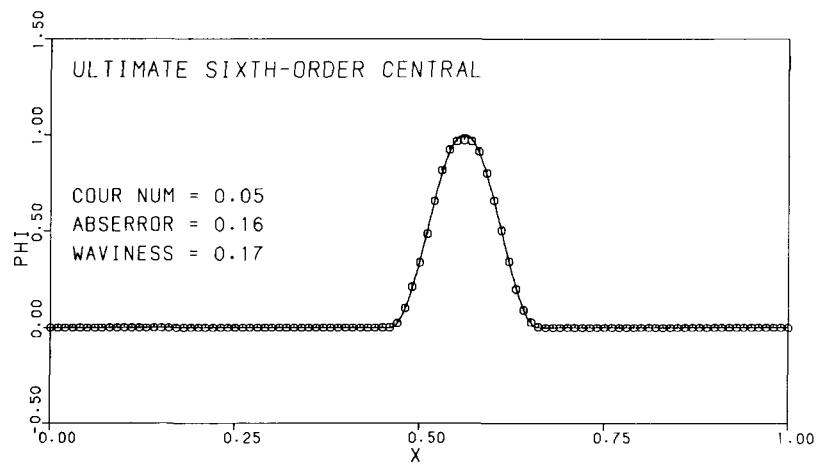
(a) c = 0.05.

FIGURE 44. - RESULTS FOR THE ULTIMATE SIXTH-ORDER CENTRAL SCHEME.

ULTIMATE SIXTH-ORDER CENTRAL

COUR NUM = 0.50
ABSERROR = 0.08
WAVINESS = 0.09

ULTIMATE SIXTH-ORDER CENTRAL

COUR NUM = 0.50
ABSERROR = 0.77
WAVINESS = 1.27

ULTIMATE SIXTH-ORDER CENTRAL

COUR NUM = 0.50
ABSERROR = 0.72
WAVINESS = 1.10
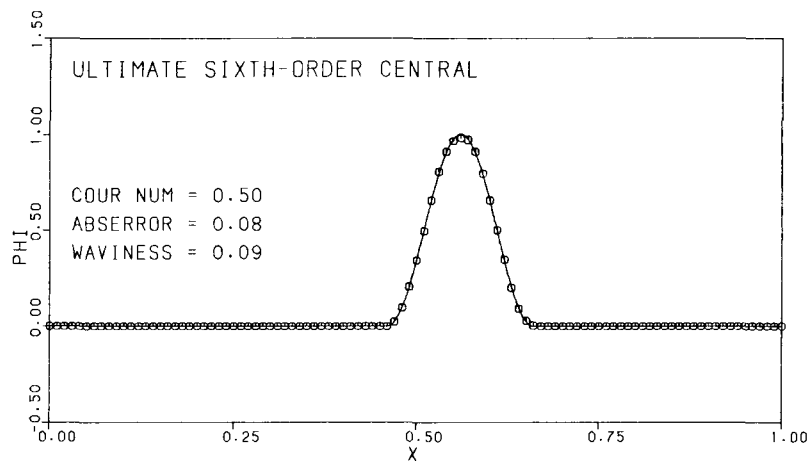
(b) c = 0.5.

FIGURE 44. - CONCLUDED.

ULTIMATE SEVENTH-ORDER UPWINDING

COUR NUM = 0.05
ABSERROR = 0.12
WAVINESS = 0.13

ULTIMATE SEVENTH-ORDER UPWINDING

COUR NUM = 0.05
ABSERROR = 0.78
WAVINESS = 1.28

ULTIMATE SEVENTH-ORDER UPWINDING

COUR NUM = 0.05
ABSERROR = 0.72
WAVINESS = 1.09
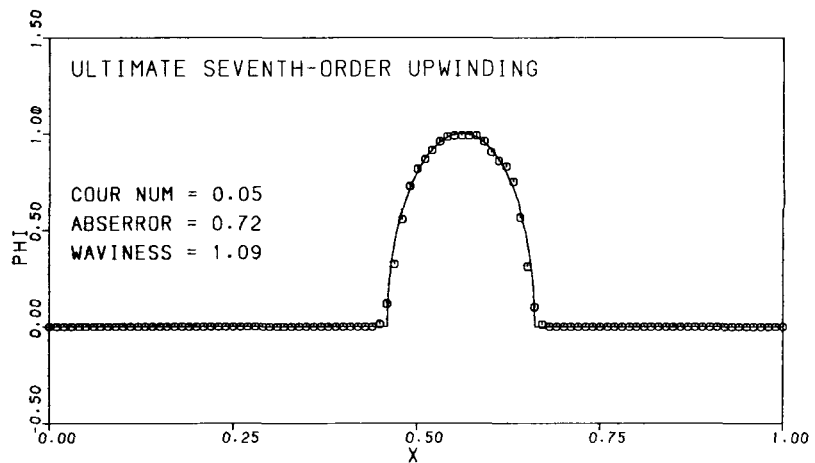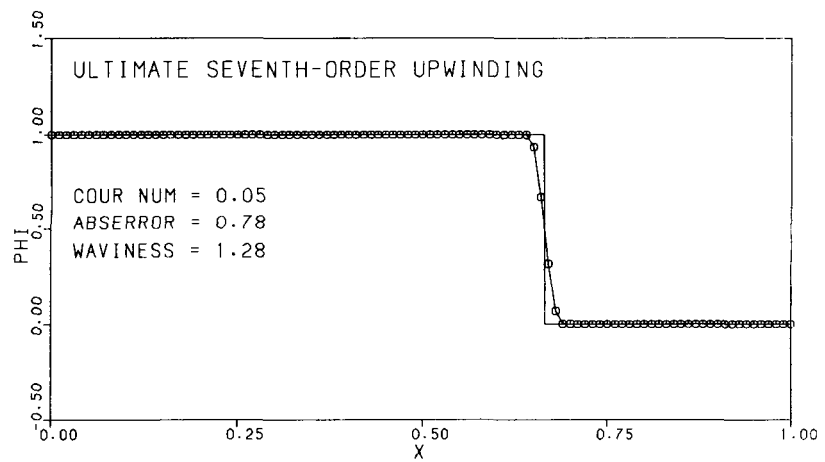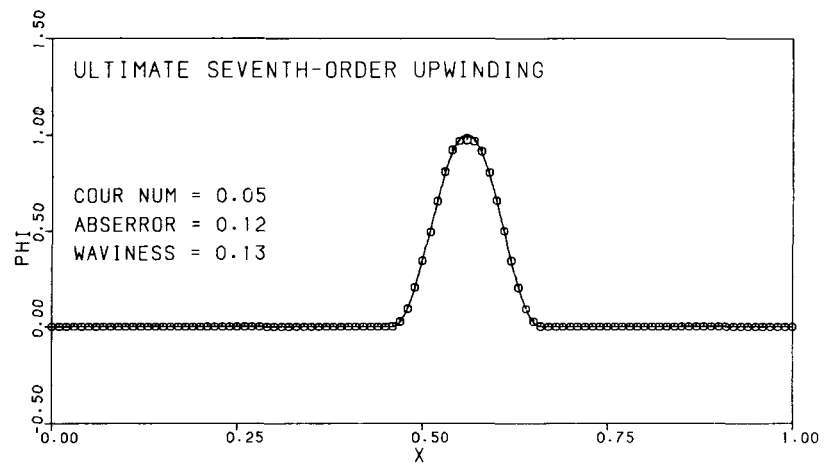
(a) c = 0.05.

FIGURE 45. - RESULTS FOR ULTIMATE SEVENTH-ORDER UPWINDING.

104
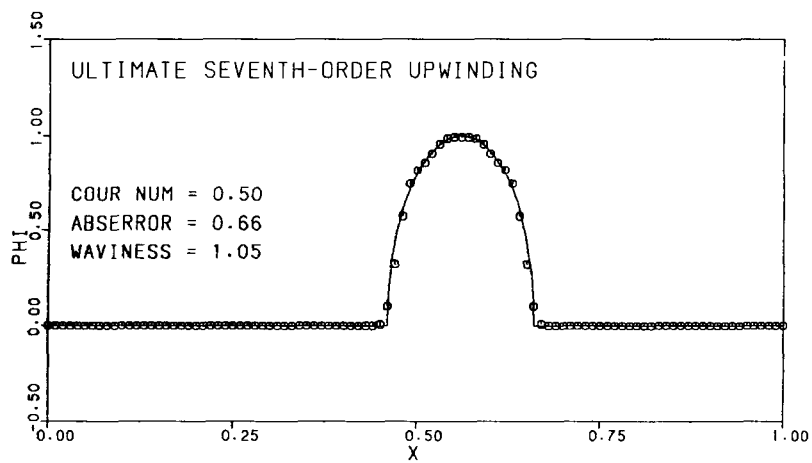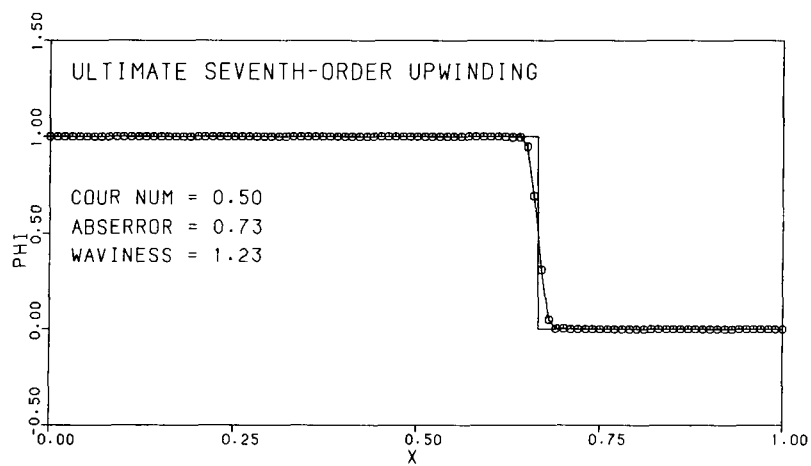
(b) c = 0.5

FIGURE 45. - CONCLUDED.
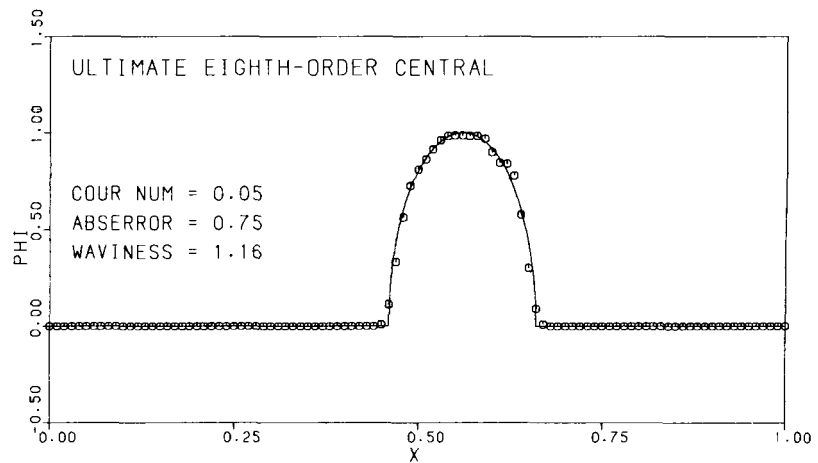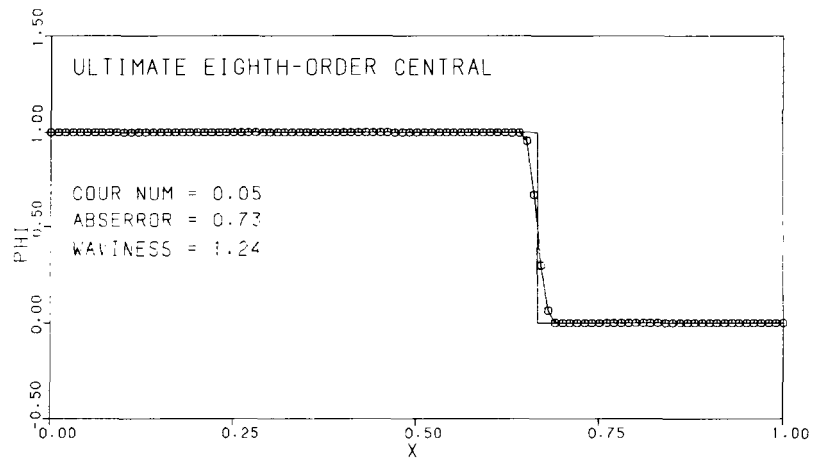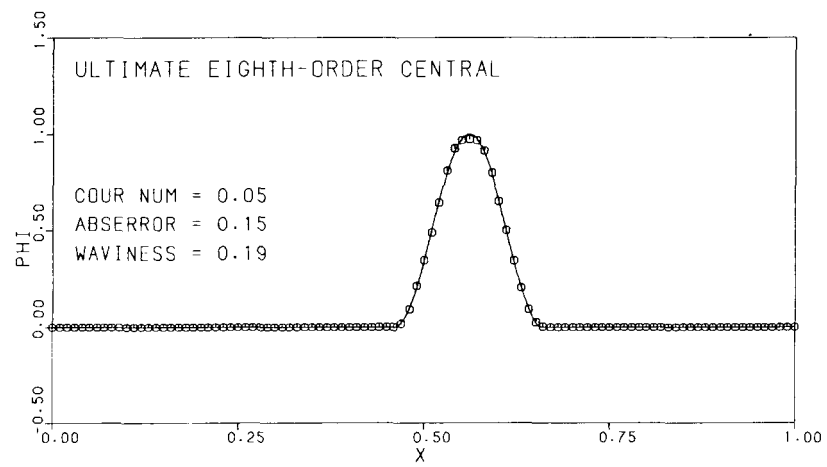
(a) c = 0.05.

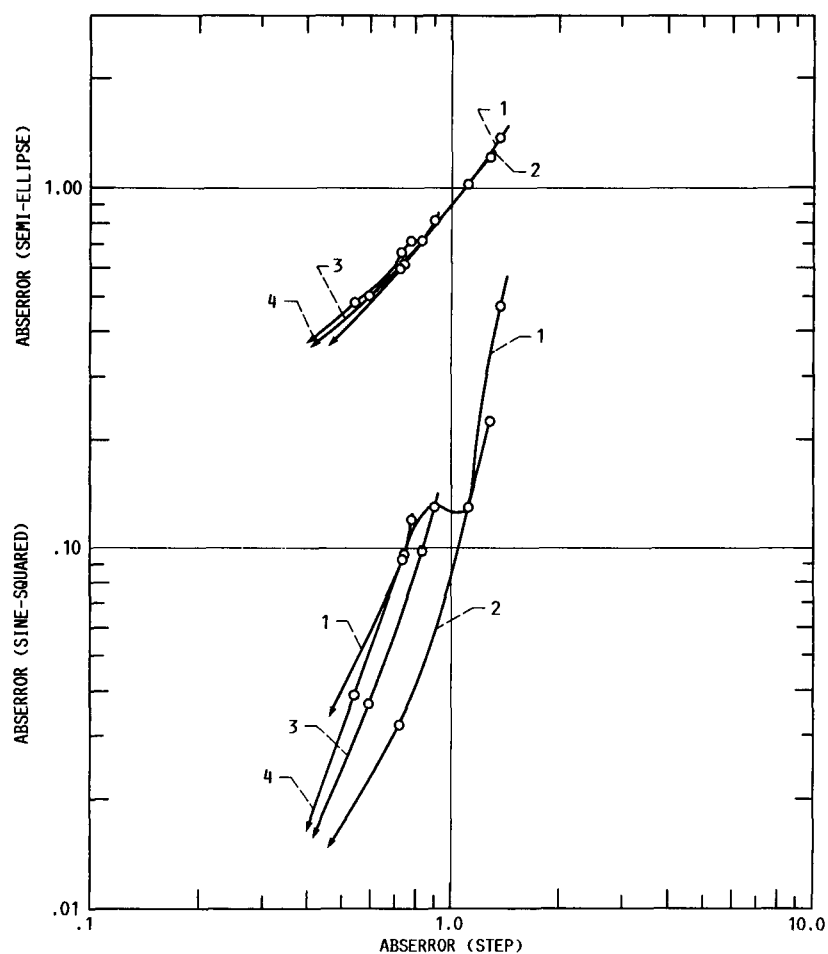FIGURE 46. - RESULTS FOR THE ULTIMATE EIGHT-ORDER CENTRAL SCHEME.
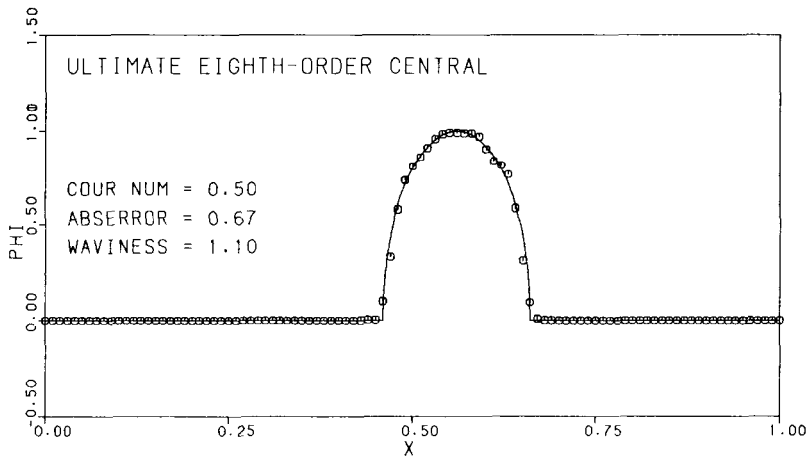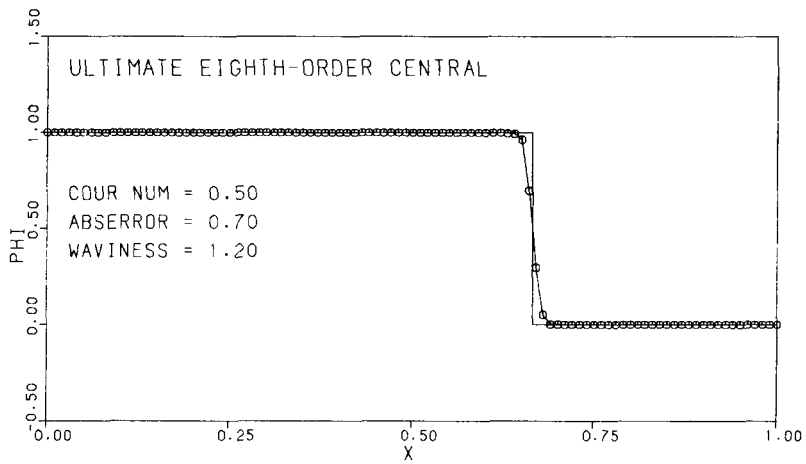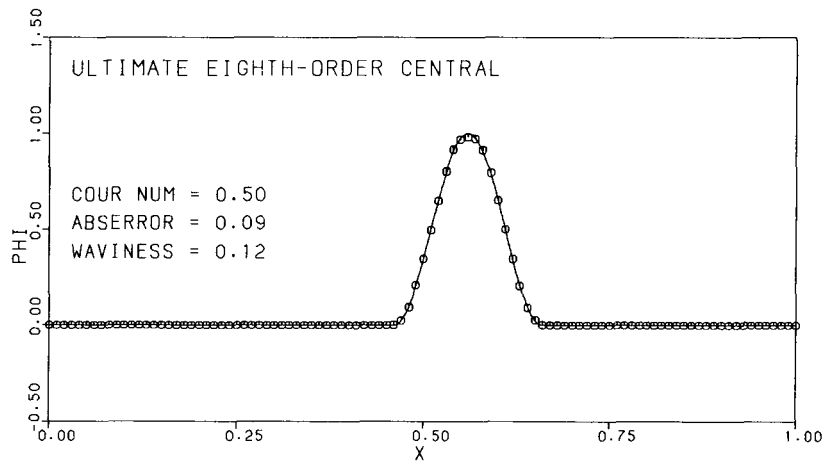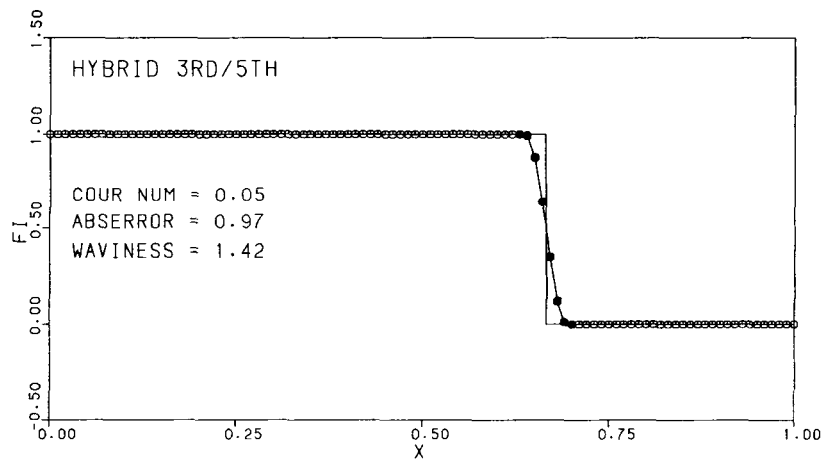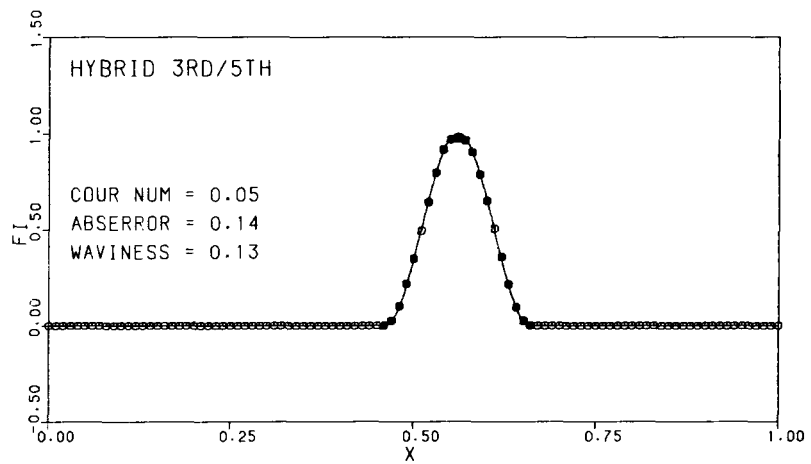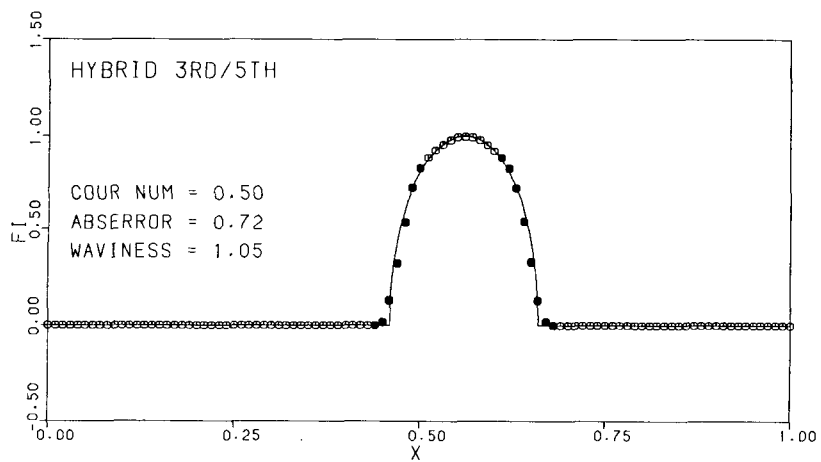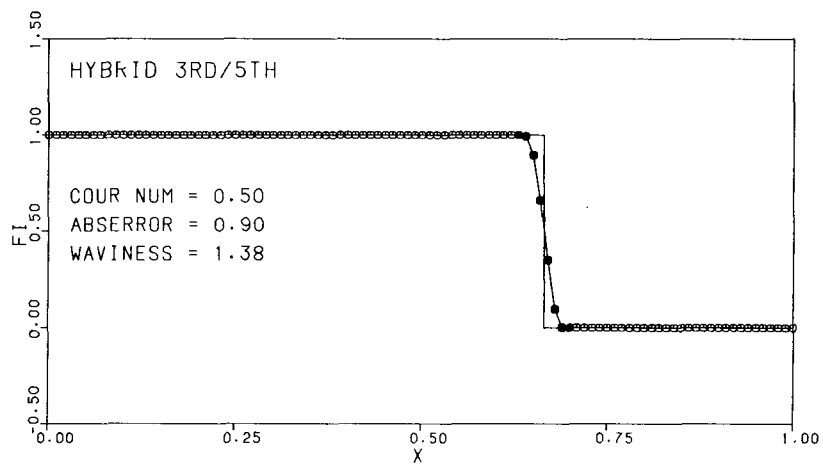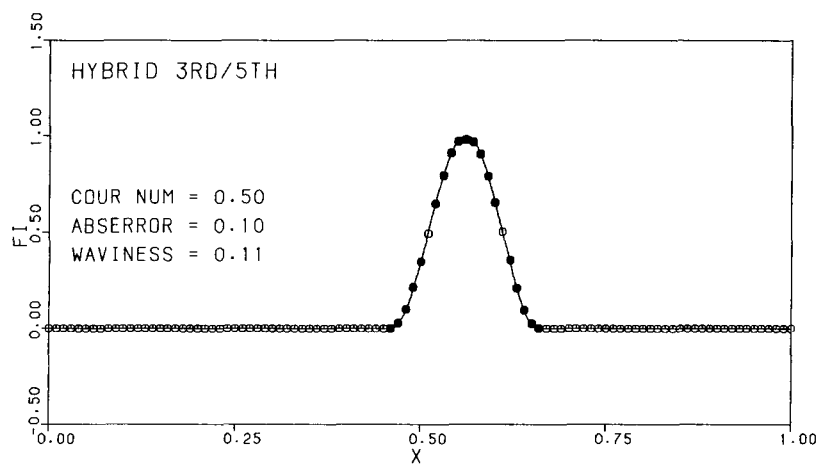
(b) c = 0.5.

FIGURE 46. - CONCLUDED.

FIGURE 47. - ABSERROR FOR THE SEMI-ELLIPSE PROFILE (UPPER CURVES) AND SINE-SQUARED PROFILE (LOWER CURVES) PLOTTED ON A LOG-LOG SCALE AGAINST ABSERROR FOR THE STEP, WITH COURANT NUMBER AS A PARAMETER RANGING FROM 0.01 TO 0.098, WITH VALUES SHOWN AT 0.1, 0.5, AND 0.9. CURVES SHOW: (1) ULTIMATE FROMM, (2) ULTIMATE QUICKEST, (3) ULTIMATE FIFTH-ORDER UPWINDING, AND (4) ULTIMATE SEVENTH-ORDER UPWINDING. ARROWS SHOW DIRECTION OF INCREASING COURANT NUMBER.
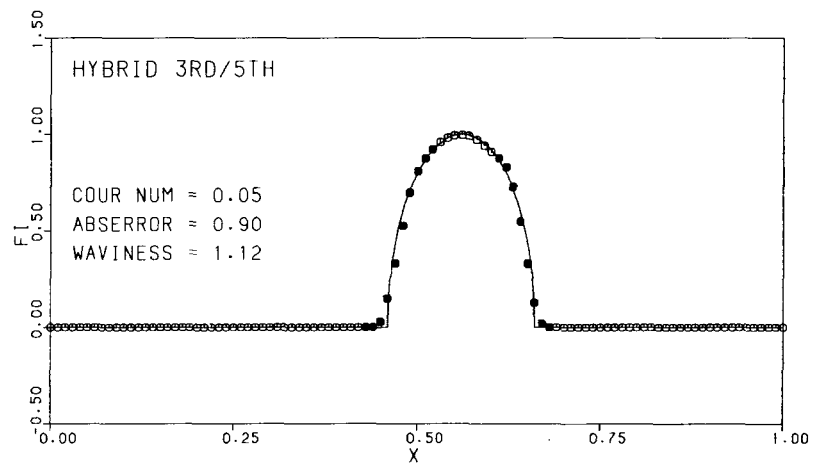
(a) c = 0.05.

FIGURE 48. - HYBRID ULTIMATE THIRD-/FIFTH-ORDER UPWINDING RESULTS. SOLID
CIRCLES SHOW NODES FOR WHICH EITHER THE LEFT OR RIGHT (OR BOTH) FACE
VALUES FOR THE NEXT TIME STEP ARE TO BE COMPUTED USING THE HIGHER-ORDER
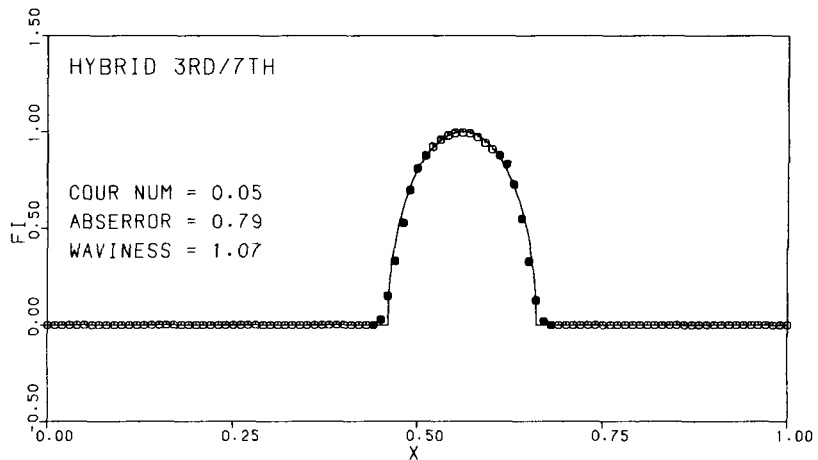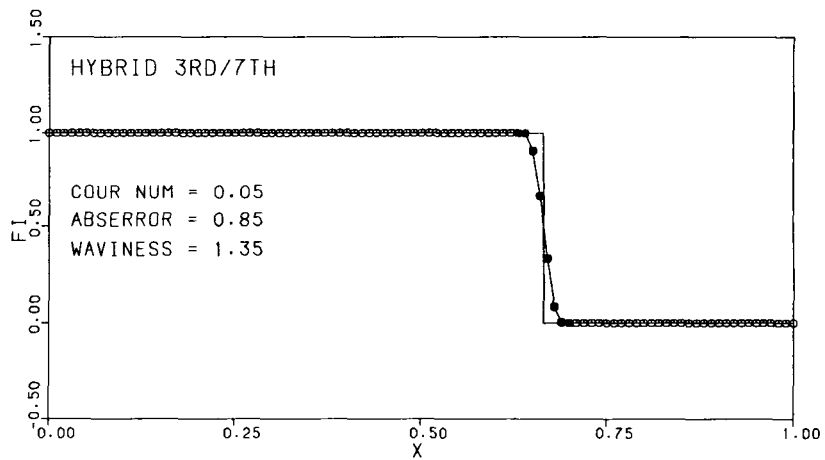SCHEME.

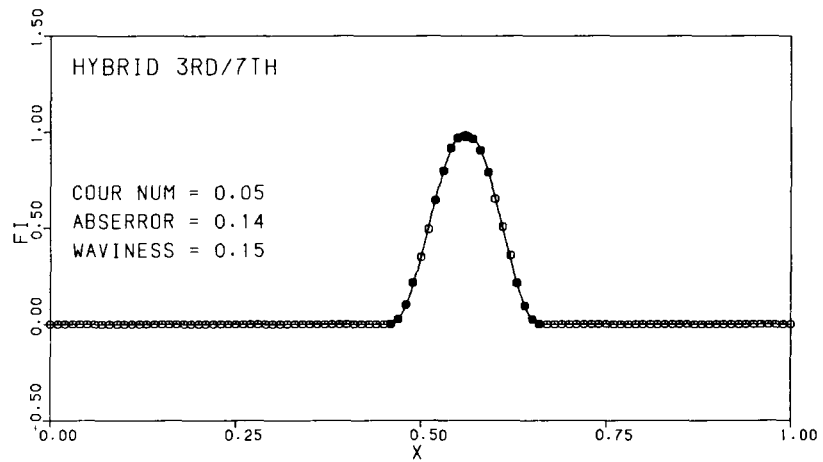(b) c = 0.5.

FIGURE 48. - CONCLUDED.

(a) c = 0.05.

FIGURE 49. - HYBRID ULTIMATE THIRD-/SEVENTH-ORDER UPWINDING RESULTS. SOLID
CIRCLES SHOW NODES FOR WHICH EITHER THE LEFT OR RIGHT (OR BOTH) FACE
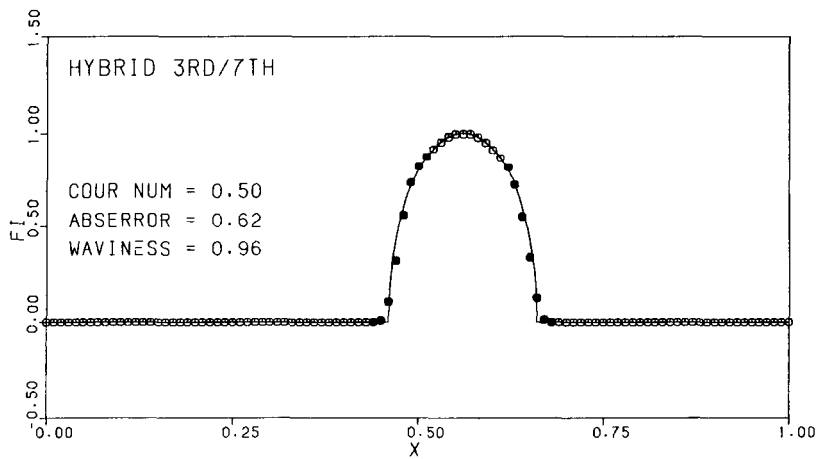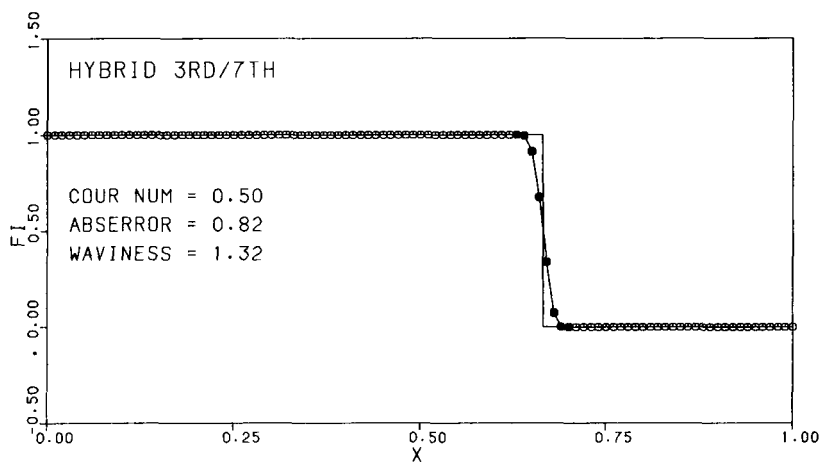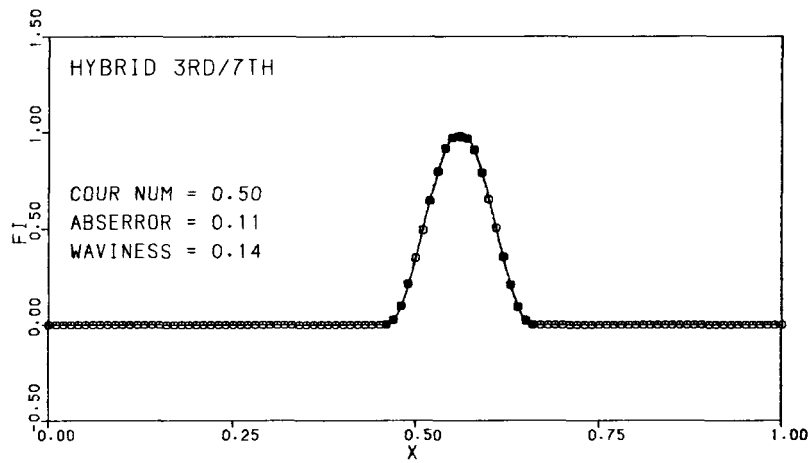VALUES FOR THE NEXT TIME STEP ARE TO BE COMPUTED USING THE HIGHER-ORDER
SCHEME.

(b) c = 0.5.

FIGURE 49. - CONCLUDED.

(a) $u_\ell > 0$, $v_\ell > 0$.   (b) $u_\ell < 0$, $v_\ell < 0$.
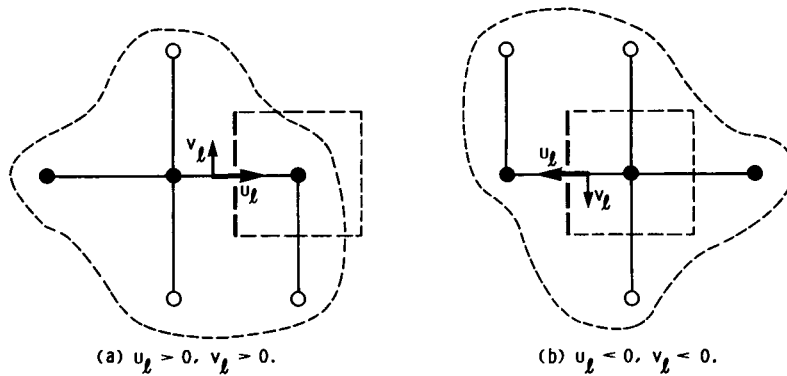
FIGURE 50. - TWO-DIMENSIONAL CONTROL-VOLUME SHOWING NODE STENCIL INVOLVED IN ESTIMATING THE LEFT-FACE VALUE USING ULTIMATE UTOPIA. SOLID CIRCLES SHOW NODES USED FOR THE UNIVERSAL LIMITER.

(a) DIFFUSE SOLUTION.   (b) NVD REGIONS.   (c) SHARP SIMULATION.
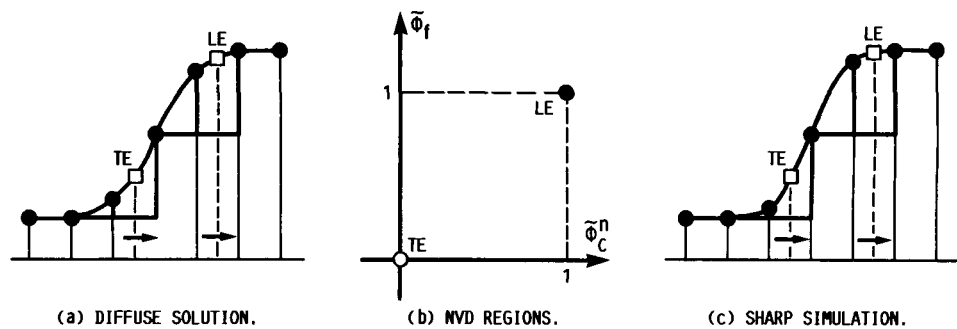
FIGURE 51. - SCHEMATIC (INVERTED) STEP SIMULATION SHOWING LEADING-EDGE (LE) AND TRAILING-EDGE (TE) BEHAVIOR.

FIGURE A.1. - SWEBY'S TVD REGION (SHADED) SHOWN. FOR REFERENCE, ROE'S SUPERBEE
SCHEME IS SHOWN BY THE HEAVY PIECEWICE LINEAR CHARACTERISTIC.

FIGURE A.2. - "EXTENDED SWEBY DIAGRAM" CORRESPONDING TO THE ULTIMATE
STRATEGY OF FIGURE 33. FOR REFERENCE, THE SUPER-C SCHEME IS SHOWN
BY THE HEAVY PIECEWISE LINEAR CHARACTERISTIC.

NASA
National Aeronautics and
Space Administration
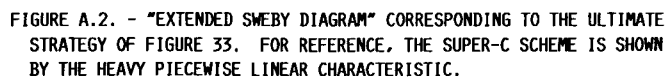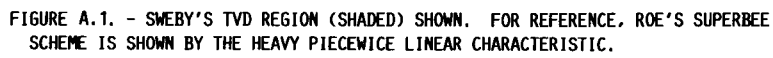
Report Documentation Page

1. Report No. NASA TM-100916 ICOMP-88-11	2. Government Accession No.	3. Recipient's Catalog No.

4. Title and Subtitle	5. Report Date
Universal Limiter for Transient Interpolation Modeling of the Advective Transport Equations: The ULTIMATE Conservative Difference Scheme	September 1988
	6. Performing Organization Code

7. Author(s)	8. Performing Organization Report No.
B.P. Leonard	E-4169
	10. Work Unit No. 505-62-21

9. Performing Organization Name and Address	11. Contract or Grant No.
National Aeronautics and Space Administration Lewis Research Center Cleveland, Ohio 44135-3191	
	13. Type of Report and Period Covered

12. Sponsoring Agency Name and Address	
National Aeronautics and Space Administration Washington, D.C. 20546-0001	Technical Memorandum
	14. Sponsoring Agency Code

16. Abstract

A fresh approach is taken to the embarrassingly difficult problem of adequately modeling simple pure advection. An explicit conservative control-volume formulation makes use of a universal limiter for transient interpolation modeling of the advective transport equations. This ULTIMATE conservative difference scheme is applied to unsteady, one-dimensional scalar pure advection at constant velocity, using three critical test profiles: an isolated sine-squared wave, a discontinuous step, and a semi-ellipse. The goal, of course, is to devise a single robust scheme which achieves sharp monotonic resolution of the step without corrupting the other profiles. The semi-ellipse is particularly challenging because of its combination of sudden and gradual changes in gradient. The ULTIMATE strategy can be applied to explicit conservative schemes of any order of accuracy. Second-order schemes are unsatisfactory, showing steepening and clipping typical of currently popular so-called "high resolution" shock-capturing or TVD schemes. The ULTIMATE third-order upwind scheme is highly satisfactory for most flows of practical importance. Higher order methods give predictably better step resolution, although even-order schemes generate a (monotonic) waviness in the difficult semi-ellipse simulation. But little is to be gained above ULTIMATE fifth-order upwinding which gives results close to the ultimate one might hope for.

17. Key Words (Suggested by Author(s))	18. Distribution Statement
ULTIMATE; Monotonic advection; Universal limiter; Nonoscillatory simulation; Conservative difference; Wiggle-free CFD	Unclassified – Unlimited Subject Category 64

19. Security Classif. (of this report)	20. Security Classif. (of this page)	21. No of pages	22. Price*
Unclassified	Unclassified	116	A06

NASA FORM 1626 OCT 86   *For sale by the National Technical Information Service, Springfield, Virginia 22161